M.Sc. Thesis Project
Renewable Energy Systems

"Hydrogen-assisted Pyrolysis-based BioSNG Production in Denmark: A Techno-economic Study"

Prof. Lasse Røngaard Clausen

Prof. Pierluigi Leone

Farshad Vaziri, M.Sc Student

February 2026

Politecnico di Torino - Technical University of Denmark

Declaration of AI use

In preparing this thesis, I made use of artificial intelligence tools to support efficiency and clarity in writing and literature handling. Specifically, AI was used primarily to summarize, paraphrase, and proofread text that I had drafted. AI was not used to create original content, generate novel results, or produce any analysis in place of my own work.

AI assistance was also used to help identify potentially relevant literature, to skim and screen papers for relevance, to format and tidy tables, to generate process flow diagrams, to transcribe data from published tables, and to convert equations into linear, copyable formats. These tasks would otherwise have required substantial time, and the use of AI helped me remain focused on the core scientific work, including critical reading of the literature, process modelling, and techno-economic analysis.

The tools used in this project included ChatGPT-5.2, Litmaps, and Nano Banana.

Abstract

This thesis evaluates a hydrogen-assisted bio synthetic natural gas pathway designed for a Danish wheat straw context. The concept separates biomass conversion into slow pyrolysis and volatile upgrading, where pyrolysis produces biochar and a volatile stream that is reformed to syngas and upgraded to methane through catalytic methanation. Renewable hydrogen is supplied via electrolysis to enable stoichiometric control and higher carbon utilisation. The process was modelled in Aspen Plus and the simulation results were used as the basis for a techno-economic analysis and sensitivity assessment. Two layouts were evaluated. One integrates alkaline electrolysis cells and the other integrates solid oxide electrolysis cells.

Under the base assumptions, the levelized cost of BioSNG production is estimated at 154.88 €/MWh for the AEC-based layout and 174.38 €/MWh for the SOEC-based layout. The SOEC layout reduces total electricity demand relative to AEC, but this advantage is offset by higher annualized capital and fixed cost assumptions. Sensitivity analysis confirms that the cost outcome is dominated by electricity related expenditures and electrolysis performance. Financing assumptions also influence results, with the SOEC layout showing higher sensitivity to WACC due to its higher capital intensity.

The work shows that hydrogen-assisted BioSNG economics depend primarily on electricity price, electrolyser performance, and capital recovery, while heat integration and co-product credits provide secondary improvements. Literature benchmarks indicate that electrolysis-intensive methane pathways are generally electricity sensitive and become more attractive under low electricity prices and credible value stacking.

Acknowledgements

I would like to express my sincere gratitude to *Prof. Clausen (DTU Construct)* for welcoming me as a visiting thesis student despite us having no prior contact. That initial trust meant a great deal to me. Throughout the project, he provided consistent guidance, constructive feedback, and valuable resources, and he invested significant time through numerous discussions and meetings. His availability, mentorship, and practical advice were pivotal in shaping both the direction and quality of this work.

I am equally grateful to *Prof. Leone (DENERG, Politecnico di Torino)* for agreeing to supervise my thesis during my visiting period at DTU. As an exchange student from Politecnico di Torino carrying out my thesis work abroad, his willingness to take on this role provided both academic continuity and essential support throughout the process.

I would also like to thank *my wife*, whose steady encouragement and emotional support carried me through a past year that was both intense and, at times, overwhelming. Her patience, understanding, and belief in me were a constant source of motivation throughout this journey.

A very special thanks goes to *my friend Benyamin* for his generosity and support during my stay in Denmark. By opening his home to me and encouraging me from the very beginning to relocate to Denmark to find a thesis opportunity, he played an important role in making this fruitful experience possible.

Finally, I dedicate this thesis to the cherished memory of my father, who passed away last year after a brave struggle with cancer, and to every soul currently enduring their own journey through this illness. He was a constant source of strength, encouragement, and belief in my ability to pursue my goals. His support made me who I am today, and he will remain in my heart forever. May he rest in peace, and may all those currently in the shadows of their battle emerge into the light of survival.

Table of Contents

List of Tables

List of Figures

Abbreviations and acronyms

Term	Meaning
AEC	Alkaline electrolysis cell
BEC	Bare erected cost
BioSNG	Bio-synthetic natural gas
CAPEX	Capital expenditure
CEPCI	Chemical Engineering Plant Cost Index
CHP	Combined heat and power
CO	Carbon monoxide
CO_2	Carbon dioxide
CRF	Capital recovery factor
DEA	Danish Energy Agency
DH	District heating
DCOALIGT	Aspen method for density of non-conventional solids
EPCC	Engineering, procurement and construction cost
FOAK	First-of-a-kind
GHSV	Gas hourly space velocity
HHV	Higher heating value
HCOALGEN	Aspen method for enthalpy of non-conventional solids
H_2	Hydrogen
H_2O	Water
KPI	Key performance indicator
LCOF	Levelized cost of fuel (bioSNG)
$LCOH_2$	Levelized cost of hydrogen
LHV	Lower heating value
NETL	National Energy Technology Laboratory
N_2	Nitrogen
O&M	Operation and maintenance
OPEX	Operating expenditure
PC	Project contingency
PEM	Proton exchange membrane electrolysis
PR-BM	Peng–Robinson EOS with Boston–Mathias modification
PtX	Power-to-X
RGibbs	Aspen equilibrium reactor block
RStoic	Aspen stoichiometric reactor block
RYield	Aspen yield reactor block
SNG	Synthetic natural gas
SMR	Steam methane reforming
SN	Stoichiometric number (syngas module) for methanation feed
SOEC	Solid oxide electrolysis cell
TAC	Total annual cost
TOC	Total overnight cost
TPC	Total plant cost
TIC	Total investment cost
TRL	Technology readiness level
TREMP	Topsoe Recycle Energy-efficient Methanation Process
WACC	Weighted average cost of capital
WGS	Water–gas shift
YSZ	Yttria-stabilized zirconia (SOEC electrolyte material)

Symbols

Symbol	Definition	Typical unit
$\dot{m}$	Mass flow rate	kg·s^{-1}
$\dot{E}_{chem}$	Chemical energy flow of a stream	MW (MJ·s^{-1})
$c_{p,eff}$	Effective heat capacity (used for biomass/biochar)	kJ·kg^{-1}·K^{-1}
T	Temperature	°C (or K)
p	Pressure	bar
ΔT_{min}	Minimum approach temperature for heat exchange	°C
η_{el}	Electrolyser electrical efficiency (overall, LHV basis)	–
η_{is}	Compressor isentropic efficiency	–
η_{mech}	Compressor mechanical efficiency	–
SN	Stoichiometric number (syngas module)	–
ρ_{cat}	Catalyst bulk density	kg·m^{-3}
$\dot{Q}$	Heating duty	MW
$\dot{C}$	Cooling duty	MW
h_{vap}	Enthalpy of vaporisation of water	MJ·kg^{-1}
i	WACC used in CRF calculation	–
n	Economic lifetime	y
C_0	Cost at base year	currency
S_0	Reference capacity	MW, kg·s^{-1}, –
n_s	Capacity scaling exponent	–

1. Introduction

1.1. Decarbonisation and the role of renewable gases

Global energy transition efforts are increasingly shaped by a dual imperative of emission reductions and sustained energy security and reliability across diverse socio-economic contexts. In this setting—as shown in figure 1.1—power-to-X (PtX) has emerged as a key complement to direct electrification, especially in sectors where full electrification remains technically difficult or economically unattractive, such as long-distance maritime transport, aviation, and heavy-duty road haulage [1]. In parallel, the scalability contrast between PtX and biomass-based pathways has become increasingly relevant. Biomass availability is constrained by land use, sustainability limits, and competing demands. By contrast, PtX fuel production can scale mainly with renewable electricity availability and access to sustainable carbon sources [2]. Electrolysis technologies also enable flexible operation that can absorb surplus renewable generation. In this way, they can act as a controllable load and support system balancing in high-renewable power systems [3].

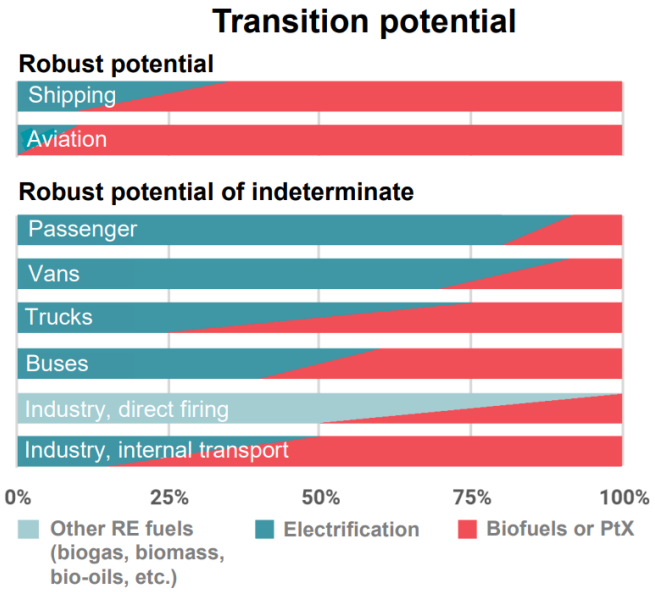

Figure 1.1: Sectoral decarbonisation options, contrasting electrification with PtX and biofuel routes. [2]

Within this broader transition, renewable gases such as biomethane, green hydrogen, and synthetic methane are often positioned as a practical bridge between variable electricity generation and end-use sectors that value dispatchability. A key advantage is their compatibility with existing gas infrastructure. This allows a gradual substitution of fossil natural gas without immediate large-scale changes to end-user equipment or a full replacement of network assets [4]. This feature is particularly relevant in energy systems with

established gas grids and district heating infrastructure, where rapid infrastructure replacement may be prohibitively costly or socially difficult—as shown for Denmark in figure 1.2. From a systems perspective, renewable gases also provide a chemical storage vector that can decouple production and consumption in time, which is attractive in wind-rich contexts where curtailment risks and seasonal variability remain structural challenges [3].

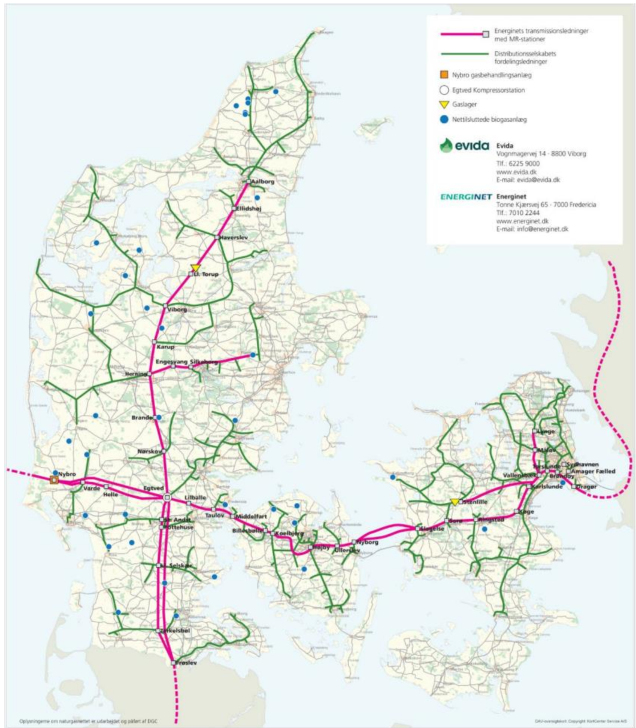

Figure 1.2: Overview of Denmark's gas grid structure, injection points, and storage connections. [4]

Against this backdrop, bio-synthetic natural gas (bioSNG) represents a pathway that couples biogenic carbon with catalytic upgrading to generate a methane-rich product compatible with gas-grid specifications. A common reference route is biomass gasification followed by syngas conditioning and methanation, producing substitute natural gas that can be blended into, or potentially substitute for, fossil-derived natural gas in existing infrastructure [5]. Beyond infrastructure compatibility, bioSNG is also discussed as a route to sector coupling. The methanation step is highly exothermic and can, in principle, support internal heat integration and external heat export where district heating networks exist [5]. This is especially relevant in Denmark, where policy and system studies frequently emphasize waste-heat utilization and cross-sector integration as practical measures to improve overall system efficiency and reduce reliance on separate thermal generation units [1].

However, experience from conventional BioSNG concepts also highlights persistent constraints that motivate alternative configurations. Key challenges include feedstock variability (composition and

moisture), throughput seasonality, and the need for extensive gas cleaning to protect sensitive catalytic steps from impurities such as alkali metals, sulfur compounds, and chlorine, all of which increase complexity and can erode net efficiency [6], [7], [8]. Methanation catalysts are particularly vulnerable to deactivation mechanisms such as coke formation and poisoning, leading to replacement cycles that materially affect operating costs and plant availability [6]. In addition, many conventional systems do not fully monetize thermal co-products. Excess heat may be rejected rather than recovered when nearby demand or infrastructure is limited. This reduces total system value and weakens the economic case [9]. Logistical penalties further compound the issue. Transporting low bulk-density biomass over long distances can quickly increase cost and emissions. Centralized large-scale plants can also face growing sourcing radii unless densification or distributed pre-processing strategies are adopted [9], [10].

The Danish context makes these trade-offs particularly tangible. Cereal straw (primarily wheat and barley) constitutes the dominant collectable agricultural residue for energy purposes, with annual agricultural activity yielding on the order of several million tonnes of residues, with cereal straw representing more than 90% of this potential [11]. Evidenced by figure 1.3, approximately half of the produced straw is currently collected, and nearly half of the collected fraction is already used for energy generation (typically district heating or CHP), which implies that any diversion to advanced fuel production competes with existing uses and must be justified by higher system value or stronger climate performance [11]. Further, spatial dispersion of residues, seasonal harvesting windows, and moisture-driven storage constraints impose real limitations on stable feedstock supply unless dedicated logistics (e.g., pelletization) and planning frameworks are implemented [9]. This is relevant because achieving high capacity factors is central to the economic feasibility of capital-intensive conversion plants. Supply disruptions directly translate into lower utilization and higher unit costs [12].

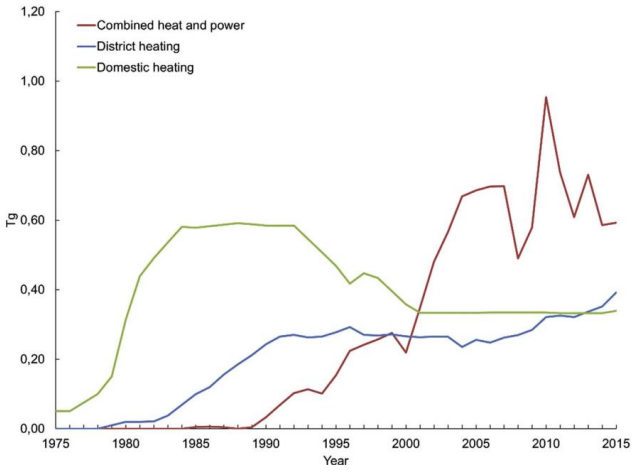

Figure 1.3: Historical Danish straw use for energy, split across district heating and CHP. [11]

These considerations motivate the interest in integrated, hybrid configurations that couple thermochemical conversion with renewable electricity inputs, rather than relying solely on a single conversion paradigm. In particular, slow pyrolysis of wheat straw is frequently highlighted as an appealing first step because it fractionates the feedstock into gaseous, liquid, and solid products whose yields can be influenced by operating conditions (temperature, residence time), while also enabling the co-production of biochar [13]. Biochar is important because, when applied to soils, it can bind biogenic carbon over extended timescales and may contribute to negative-emission accounting under suitable sustainability and certification frameworks [10]. At the same time, reforming the volatile fraction can produce a syngas stream that is suitable for methanation. Integrating electrolytic hydrogen enables stoichiometric control. This capability is increasingly relevant in wind-rich energy systems where flexible electrolysis can also provide system-balancing value [3].

Finally, the motivation is not only to show that a pathway can work in principle, but to assess how it performs as a whole. This includes whether heat recovery can reduce external utility needs. It also includes whether surplus heat can be exported through district heating where temperature levels and offtake conditions permit [14]. Another key question is whether the economics remain attractive under realistic electricity prices, feedstock logistics, catalyst durability, and financing assumptions. Taken together, these drivers highlight the need for research that compares alternative plant configurations using integrated process modelling. Such studies can clarify how heat integration and co-product valorisation affect the practical role of these pathways in decarbonisation contexts such as Denmark [1], [9], [14].

1.2. Limits of conventional bioSNG routes

Conventional bioSNG production is most commonly framed as biomass gasification followed by syngas conditioning and catalytic methanation. While conceptually straightforward, this route becomes materially constrained once the target shifts from “a combustible product gas” to grid-quality methane—shown in table 1-1— and stable, long-term operation. The core problem is that raw syngas from biomass gasifiers is intrinsically heterogeneous. It contains particulates, condensable tars, and reactive trace species that must be removed or converted before methanation, because nickel-based methanation catalysts are vulnerable to fouling, poisoning, and sintering when exposed to contaminants above tolerance thresholds [15]. Even minute concentrations of sulfur-, chlorine-, or alkali-containing compounds can sharply shorten catalyst lifetime, which forces designs toward extensive cleaning trains and higher replacement frequencies [6], [7], [15]. In addition, impurity tolerances can become even stricter when high-performance units are integrated

upstream or downstream. For example, some low-temperature methanators require impurity levels below the ppm range, and SOEC-related systems also tolerate only minimal contamination [16].

In practice, this translates into a non-trivial syngas cleaning and conditioning burden that affects both cost and efficiency. Mechanical interception steps (e.g., cyclones and fabric filters) reduce bulk solids load, but their effectiveness is limited for tar-bound particulates. Typical reported capture ranges are 30–70% for cyclones and 0–50% for fabric filters under conditions aligned with syngas cooling [6]. Consequently, mechanical cleaning is rarely sufficient on its own and must be coupled with secondary treatments targeting tar conversion or removal. Tar management is repeatedly identified as a critical bottleneck. Physical removal methods may reduce tar presence without altering its chemical nature [17], while catalytic reforming approaches can crack heavy hydrocarbons into lighter gases, thereby improving both gas cleanliness and chemical energy recovery into H_2 and CO suitable for methanation [18]. Downstream of tar control, further polishing is typically required for sulfur and chlorine (e.g., sorbents such as ZnO for H_2S, alkaline materials for HCl), adding additional unit operations, pressure drops, and thermal penalties [7]. Collectively, these constraints mean that conventional bioSNG is often not limited by methanation chemistry per se, but by the complexity required to produce a catalyst-compatible feed reliably and economically [6], [7], [15].

A second, system-level limitation is that many conventional concepts struggle to consistently capture the value of co-generated heat. Even when thermodynamic potential exists, excess heat is vented rather than recovered due to insufficient nearby infrastructure or limited ability to match temperature levels and demand profiles, which worsens overall energy return and leaves potential revenue untapped [9]. This is particularly relevant for rural, biomass-rich areas where district heating density may be lower, and where siting decisions can determine whether heat integration becomes a benefit or an unrealized opportunity [9]. A third limitation concerns logistics and utilisation rates. Economic feasibility depends heavily on high capacity factors to distribute capital costs over sustained output, but maintaining such utilisation requires steady feedstock inflows. Disruptions directly lead to underutilized assets and higher unit costs [12]. Biomass transport can further erode feasibility. Low bulk density materials transported over long distances increase cost and reduce environmental benefit through additional fuel use [10].

Finally, many conventional designs are configured for steady operation, which can limit responsiveness. Standard designs typically aim at stable methane output, with relatively limited capability to adjust product strategy in response to changes in electricity prices, policy incentives, or competing markets for renewable fuels and chemical intermediates [12]. In parallel, the economic case is frequently sensitive to external conditions such as carbon pricing, support schemes, and compliance costs associated with grid injection standards (monitoring calorific value and contaminant levels), which can disadvantage bioSNG relative to

fossil methane in the absence of supportive policy mechanisms [19]. The combined effect: technical vulnerability to impurities and catalyst stability, sizeable cleaning/conditioning chains, constrained heat monetisation, dependence on stable logistics and high utilisation, and exposure to policy and market structures creates a credible rationale for rethinking bioSNG configurations beyond incremental optimisation [6], [9], [10], [12], [19].

Table 1-1: Danish gas-grid quality requirements for SNG. [7]

Gas characteristic	Required value or span of values
General quality requirements	Gas free of compounds causing blockage, malfunction, corrosion of grid installations/equipment.
Hydrocarbons	Minimise unsaturated/aromatic hydrocarbons; prevent condensation; dew point <−5°C (≤4 bar) or <0°C (>4 bar).
Water content	Keep low; dew point <0°C (>4 bar) or <ambient; collect condensate if needed.
Dust	Remove dust completely.
Sulfur compounds (mg/m³n)	Corrosion limits: H2S <5; other S <10; odorants min: THT 10.5, mercaptan 4.0.
Wobbe index (heat effect on gas burner)	51.9–55.8 MJ/m³n under normal conditions.
Relative density (dry gas relative to dry air)	<0.7

This motivates the research gap addressed in this thesis. there is a need for integrated, hybrid bioSNG concepts that better exploit renewable electricity as a controllable input, improve stoichiometric control for methanation, and valorise co-products (notably biochar and exportable heat) more explicitly. Literature increasingly discusses integration directions such as catalytic reforming strategies to convert heavy hydrocarbons into syngas precursors, electrified reforming concepts with precise thermal control [20], and the use of electrolysis to adjust hydrogen availability and improve overall system efficiency [12], [19]. However, many studies treat these elements in partial scope (e.g., focusing on gasifier selection or cleaning trains, or analysing electrolysis separately) and therefore do not consistently quantify the full plant-level trade-offs between electrolysis technology choice, heat integration and export potential, cost structure, and LCOF sensitivity under a unified boundary and comparable bioSNG output. The present work addresses this gap by developing a plant-wide Aspen-based model of a pyrolysis–reforming–electrolysis–methanation pathway and applying a consistent performance and techno-economic framework to compare AEC- and SOEC-based layouts, including explicit heat-integration assessment and systematic sensitivity analyses.

1.3. Aim and research questions

The aim of this thesis is to develop a consistent, plant-wide process model for an integrated pyrolysis–reforming–electrolysis–methanation pathway to grid-quality bioSNG from wheat straw—demonstrated in figure 1.4, and to use this model to quantify the main technical and economic trade-offs between two alternative hydrogen-supply configurations: AEC-based and SOEC-based electrolysis integration.

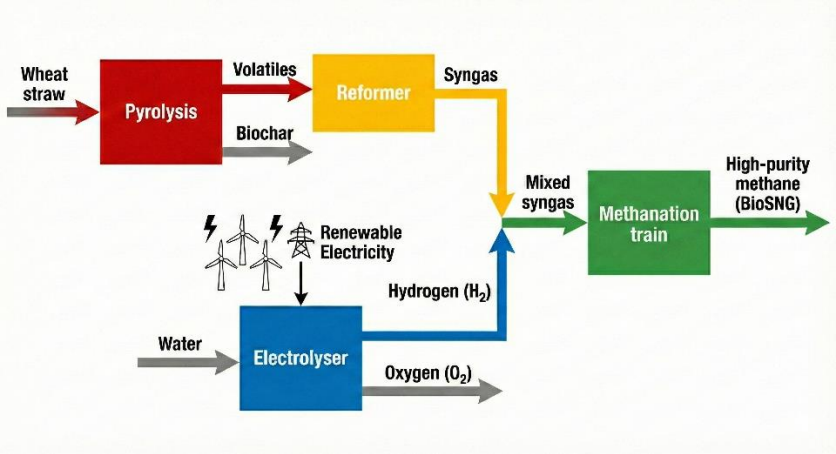

Figure 1.4: Simplified process flow diagram of the present study.

Accordingly, the thesis addresses the following research questions:

- Process feasibility and performance: Under a unified boundary and consistent assumptions, what are the resulting mass and energy balances, key performance indicators, and bioSNG output characteristics for the two layouts?
- Heat integration and export potential: To what extent can internal heat demands be satisfied through process integration, and what prospects arise for each layout under representative heat export programs?
- Economic competitiveness: What are the total annual expenses and base-case LCOF for each layout when subsystem sizing is coupled to literature cost bases?
- Robustness and key drivers: How sensitive is the LCOF to major uncertainty and variability drivers and which factors dominate the cost of production?

1.4. Scope, system perspective, and key delimitations

This thesis adopts a plant-gate (cradle-to-gate) system perspective for the core technical and economic assessment. The model boundary extends from biomass input at the pyrolysis section inlet to dry bioSNG at the plant fence, and explicitly includes the integrated electrolysis-based hydrogen supply, the major compression/pumping duties, and the principal heating/cooling duties required for plant-wide heat integration and export assessment. The analysis is therefore focused on the integrated conversion chain and on comparing AEC- vs. SOEC-based layouts under a unified boundary and comparable bioSNG output.

The plant is evaluated at steady state and fixed nominal load, consistent with the base-case operating assumptions used throughout the simulation and techno-economic analysis. Electricity is treated as an

external renewable input characterised by an assumed market price, while biochar and exportable heat are treated as co-products through revenue credits within the economic boundary.

Key delimitations applied in this work are:

- Upstream biomass logistics (cultivation, harvesting, collection, transport, and pelletisation/densification) are excluded from the core process model boundary.
- Downstream distribution and end-use of bioSNG (gas-grid transport and final combustion) are excluded.
- Detailed gas clean-up trains (e.g., tar filtration and sulphur removal) are not modelled explicitly; their effects are treated through simplifying assumptions consistent with the chosen process definition.
- Environmental/LCA assessment is not performed in the present thesis; a full LCA would require expanded cradle-to-grave boundaries and explicit methodological choices for co-product treatment (e.g., biochar sequestration crediting and district-heating displacement), which are outside the current scope, [10], [14], [21].
- Dynamic operation and dispatch optimisation are not considered; the analysis represents nominal continuous operation, with sensitivity analyses used to probe the impact of key uncertainties rather than modelling time-resolved operation [12], [22].

1.5. Thesis outline

Chapter 3 defines the process concept, system boundaries, and modelling approach used to represent the integrated process pathway. Chapter 4 presents the simulation results and key performance indicators, including carbon utilisation, electricity demand, and heat-integration and export potential. Chapter 5 develops the techno-economic methodology and reports the investment and operating costs, total annual expenses, and base-case levelized cost of bioSNG (LCOF). Chapter 6 evaluates the robustness of the results through sensitivity analyses (electrolyzer efficiency, electricity price, and WACC) and an uncertainty-band assessment. Finally, the concluding chapters summarise the main findings, discuss limitations and implications, and propose directions for future work.

2. Literature review and theoretical framework

2.1. Feedstock context and wheat straw characteristics

Wheat straw is an attractive bioSNG feedstock in a Danish context primarily because it is a large-volume agricultural residue rather than a dedicated energy crop, and therefore does not directly introduce land-use change pressures. In rural Denmark, the dominant collectable residue stream is cereal straw (mainly wheat and barley). Reported national residue generation—based on figure 2.1—is on the order of ~6 Tg per year, with cereal straw representing more than 90% of this potential [11]. However, only about half of the produced straw is collected, and of the collected fraction nearly half is already used for energy, typically combustion for district heating or CHP. Straw used for energy peaked at 1.6 Tg in 2010 and was 1.3 Tg in 2015, of which 1.0 Tg was used for CHP and district heating [11]. In addition, a substantial fraction is deliberately left unharvested to preserve soil organic carbon or due to logistical constraints, and straw also has established non-energy uses such as livestock bedding (27% of harvested straw) and incorporation into soils (50% of the harvested straw left on field) [9]. These patterns imply that the "technical potential" of straw does not translate directly into a freely available industrial feedstock and any advanced conversion route must compete with existing value chains and respect agronomic sustainability constraints [9], [11].

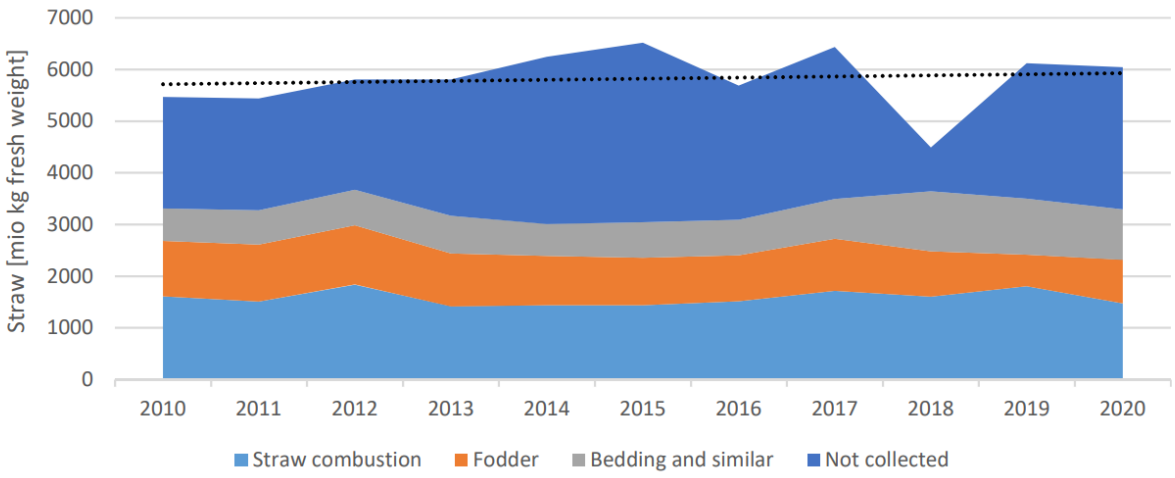

Figure 2.1: Danish straw uses 2010–2020 split into combustion, fodder, bedding, and not collected. [21]

A second defining characteristic is seasonality. Straw availability is concentrated in relatively short harvesting windows, whereas conversion facilities are generally designed for near-continuous operation to maintain high utilisation and acceptable unit costs. Bridging this mismatch requires logistics and storage strategies that can preserve feed quality throughout the year [11]. Estimates under dry-matter assumptions suggest that approximately 2.5 million tonnes of relatively dry straw may be storable annually using

conventional collection practices, although this is highly sensitive to weather conditions during harvest [21]. A “commonly used” harvest moisture limit is 20% (fresh basis), but <18% is preferred by straw buyers/utilities [11]. Wet straw introduces practical limitations. It increases the risk of microbial degradation (handling and health risks) and self-heating during storage, reduces available dry matter, and can create safety risks over long storage periods [21]. For these reasons, robust feedstock preparation and storage concepts are not peripheral issues but central determinants of whether straw-based thermochemical routes can operate reliably at high capacity factors [9], [11], [21].

From a physical-handling perspective, straw’s low bulk density increases transport and storage burdens. Densification measures such as baling and, particularly, pelletisation can reduce hauling energy per unit mass and improve handling stability, but they impose additional capital and operational requirements and typically require sufficiently dry material to avoid pellet integrity problems or die blockage [23]. Typical straw characteristics are shown in table 2-1. In practice, densification generally demands moisture levels below roughly 12%, which motivates either effective field drying or mechanical drying before pellet production [23]. Because transport costs rise rapidly with distance for bulky biomass, supply-chain designs often consider decentralised pre-processing (drying and densification) near collection zones as a means to stabilise feed properties while reducing the effective transport penalty to a central conversion site [9], [21].

Table 2-1: Typical straw moisture, ash content, and LHV ranges used for pyrolysis. [8]

Raw material	Moisture content, before treatment (Weight %)	Ash content* (Weight % on dry substance)	Lower heating value, (dry/ash free) (MJ/kg)
Straw	10–15	4–10	17–18

Moisture content is also a process-relevant variable. For pyrolysis-based pathways, operational practice often targets a feed moisture range on the order of 10–25%, depending on reactor configuration and available pretreatment infrastructure [8]. Lower moisture improves thermal efficiency because less heat is diverted to water evaporation prior to devolatilisation; however, achieving low moisture may require additional drying energy or equipment (drying from 13% to 10% moisture needs ~11 kWh/ton heat and pelletising needs ~23 kWh/ton of electricity) [8]. For integrated configurations that include reforming, moisture variability can propagate beyond the pyrolysis step. Varying inherent water inputs translate into varying steam availability for reforming reactions, complicating mass-balance predictability and operational control [8]. Consequently, several process simulation studies adopt standardised moisture levels, often around ~10% after drying, to ensure comparability across cases [8]. A practical design compromise discussed in the literature is to target approximately 10–12% moisture at plant gate, balancing achievable drying under local conditions with the needs of stable thermochemical operation [8].

The chemical composition of wheat straw—demonstrated within figure 2.2—largely explains both its conversion potential and its operational challenges. Structurally, wheat straw is lignocellulosic, typically reported with a relatively high carbohydrate fraction, for example approximately 40% cellulose, 32% hemicellulose, 20% lignin, and ~8% extractives in representative datasets [24]. The comparatively lower lignin fraction (relative to many woody feedstocks) tends to favour higher volatile yields under pyrolysis, which is beneficial when the process concept relies on upgrading the volatile fraction into synthesis gas and then methane [10], [24]. Thermal decomposition proceeds in characteristic stages. Hemicellulose typically decomposes around 200(220)–300(320)°C, cellulose around 300(350)–400(420)°C, and lignin over a broader window extending beyond 500°C, which contributes to sustained char formation even after most carbohydrate-derived volatiles have evolved [24]. These traits are directly relevant to process design because they influence the distribution between volatile products and solid char, as well as the reactivity and reformability of the evolved vapours [24].

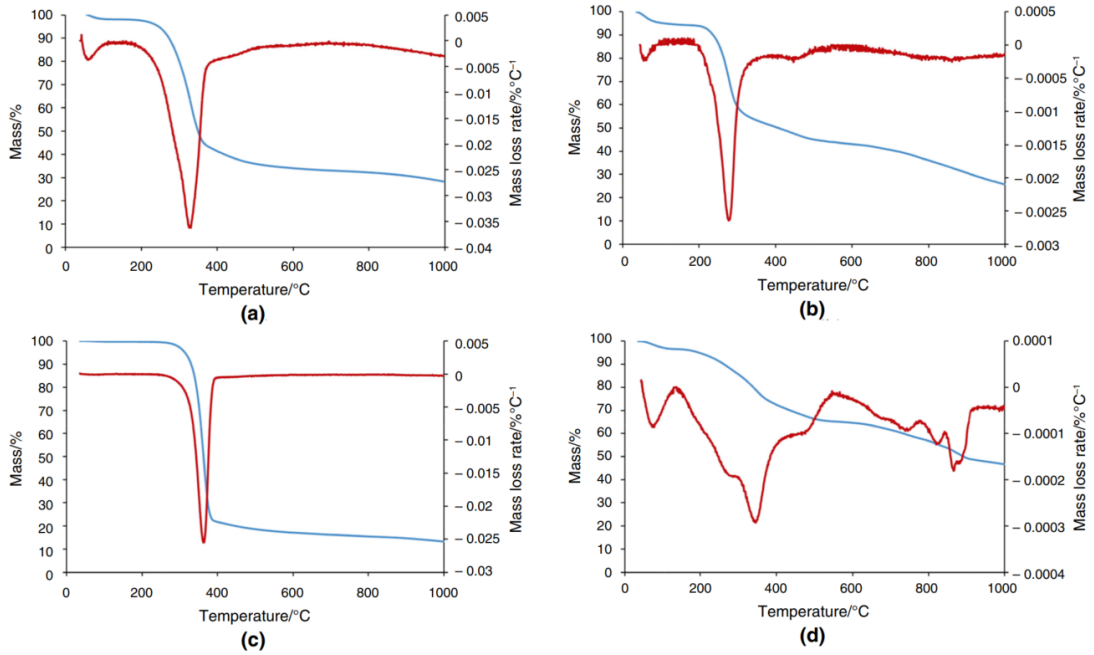

Figure 2.2: TGA and DTG curves for wheat straw residue (a), hemicellulose (b), cellulose (c), and lignin (d). [24]

At the same time, straw's inorganic fraction requires attention. Wheat straw, containing a relatively high ash content, often contains silica and relatively elevated alkali metals (notably potassium), which can increase slagging/fouling tendencies in high-temperature systems and may contribute to catalyst-related risks if not adequately managed [20], [23], [24]. Moisture during storage can further alter ash chemistry because some alkali species are mobile in aqueous phases; prolonged exposure to residual liquid water can drive leaching and redistribution of minerals, with potential implications for downstream high-temperature

behaviour [24]. This reinforces that feedstock "quality" is not static and it evolves with handling and storage conditions and can affect both thermal performance and operational reliability [24].

2.2. BioSNG production pathways

2.2.1. Gasification, syngas conditioning, and catalytic methanation

The conventional and most widely discussed route to bio-synthetic natural gas (bioSNG) is based on biomass gasification, followed by syngas cleaning (conditioning) and catalytic methanation. In this pathway, the gasifier converts solid biomass into a raw product gas containing primarily CO, H_2, CO_2, and smaller fractions of CH_4, along with undesired species such as particulates, condensable tars, and reactive trace contaminants. Evidenced by figure 2.3, the choice of gasification technology influences raw gas composition, impurity load, downstream unit sizing, and ultimately overall plant efficiency and economics over the full operating lifetime [5], [15].

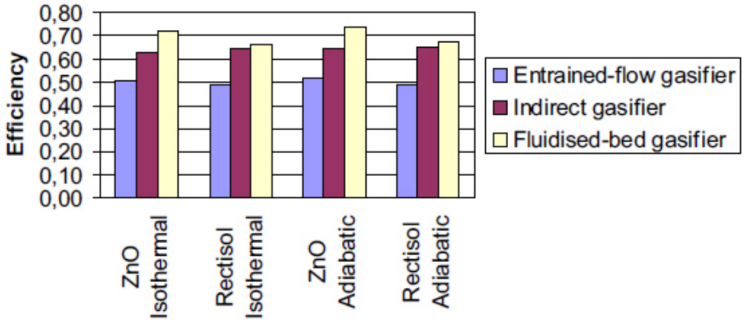

Figure 2.3: SNG efficiency comparison across gasifier types, cleanup systems, and methanation concepts. [7]

A range of gasifier concepts has been developed for biomass-to-SNG applications, with trade-offs primarily governed by operating temperature regime, oxidizing medium, and solids handling—illustrated in figure 2.4. For example, fluidized-bed gasifiers (bubbling or circulating) are frequently highlighted due to their tolerance toward mixed biomass particle sizes and relatively uniform temperature profiles, but they often carry higher ash/particle entrainment to downstream units, increasing the burden on filtration ahead of catalytic steps [5], [25]. In contrast, entrained-flow gasifiers operate at very high temperatures (typically above $1200°C$ in slagging mode with oxygen), which largely eliminates tar formation but requires significant feed pre-treatment (fine grinding below $1mm$ down to $0.1mm$) and higher upfront investment; the resulting syngas generally contains little to no methane due to thermal cracking, which implies that essentially all methane must be produced downstream via methanation [15]. Dual fluidized-bed (DFB) concepts decouple combustion and gasification zones and can produce nitrogen-free product gas without

pure oxygen, but may operate in temperature windows where tar formation is non-negligible, again increasing the importance of downstream conditioning [5]. Overall, reactor selection becomes a system decision in which lower capital intensity can come at the cost of higher downstream clean-up demands, while premium “cleaner syngas” designs may be economically justified only if long, stable operation and robust feed supply chains can be ensured [15].

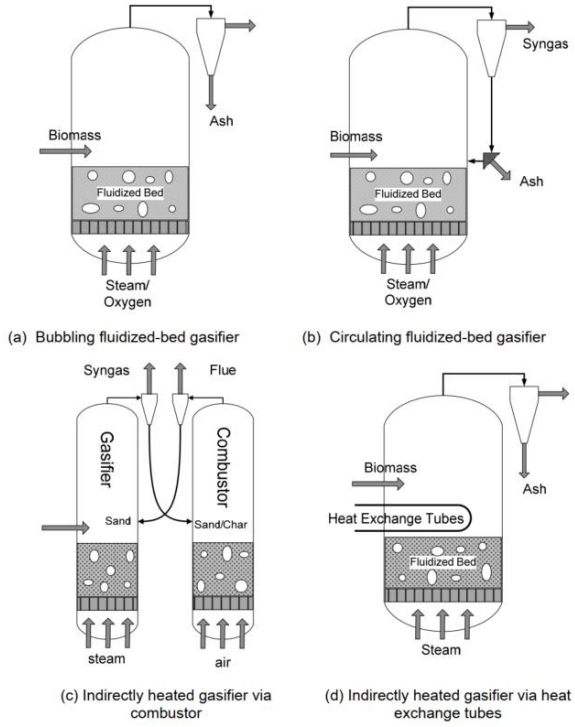

Figure 2.4: Fluidized bed gasifier variants. [15]

Independent of gasifier type, syngas cleaning and conditioning is typically the defining complexity in conventional BioSNG plants, because methanation catalysts (most commonly Ni-based systems) are highly sensitive to impurities. Raw syngas inevitably contains solid particulates, condensable tars, and reactive trace species that must be removed or converted to meet methanation inlet specifications [15]. Even small concentrations of sulfur, chlorine, or alkali metals can drastically shorten catalyst lifetime through poisoning or accelerated deactivation, which is why many designs include extensive multi-step cleaning before methanation [6], [7], [15]. In practice, the conditioning chain often begins with coarse particulate removal. Cyclones and fabric filters are commonly used but show limited capture efficiencies for tar-bound or fine aerosols; reported capture ranges are approximately 30–70% for cyclones and 0–50% for fabric filters under conditions aligned with syngas cooling [6]. As a result, mechanical cleaning is rarely sufficient and must be complemented by tar-focused measures [6], [17].

Tar management is repeatedly identified as a principal bottleneck. Physical removal approaches (e.g., scrubbing, electrostatic precipitation) can reduce tar presence but do not necessarily change the chemical nature of the remaining tar species [17]. By contrast, catalytic reforming approaches can actively crack complex hydrocarbons into lighter gases, thereby both cleaning the syngas and recovering chemical energy into H_2 and CO that contribute directly to methanation feed quality [18]. Integration concepts such as catalytic filter candles combine solids interception and steam-assisted tar reforming in a single unit operation, potentially shortening the clean-up chain while introducing maintenance and fouling considerations that must be managed over time [18]. After tar mitigation, polishing steps typically target H_2S and HCl using sorbent beds (e.g., ZnO for sulfur and alkaline sorbents for chlorine), arranged in temperature-appropriate sequences to maximize media lifetime and protect downstream catalysts [4], [7], [18].

Conditioning is not only about impurity removal; it also includes stoichiometric adjustment for methanation. Depending on gasifier type and operating mode, the raw syngas may not meet the desired H_2/CO balance for efficient methane synthesis, motivating insertion of water–gas shift units and steam management strategies to tune reactive ratios [17]. In many cases, CO_2 management is also required to satisfy grid-injection and methane-purity requirements; removal via physical solvents (Rectisol; removing CO_2 to <10 ppm, total sulfur <0.1 ppmv) or amine scrubbing (a-MDEA is described with CO_2 purity >99.4% in the capture stream) is often practiced, particularly when high methane purity and stable calorific value are targeted [5], [7], [15]. This increases both CAPEX and OPEX and introduces additional heat duties and regeneration requirements, reinforcing that the conventional route's feasibility depends strongly on how well the cleaning/conditioning chain is designed and integrated thermally [7], [15].

From a system-integration perspective, conventional BioSNG pathways can achieve high efficiencies under favorable conditions, but their performance is strongly contingent on heat recovery and operational stability. Literature discussions note that co-produced heat can represent a substantial share of the biomass input energy (on the order of 20–25% on an LHV basis), and that overall efficiency can improve significantly when this heat is effectively recovered and exported (e.g., to district heating networks) rather than rejected. TREMP context reports up to ~85% of methanation reaction heat recovered and ~3.0–3.5 kg steam/Nm³ SNG [7], [9]. However, many conventional systems struggle to monetize heat in practice due to infrastructure limitations or mismatch between temperature levels and local demand [7], [9]. Furthermore, conventional plants are sensitive to biomass logistics and utilization rate. Centralizing the process can exploit economies of scale, but it may increase transport penalties for low-density biomass, while smaller distributed sites may reduce logistics costs but suffer from reduced economies of scale and potentially less favorable efficiency [9], [10]. Finally, conventional designs are often characterised by limited operational

flexibility and product adaptability relative to emerging hybrid concepts that integrate variable renewable electricity (e.g., via electrolysis) and can adjust synthesis conditions in response to market drivers [12].

2.2.2. Rationale for an alternative pathway

An alternative to the conventional gasification-based BioSNG route is to separate biomass conversion into two deliberate steps: (i) slow pyrolysis to fractionate wheat straw into a solid carbonaceous stream and a volatile stream, and (ii) direct upgrading of the volatiles to methanation-ready syngas via reforming—illustrated by types in figure 2.5, followed by catalytic methanation. Pyrolysis vapours have a very high condensable fraction (bio-oil) with complex oxygenated chemistry and poor fuel properties, motivating direct reforming rather than storage/handling. The fundamental motivation is to redesign where the difficult chemistry is handled. Instead of producing a raw syngas in a gasifier and then investing heavily in downstream conditioning to protect methanation catalysts, the pyrolysis–reforming approach aims to (a) control the formation and handling of heavy organics and (b) convert them into useful syngas components within the reforming step, thereby improving both process robustness and carbon utilisation toward the final fuel. [6], [26], [27].

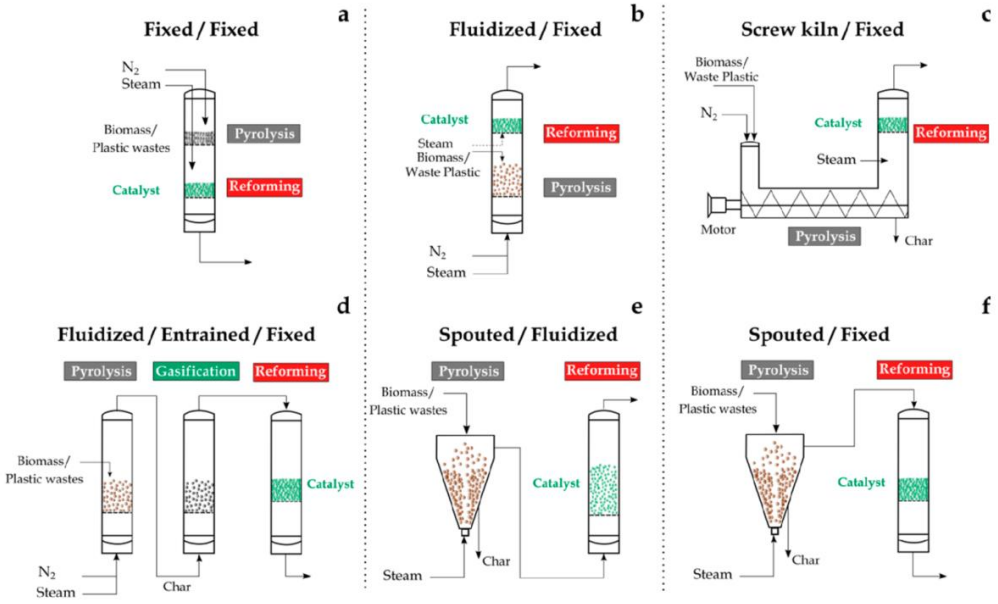

Figure 2.5: Reactor configurations for pyrolysis with in-line catalytic steam reforming. [28]

A key feature is the use of slow pyrolysis as a conditioning step rather than only a fuel-production step. Slow pyrolysis operates at relatively low heating rates and long vapour residence times, favouring char formation and enabling tunability of product distribution via temperature and residence-time control [28].

For wheat straw specifically, devolatilisation occurs in stages, which implies that vapour composition entering any downstream reformer is inherently transient and depends strongly on the pyrolyser operating window [24]. In integrated schemes, this motivates careful control of vapour transfer such that volatiles can be fed to reforming without intermediate condensation, avoiding issues associated with bio-oil handling (polymerisation, phase separation) and instead reforming higher hydrocarbons in situ [27].

The second rationale relates to value stacking through biochar. Slow pyrolysis retains a substantial share of biogenic carbon in biochar, typically on the order of 35–60% of the input carbon depending on operating conditions, which can be monetised either as a product in specialised markets or via climate-credit frameworks when applied to soils under suitable permanence assumptions [8]. Various sources are compared in table 2-2.

Table 2-2: CO2-eq removal per tonne biochar, unit net cost of biochar production, and unit cost per tonne of CO2-eq mitigation (costs in EURO in 2021 year value). [29]

Source	CO_2-eq removal per ton biochar	Cost (EUR per ton biochar)	Cost (EUR per ton of CO_2-eq removal)
McCarl et al. (2009), fast pyrolysis, maize residues	24.39	3465	142
McCarl et al. (2009), slow pyrolysis, maize residues	4.24	369	87
Teichmann (2015), slow pyrolysis, straw	3.09–4.77	132–252	28–81
Shackley et al. (2011), slow pyrolysis, straw	1.49	238–392	159–263
Shackley et al. (2011), slow pyrolysis, sludge	0.92	(−192)–334	(−208)–363
EA Energi analyse (2020), slow pyrolysis, incl. pyrolysis oil CO_2 impacts	—	—	117
EA Energianalyse (2020), slow pyrolysis, excl. pyrolysis oil CO_2 impacts, including green premium	—	—	65
Energistyrelsen (2022), 2022 CO_2 price	—	—	83
Det Økonomiske råd (2020), CO_2 price to meet 2030 targets	—	—	161
Average carbon offset price EU ETS 2021 (ICAP, 2022)	—	—	40

In a Danish agricultural context, this co-product also carries an additional systems argument as returning straw-derived biochar to fields can partially return minerals (e.g., P, K, Mg) —illustrated in table 2-3— and mitigate nutrient depletion concerns associated with sustained residue removal, strengthening the

sustainability narrative beyond fuel substitution alone [30]. In other words, the pyrolysis route is not only about producing a reformable vapour stream; it is also about embedding a potentially durable carbon-storage mechanism inside the BioSNG value chain [8], [10], [30].

Table 2-3: Nutrient concentrations P, K, Mg in biochar and ash products (wheat straw). [30]

Sample	**Fe**	**K**	**Mg**	**P**	**Zn**
Wheat straw	1.77 ± 0.16	10.20 ± 0.09	1.40 ± 0.16	2.00 ± 0.18	0.35 ± 0.04
Biochar	0.23 ± 0.03	36.00 ± 0.40	2.30 ± 0.03	4.20 ± 0.06	0.15 ± 0.01
Oxidation ash	2.96 ± 0	193.70 ± 2.06	11.80 ± 0.25	22.00 ± 0.51	not determined
Gasification ash	2.28 ± 0.17	173.00 ± 3.73	11.50 ± 0.23	20.70 ± 0.33	0.16 ± 0.01

A third motivation is process integration and heat management. The pyrolysis and reforming steps are endothermic (or demand high-grade heat), while methanation is strongly exothermic; literature repeatedly highlights that overall plant performance improves when hot and cold streams are matched across unit boundaries rather than optimised in isolation [31], [32]. Within a pyrolysis–reforming–methanation chain, sensible heat from hot char and hot vapours can be recovered to preheat incoming feeds or generate steam for reforming, and the methanation reaction enthalpy can be exploited for internal duties and/or district heating export where temperature levels allow [14], [31], [32]. This is particularly relevant for rural Danish settings where district heating infrastructure exists and where heat export can provide an additional revenue stream and a system-efficiency lever [14].

Finally, the pathway becomes especially compelling when paired with renewable electricity integration through electrified reforming and electrolysis. Electrified catalytic reforming concepts can replace combustion-based heat supply with controllable electrical heat input, which has been reported to enable improved temperature uniformity and faster thermal ramp-up relative to conventional fired configurations [20]. In parallel, electrolysis provides a direct lever for stoichiometric control. Deviations in steam-to-biomass ratio, volatile composition, or reformer conversion can be compensated by hydrogen injection to meet methanation requirements, reducing reliance on extensive shift/conditioning trains and enabling a more controlled approach to meeting grid-gas specifications [6], [12]. This integrated framing (i.e., slow pyrolysis for fractionation and biochar co-production, direct volatile reforming for syngas generation without bio-oil handling, electrolysis for stoichiometric control, and methanation for final methane synthesis with recoverable heat) defines the rationale for the pathway investigated in the present thesis.

2.3. Technology background for the integrated concept

2.3.1. Slow pyrolysis fundamentals and biochar as co-product

Slow pyrolysis refers to thermochemical conversion under moderate heating rates and extended residence times, which allows biomass to decompose into three main product groups, solid biochar, condensable organics, and permanent gases—illustrated in figures 2.6 and 2.7 and table 2-4 for straw—without the rapid quenching characteristic of fast pyrolysis [28]. In typical implementations, heating rates are kept below approximately 40 °C·min^{-1} and reactor configurations such as fixed-bed, moving-bed, or auger systems are used to sustain longer vapour–solid contact times and promote secondary cracking within the reactor volume [28]. This operating philosophy makes slow pyrolysis particularly relevant for integrated schemes. Residence-time and temperature control can be used not only to steer char yield, but also to shape the volatile composition in a way that supports downstream catalytic upgrading reforming rather than treating tar suppression as a separate stand-alone problem [26].

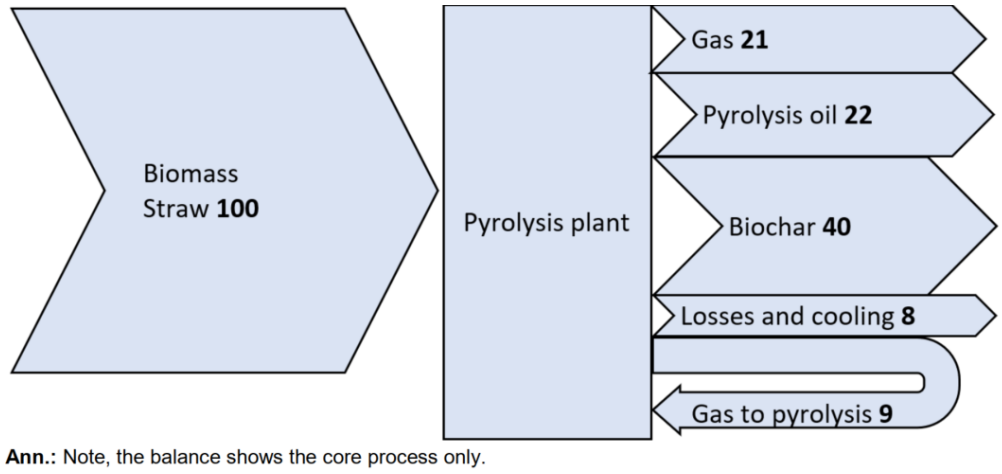

Figure 2.6: Energy balance for slow pyrolysis of straw. [8]

Temperature is a decisive parameter because it shifts both yield distribution and product properties. At low-to-moderate peak temperatures (~500 °C), biochar yields commonly remain high (often on the order of 30–35 wt.% of dry feed) with gas and liquid fractions comprising the remainder [33]. Increasing the peak temperature generally reduces char yield while increasing permanent gas formation and promoting a more carbonised, aromatic char structure [8], [33]. These trends are closely linked to the staged thermal degradation of lignocellulosic biomass [24]. This staged volatilisation means that the vapour stream composition entering any downstream reformer is inherently dependent on the pyrolyser temperature window and residence-time regime, and can be transient if not stabilised through process design [24], [33].

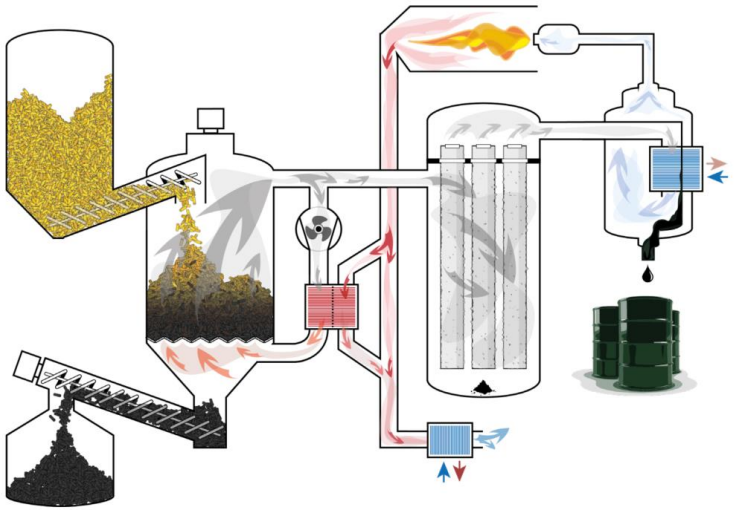

Figure 2.7: SkyClean pyrolysis process design with oil and heat as end products. [33]

Maintaining an inert or oxygen-free atmosphere is essential to avoid undesired combustion and oxidation losses. Laboratory and pilot practices often employ nitrogen purge/blanketing to displace air before heating and to stabilise reactor atmospheres; purge rates on the order of 6 $L \cdot min^{-1}$ (for 20 minutes before heating) have been reported for small reactors [30]. Post-reaction cooling strategy also matters as biochar can ignite at relatively low temperatures (as low as ~200 °C). Hot char can oxidise rapidly if exposed to air, so controlled cooling, via inert-gas cooling chambers, controlled quenching, or water sprays has been used to stabilise biochar for storage or soil application without compromising fixed-carbon content [33]. Where slow pyrolysis is integrated with downstream upgrading, many studies emphasise avoiding condensation of vapours into bio-oil and instead transferring volatiles directly to a reformer, because condensation introduces additional challenges (e.g., polymerisation and phase separation) that complicate handling and can reduce overall carbon and energy recovery [27].

A major reason slow pyrolysis is frequently highlighted in straw-based fuel pathways is the opportunity to treat biochar as a deliberate co-product, rather than as a low-value residue. Biochar formation typically retains a substantial fraction of the feedstock's biogenic carbon (often reported in the range of 35–60% of the input carbon, depending on pyrolysis conditions), which supports negative-emission narratives when biochar is returned to soils under suitable permanence assumptions (half-life ~150–5000 years) [8]. Stability is commonly linked to the degree of aromaticity achieved during conversion; operating conditions with moderate heating rates and peak temperatures around 500–600 °C favour aromatic structures that are resistant to microbial mineralisation over long timescales [8], [24]. A frequently used indicator is the molar H/C ratio, where values below approximately 0.4 are associated with high permanence potential in soil environments (70% remaining after 100 years for $H/C_{org} \leq 0.4$; 50% for 0.4–0.7) [29]. For straw-derived biochars, fixed-carbon contents approaching 70–75 wt.% are reported, and when translated into CO_2-

equivalent crediting under conservative permanence factors, sequestration potentials on the order of ~1.45 to 4.77 tCO_2-eq per tonne of biochar have been discussed [21], [29].

Beyond carbon storage, straw-derived biochar has a distinct agronomic and materials profile because slow pyrolysis concentrates much of the inorganic ash into the solid fraction. Wheat straw typically contains significant silica and notable alkali content (e.g., potassium), and these minerals largely remain in the char after pyrolysis [30], [33]—illustrated in figure 2.8. This concentration effect can be beneficial in land-application contexts because elements such as potassium and phosphorus can return to soils as plant-available nutrients, partially offsetting nutrient removal associated with straw harvesting [30]. At the same time, the inorganic/trace-metal profile constrains certain applications and motivates good feedstock handling (e.g., avoiding excessive soil contamination) if biochar is to be marketed for higher-value uses such as filtration media or precursor material for activated carbon [30]. The literature also notes a practical value-stacking logic. Revenue from biochar sales or climate-credit mechanisms can improve the resilience of BioSNG plant economics, especially where the fuel product competes with low-cost fossil natural gas [31].

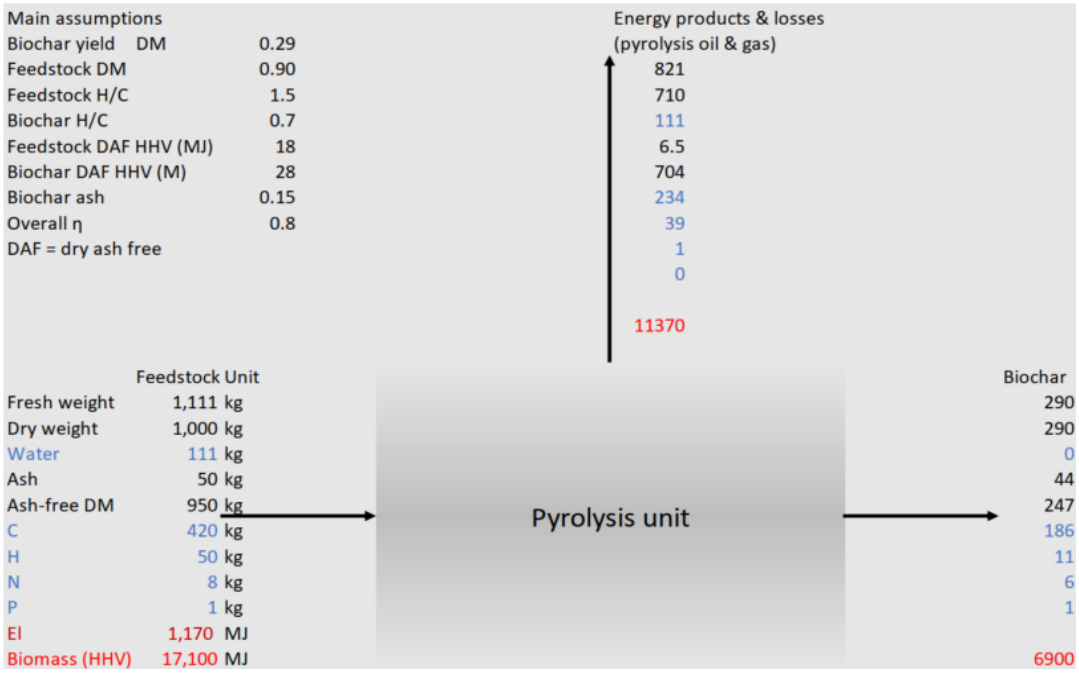

Figure 2.8: Stiesdal SkyClean A/S (2022) energy and mass balance for biochar production based on straw. Blue colour shows water and elements, and red colour shows energy. [29]

Table 2-4: Mass, energy, and carbon balance by conversion of 1 tonne of straw (Stiesdal SkyClean A/S, 2022). Energy as HHV. HHV for biochar, 28.26 MJ/kg; HHV for oil, 32.8 MJ/kg. [29]

Category	Stream	Mass balance (kg)	Mass balance (AR basis)	Mass balance (DM basis)	Energy balance (GJ)	Energy balance (%)	Carbon balance (kg C)	Carbon balance (%)
Input	Straw AR	1000	100%	—	16.5	100%	426	100%
Input	Straw DM	900	90%	100%	16.5	100%	426	100%
Input	Moisture	100	10%	11%	0.0	0%	0	0%
Output	Biochar	263	26%	29%	7.4	45%	189	44%
Output	Oil	107	11%	12%	3.5	21%	76	18%
Output	Gas	630	63%	70%	5.5	34%	161	38%

2.3.2. Reforming options, with emphasis on electrified/catalytic concepts

In an integrated pyrolysis-to-bioSNG pathway, the reformer is the unit that converts a chemically complex volatile stream (light gases plus oxygenates and tar-like species) into a methanation-suitable syngas—based on reactions in table 2-5—primarily by cracking higher hydrocarbons, reforming methane and light organics, and shifting the H_2/CO balance toward the stoichiometry required downstream [6], [27], [34]. From a system perspective, reformer "performance" is therefore not only a matter of high conversion, but also of delivering stable syngas quality under realistic feed variability while embedding manageable heat supply and integration opportunities within the overall plant [32].

A first high-level distinction is between thermal (non-catalytic) reforming and catalytic reforming. Thermal reformers rely on high temperatures (often up to 1300°C) to promote tar destruction and hydrocarbon cracking, typically inside refractory-lined chambers designed to withstand corrosive environments associated with alkali-laden biomass vapours [6]. While such high-severity operation can suppress persistent heavy tars, it generally requires substantial high-grade heat input and careful management of soot/carbon formation when steam availability is limited [20]. Catalytic reforming, in contrast, aims to achieve high carbon conversion and tar destruction at comparatively lower temperatures by leveraging active metal surfaces (commonly Ni-based), which can improve the effective hydrogen yield and reduce downstream conditioning effort by producing syngas with a more favorable H_2/CO ratio for methanation

[34]. However, catalyst durability becomes the central challenge because straw-derived vapours and aromatics promote coke formation and gradual deactivation if operating conditions are not carefully controlled [6], [26].

Table 2-5: Main reactions involved in the reforming of the volatiles derived from biomass and waste material. [28]

Bio-oil cracking	$C_nH_mO_k \rightarrow C_xH_yO_z + C_aH_b + CH_4 + CO + CO_2 + C$
Hydrocarbons (HCs) cracking	$C_nH_m \rightarrow CH_4 + C_aH_b + C$
Bio-oil steam reforming	$C_nH_mO_k + (n-k)H_2O \rightarrow nCO + \left(n + \frac{m}{2} - k\right)H_2$
Methane steam reforming	$CH_4 + H_2O \rightleftharpoons CO + 3H_2 \qquad \Delta H = 206{,}3 \text{ kJ mol}^{-1}$
HCs steam reforming	$C_nH_m + nH_2O \rightarrow nCO + \left(n + \frac{m}{2}\right)H_2$
Water gas shift (WGS)	$CO + H_2O \rightleftharpoons H_2 + CO_2 \qquad \Delta H = -41{,}2 \text{ kJ mol}^{-1}$
Interconversion	$C_nH_mO_k \rightarrow C_xH_yO_z$

Across both thermal and catalytic routes, the heat-supply concept is decisive. Heating can be provided via external combustion, indirect heat transfer through solids (e.g., sand or ceramic spheres), or direct electrical resistance, and the choice is closely tied to viable reactor configuration and achievable temperature uniformity [20]. Combustion-driven radiant heating can introduce steep temperature gradients, while electrically heated bodies can sustain tighter temperature tolerances, which is particularly valuable for preventing cold zones where tars may condense and initiate fouling [6], [20]. In practical reformers processing heterogeneous pyrolysis vapours, inlet gas maldistribution is a well-known risk factor that can create local cold regions and accelerate condensation-driven fouling, motivating design features such as staged injection points along the reactor length to distribute steam or CO_2 more evenly and stabilize reaction stoichiometry [27].

With respect to reaction environment, several reforming “modes” are reported in the literature—shown in figure 2.9. Partial oxidation (POX) converts hydrocarbons with limited oxygen into syngas via exothermic reactions, requiring no external heat. Catalytic partial oxidation (CPO) enhances POX using catalysts to improve selectivity and reduce temperature. Autothermal reforming (ATR) integrates POX with steam reforming, balancing exothermic and endothermic reactions to achieve thermal neutrality and flexible syngas composition control. Catalytic steam reforming (CSR) is often emphasized for biomass vapours because steam promotes hydrogen-rich syngas and helps suppress carbon laydown, but the steam-to-carbon ratio must be controlled for stabilizing catalyst surfaces under mixed oxygenate/aromatic loads, and to maintain integrity and suppress soot/coke formation under high-temperature service [6], [20]. Dry

reforming (with CO_2) can shift the product toward higher CO but typically yields lower H_2 unless hybridized with steam, and partial oxidation routes can simplify heat supply by generating heat internally but interact differently with downstream conditioning and electrolysis-based hydrogen supplementation [17], [27]. In all cases, the syngas H_2/CO ratio remains a critical quality variable. Off-stoichiometric syngas reduces methane yield unless compensated by hydrogen injection from electrolysis [34].

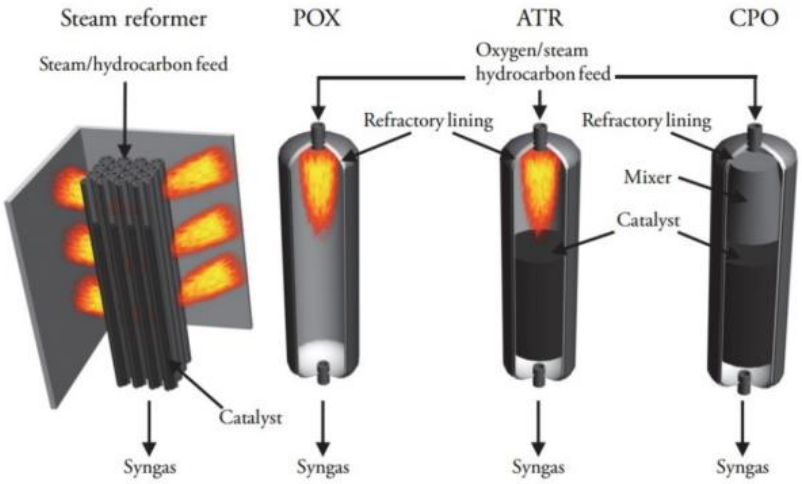

Figure 2.9: Illustration of most common reformer types. [6]

Within this landscape, electrified catalytic steam reforming (eCSR) —illustrated and compared with conventional types in figure 2.10— has received growing attention because it combines catalytic conversion with direct electrical heating of the reformer structure, enabling precise thermal control and shorter start-up time [20]. Electrified concepts are commonly discussed in connection with structured catalyst geometries, such as metal lattices, monoliths, or periodic open cellular structures (POCS), because these structures provide high geometric surface area while maintaining low pressure drop, and they can be heated directly by Joule heating through conductive supports (e.g., FeCrAl alloys) [6], [20]. Reported operating windows for electrically heated structured reformers are commonly in the range of 700–900°C (with S/C ratios of 4/6/8/10, and S/B ratios of 0.15-4), where high tar conversion is achievable while temperature uniformity reduces local condensation risks and hence mitigates coking initiation [6], [20]. In addition, electrified heating can shorten warm-up times and improve syngas quality consistency under load changes, which becomes relevant when reforming is coupled to intermittent renewable electricity and to electrolysis operation schedules [20].

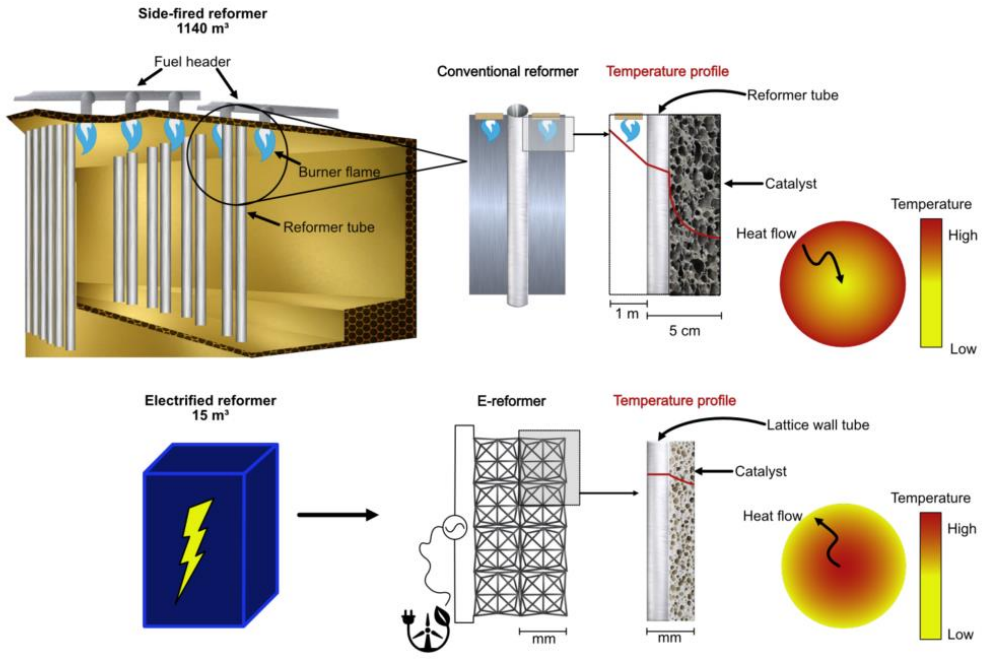

Figure 2.10: Conventional (fired) reformer vs electrified reformer. [6]

Reformer reactor configuration is an additional design dimension, because geometry governs residence time distribution, pressure drop, heat transfer, and catalyst lifetime. Literature highlights several viable options such as conventional packed beds (simple but susceptible to channeling and axial gradients), radial-flow fixed beds (reduced gradient effects), fluidized beds (excellent gas–solid contact and catalyst renewal but more complex solids handling), and structured catalysts such as monolithic honeycombs or additively manufactured POCS (good flow uniformity and favorable heat transfer) [28], [35]. In electrified reformers, the structured options are particularly attractive because they support embedded heating and enable segmented heating zones, e.g., higher-temperature upstream zones for heavy tar breakdown followed by downstream zones tuned for syngas adjustment without requiring multiple separate vessels [6]. These design choices are closely linked to the dominant deactivation mechanism in biomass volatile reforming, namely carbon deposition. Filamentous carbon growth and progressive encapsulation of Ni crystallites can reduce activity over time, and mitigation approaches include adjusting steam ratios and applying periodic oxidation/regeneration strategies during scheduled downtime [6], [27], [36].

Overall, the literature frames reformer selection as a multi-variable optimisation problem balancing (i) tar destruction and syngas quality stability, (ii) heat-supply strategy and temperature uniformity, (iii) pressure drop and integration proximity to downstream units, and (iv) long-term catalyst durability under straw-derived impurity and aromatic loads. Within that framing, electrified catalytic reforming is emphasized because it provides a controllable heat-supply mechanism compatible with renewable electricity integration, while structured catalyst designs can mitigate classical packed-bed limitations (cold spots,

maldistribution, and coking) that otherwise dominate operational risk in straw-volatile upgrading. In this setting, because the volatiles from the pyrolysis contain trace amounts of sulfur, it is important to use sulfur tolerant catalysts.

2.3.3. Electrolysis options (AEC vs. SOEC) and integration implications

Electrolysis is introduced in integrated BioSNG concepts primarily as a stoichiometric control lever. By supplying renewable H_2, the overall H_2/CO ratio entering methanation can be adjusted without relying exclusively on upstream shift chemistry or reformer retuning, thereby stabilising methane yield and product quality when biomass-derived syngas composition varies [3], [12], [34]. In practice, the choice of electrolyser technology is not neutral at plant level, because it affects not only electricity consumption but also the temperature level of recoverable (or required) heat, pressure integration, operational flexibility, and durability constraints over long campaigns (for 1 MWh electricity input, AEC produces 0.67 MWh H_2 (LHV) while SOEC produces 0.97 MWh H_2 (LHV) but requires 0.26 MWh heat) [3], [12]. Technology differences and their implications are illustrated and compared via figures 2.11, 2.12 and tables 2-6, 2-7.

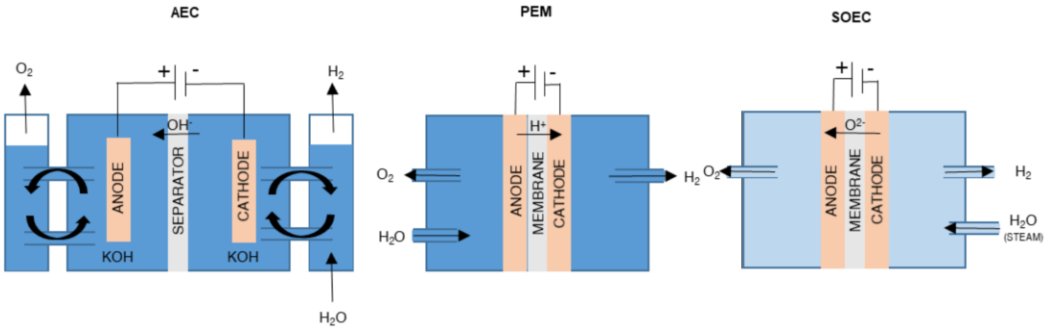

Figure 2.11: Stack-level schematic comparison of AEC, PEM, and SOEC highlighting key differences. [4]

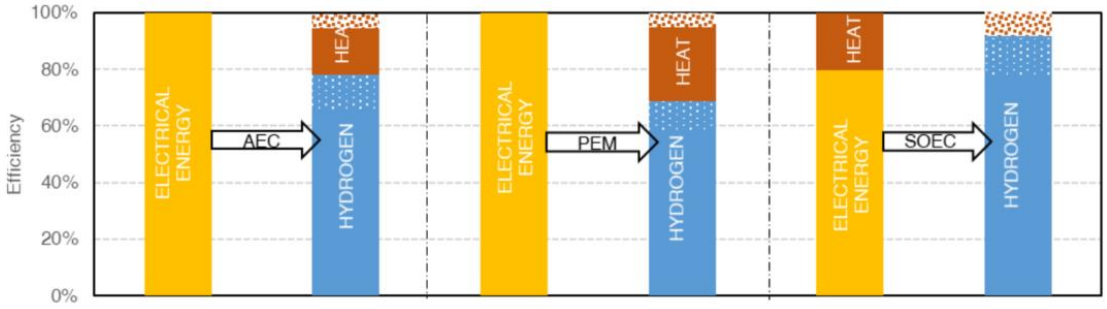

Figure 2.12: Efficiency comparison between AEC, PEM, and SOEC. Dotted orange bar is the heat loss while solid orange bar is the recoverable heat. Blue bars show the chemical energy of the hydrogen based on LHV (solid blue) and HHV (dotted blue). [3]

Alkaline electrolysis cells (AEC) represent the most established option and operate by transporting hydroxyl ions through an alkaline electrolyte (typically KOH/NaOH at roughly 25–40 wt.%), producing H_2 at the cathode and O_2 at the anode [14], [37]. Typical industrial AEC operating temperatures lie in the moderate range of 70–90°C, which reduces ohmic losses relative to ambient conditions without imposing the material challenges associated with high-temperature electrolysis [14], [37]. A practical advantage is the use of relatively abundant electrode materials (e.g., nickel-based catalysts and stainless steel alloys) and diaphragm-based separation, which supports comparatively cost-effective capacity deployment and long lifetimes in mature designs [14], [37].

Reported specific energy consumption values for industrial AEC operation are often in the range of 50 kWh per kg of H_2 under well-maintained conditions [8], [37]. From an integration standpoint, AEC systems can be operated pressurised (to several bar), reducing downstream compression demand before H_2 is blended into methanation feeds or injected into pressurised process networks, although this introduces mechanical constraints across diaphragms and cell assemblies [3]. Importantly for plant-wide heat integration, AEC operation rejects low-grade heat (in temperature range of 60–70°C) through the stack and auxiliaries (rectifiers, circulation loops, separators), typically at temperature levels aligned with district heating or other low-temperature uses (recoverable heat in the range of 0.16 MWh per 1 MWh electricity). The magnitude of this heat increases as electrochemical efficiency decreases, meaning stack ageing can simultaneously degrade electrical performance while increasing available waste heat [3]. Durability and operational robustness remain tied to water purity and electrolyte integrity; issues such as electrode passivation, diaphragm fouling, and carbonate scaling (if CO_2 enters the electrolyte circuit) are noted as relevant degradation mechanisms in integrated systems [34].

Table 2-6: Comparison of the energy balance between the electrolyser technologies for an input of 1 $MWh_{el.}$ [3]

Technology	Input: Electricity	Input: Heat	Output: Hydrogen	Output: Recoverable heat	Output: Heat loss
AEC	1 MWh	–	0.67 MWh (20 kg)	0.16 MWh	0.05 MWh
PEM	1 MWh	–	0.58 MWh (17 kg)	0.26 MWh	0.05 MWh
SOEC	1 MWh	0.26 MWh	0.97 MWh (29 kg)	–	0.1 MWh

Solid oxide electrolysis cells (SOEC) operate at high temperature (typically >600°C) and exploit oxide-ion conduction through a dense ceramic electrolyte (commonly YSZ) with Ni–YSZ fuel electrodes and mixed-conducting oxygen electrodes (e.g., LSM-type materials) [3], [12], [37]. At these temperatures, part of the reaction enthalpy can be supplied as heat, reducing the required electrical input; under effective heat

integration, electrical consumption can drop by roughly ~20% relative to low-temperature electrolysis, provided adequate high-grade heat is available to support steam electrolysis operation [3]. This makes SOEC particularly attractive when the broader plant has stable high-temperature heat sources. Literature emphasises that the steam feed should be superheated close to stack inlet temperature to minimise endothermic burden inside the cell and avoid cold spots, with candidate sources including sensible heat from hot reformer outlet streams, recovered methanation heat, and in some layouts even staged recovery from hot char/pyrolyser systems [3], [20], [31], [34]. SOEC integration can also benefit from operating at matched pressures with downstream synthesis units, thereby avoiding depressurisation–repressurisation cycles and reducing compression penalties. However, pressurisation must be balanced against sealing and mechanical reliability constraints for ceramic stacks [3]. Beyond steam electrolysis, SOECs can tolerate co-feeding of CO_2 and steam, enabling co-electrolysis to produce syngas directly and potentially bypass parts of conventional reforming requirements in BioSNG schemes [38]. High-temperature operation accelerates degradation mechanisms (e.g., Ni coarsening, component interdiffusion, thermal cycling damage), and tight control of temperature gradients is required. Engineering practice may limit stack temperature variation to very small values under steady operation to avoid mechanical stress and maintain durability [12]. Operational strategies such as moderating current density (e.g., using around 0.5 A/cm² rather than higher short-term test loads) are noted as approaches to extend lifetime while maintaining acceptable hydrogen production for integrated systems [39].

Taken together, these characteristics imply distinct integration consequences for BioSNG plants. AEC offers maturity, moderate-temperature operation, and meaningful low-grade heat recovery that can align with district heating, but it does not intrinsically exploit high-grade process heat to reduce electricity consumption. SOEC, in contrast, can reduce electricity demand by substituting part of the energy input with heat, but it introduces a stronger dependence on high-temperature heat-integration architecture and careful thermal management; it can therefore shift the plant's heat-integration priorities and may change the overall economic ranking depending on electricity price, available recoverable heat, and financing conditions [40].

Table 2-7: Comparison of AEC, PEM, SOEC including TRL, temperatures, efficiency, DH suitability. [14]

Technology	Technology readiness level (TRL)	Operation	Input	Output	Efficiency (including heat input)	Regulation ability	Expected technical lifetime	Relevant for district heating
AEC	9	65–90°C; 1–35 bar	Electricity; Water	Hydrogen; Oxygen; Heat	65% H_2 (LHV); 10% DH; 25% heat loss	Cold start: ~30 min; Warm: up: ~sec; down: ~mS (10–100%)	25 years	Yes
PEM	8–9	50–80°C; 1–50 bar	Electricity; Water	Hydrogen; Oxygen; Heat	64% H_2 (LHV); 10% DH; 26% heat loss	Cold start: <20 min; Warm: up/down: <1 sec (5–100%)	20 years	Yes
SOEC	7	>600°C; 1–10 bar	Electricity; Water; Heat (evaporation)	Hydrogen; Oxygen (Heat)	75% H_2 (LHV); 7% DH; 18% heat loss	Cold start: 12 timer; Warm: up/down: ~sec (0–100%)	10 years	To a lesser extent

2.3.4. Methanation fundamentals, multi-stage adiabatic operation, and heat recovery

Methanation converts the carbon oxides in biomass-derived syngas to methane via the reversible hydrogenation reactions:

$$CO + 3H_2 \rightleftharpoons CH_4 + H_2O$$

$$CO_2 + 4H_2 \rightleftharpoons CH_4 + 2H_2O$$

Both reactions are highly exothermic (standard reaction enthalpies at 298 K are strongly negative) [41], which means that large heat duties are released wherever high conversions are achieved. A useful rule-of-thumb is that the released heat can correspond to a significant fraction of the syngas chemical energy (on the order of ~20% of the LHV scale), which makes methanation simultaneously a thermal-management challenge and a central integration opportunity in BioSNG schemes [42]. From a thermodynamic standpoint, methanation reduces the total number of moles in the reacting mixture; therefore, higher pressure favours equilibrium conversion toward methane (Le Chatelier), and pressurised operation is commonly used to push equilibrium and reduce downstream compression needs [43], [44]. Conversely, higher temperature disfavors equilibrium methane yield even though kinetics will improve; for CO methanation, equilibrium calculations show that increasing temperature reduces achievable methane mole fraction at constant pressure, motivating staged cooling if higher-temperature beds are used to overcome activation barriers [44]. Different methanation concepts are illustrated in figure 2.13.

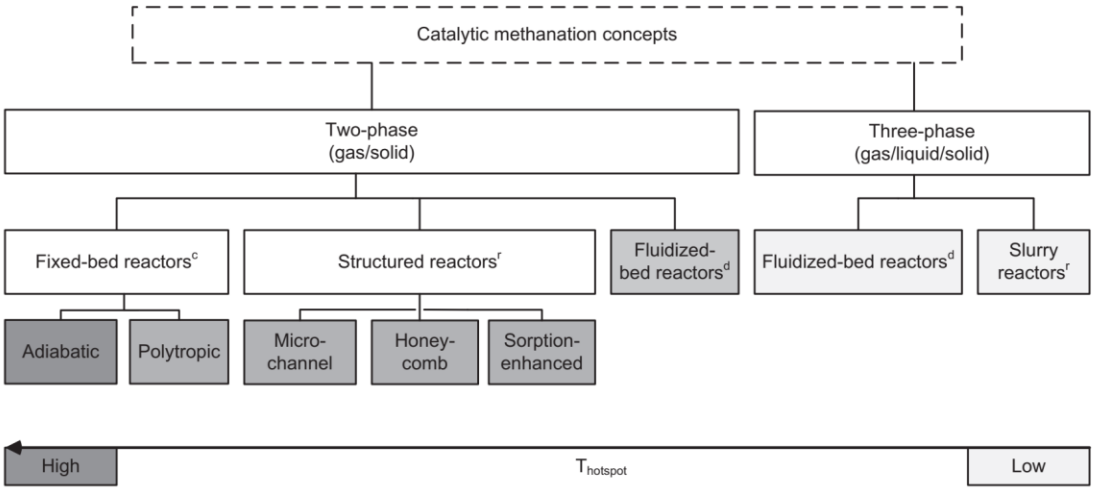

Figure 2.13: Overview of different methanation concepts; commercial (c), demonstration (d), research (r). [44]

These thermodynamic characteristics translate directly into the common industrial design choice of multi-stage adiabatic methanation with intercooling [44]. Under near-stoichiometric feeds, adiabatic beds can experience sizeable temperature rises (several hundred degrees), which pushes the reactor toward less favourable equilibrium conditions and accelerates deactivation risks such as sintering and carbon deposition on Ni-based catalysts [36], [43]. Multi-bed adiabatic arrangements with intermediate cooling steps—illustrated in figure 2.14— are therefore widely implemented to keep each stage within a practical operating window, preserve catalyst integrity, and sustain high methane selectivity—evident in table 2-8—over long campaigns [36]. The need for thermal moderation is further reinforced by kinetic and surface effects in co-methanation. Experimental evidence indicates that CO preferentially adsorbs on Ni active sites over CO_2 even at low CO fractions (around 1 mol.%), which can suppress CO_2 conversion relative to purely thermodynamic expectations and makes staged operation and tailored temperature profiles relevant for achieving robust overall conversion [43]. In addition, methane itself becomes a liability at elevated temperatures; above roughly 400°C, methane cracking can contribute to solid carbon deposition, with the risk becoming notable in temperature windows that can occur locally in adiabatic beds without adequate cooling or dilution [43], [45].

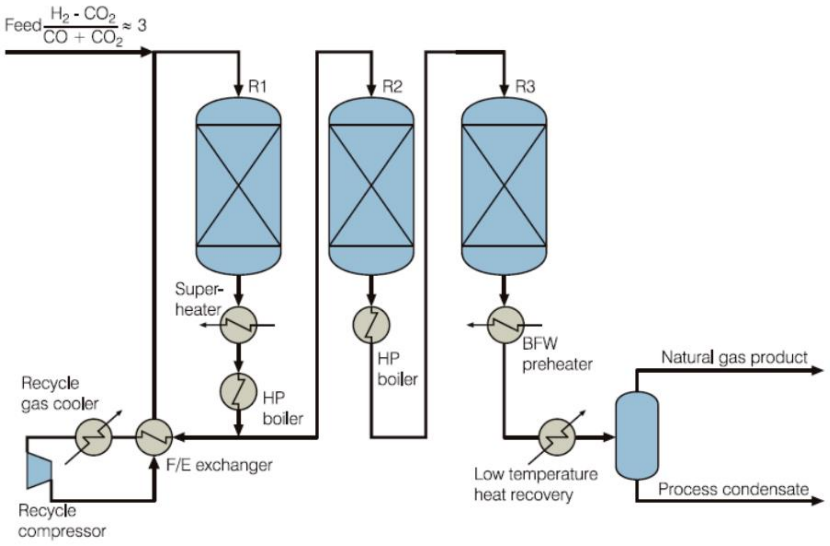

Figure 2.14: Flow sheet example of Haldor Topsøe TREMP methanation technology (2009). [7]

Table 2-8: Typical TREMP BioSNG product composition and impurity levels relative to grid limits. [7]

Producer gas component (mole %)	**TREMP average product**
CH_4	94–98
CO_2	0.2–2
H_2	0.05–2
CO	< 100 ppm
N_2 + Ar	2–3
HHV, MJ/Nm³	37.4–38.4

Intercooling between adiabatic beds can be implemented either as direct quenching or indirect heat exchange. Direct quenching (e.g., by mixing with cool recycle gas or injecting steam) can rapidly reduce temperature but introduces dilution effects that reduce reactant partial pressures; therefore, the mass balance must ensure that hydrogen remains sufficient for the desired per-pass conversion after mixing [46]. Steam quenching can additionally influence internal equilibria via water–gas shift activity, potentially supporting H_2 formation when outlet ratios are marginal [8], although excessive steam increases volumetric flow and cooling duty [46]. Indirect intercooling through heat exchangers provides tighter temperature control without changing composition, and it is commonly used to recover sensible heat into boiler feedwater or district-heating loops [32], [46]. Practical design rules-of-thumb highlighted in the literature include

limiting the outlet temperature rise per bed to avoid runaway behaviour and hotspot-driven deactivation, with the exact threshold depending on inlet composition and the relative shares of CO and CO_2 conversion [46].

The thermal release from methanation is therefore not treated merely as a penalty to be removed; it is frequently framed as a resource to be harvested through purposeful heat recovery design. Literature discussions indicate that roughly 20–25% of the chemical energy in the syngas feed can emerge as surplus thermal energy in product gas streams, and that this fraction can meaningfully displace external utilities in endothermic units (e.g., reforming or pyrolysis) if recovered through a matched heat exchanger network [47]. Intercoolers become prime interfaces for recovery because they already exist for temperature control; designing them as dual-purpose exchangers enables transfer of heat into useful circuits, such as steam generation for catalytic steam reforming (~2560 kcal per Nm³ SNG heat evolved and ~3.2 kg HP steam at ≈100 bar g / 540°C produced per Nm³ SNG, theoretically) [32], [41]. This integration logic strengthens in electrified configurations. When reforming heat is supplied electrically rather than by combustion, recovered methanation heat can offset electric heater duty (via steam preheating) and reduce plant-wide electricity draw [20]. Likewise, when SOEC is integrated upstream, recovered heat at suitable temperature levels can support steam generation to the electrolyser, thereby reducing the electrical burden associated with preparing high-temperature steam feeds and improving net electrical utilisation at the plant level [12], [16], [38].

Finally, methanation heat recovery links naturally to district heating in Danish system settings. Intercooler heat can be routed into municipal networks where temperature levels and offtake conditions permit, replacing fossil-derived heat and creating an additional revenue stream [14]. Because the thermal profile differs by bed position (early beds generally delivering higher-grade heat and later beds delivering mid-grade heat) selective routing (high-grade to endothermic chemical duties; mid-grade to district heating or feed preheating) is discussed as a way to maximize utilisation rather than blending into a single mixed stream that cannot satisfy higher-temperature needs [32], [41]. The same logic can be extended to other upstream sections (e.g., maintaining hot-gas filtration temperatures for tar cracking or supporting biomass drying) when materials and fouling constraints are managed appropriately [6], [18]. Overall, staged adiabatic methanation is best understood as a tightly coupled unit within the broader BioSNG plant. It is simultaneously the final chemical upgrading step, a dominant source of recoverable heat—evident by figure 2.15, and a unit whose operability depends on careful management of stoichiometry, temperature rise, and catalyst protection mechanisms.

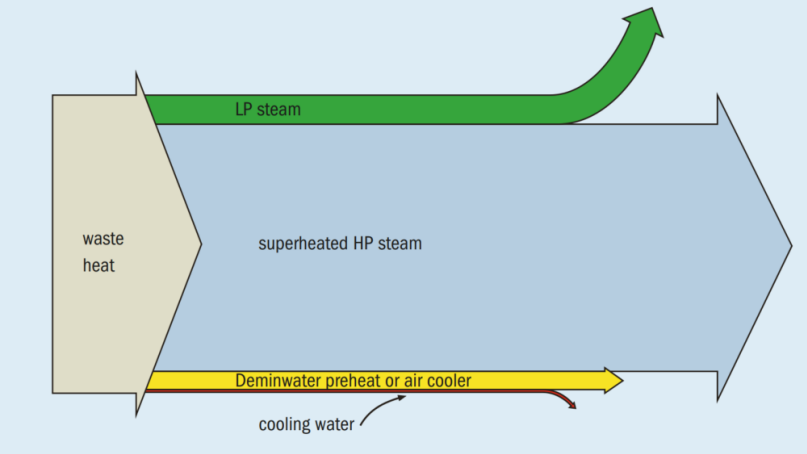

Figure 2.15: Typical heat recovery in TREMP unit. [41]

2.4. Heat integration and export potential

Heat integration is a central design lever in integrated BioSNG plants because the process inherently couples strongly endothermic sections (e.g., pyrolysis/reforming duties and, in the SOEC case, high-temperature steam preparation) with strongly exothermic sections (most notably multi-stage methanation). When these hot and cold demands are treated in isolation, the plant risks simultaneously rejecting valuable heat in coolers while purchasing external utilities to satisfy heating duties elsewhere. Conversely, a deliberately integrated heat-exchanger network can recycle a significant fraction of internally available heat, reduce external utility reliance, and improve both overall efficiency and levelized production cost [16], [32].

A common and transparent way to evaluate plant-wide heat integration potential is composite curve (pinch) analysis, where all hot and cold process streams are aggregated and plotted as enthalpy–temperature profiles after imposing a minimum approach temperature (ΔT_{min}). This provides a graphical identification of the pinch point and clarifies (i) how much heat can be internally recovered, (ii) where external heating/cooling utilities remain necessary, and (iii) which temperature intervals host the most valuable match opportunities [16]. In integrated BioSNG configurations, literature examples show that when ΔT_{min} is set in the order of 5–20 K, meaningful overlap often emerges between methanation exotherms (e.g., in the 200–350°C range) and cold demands such as steam generation for reforming or preheating duties, enabling cross-integration without intermediate utilities [32], [34]. The same analysis also reveals that if most surplus heat lies at temperature levels that do not overlap with process cold demands, the surplus cannot be fully exploited, at

least without additional technologies (e.g., heat pumps) to lift low-grade waste heat to usable levels [12], [34].

Beyond identifying “where the heat is,” the practical implementation is typically discussed in terms of internal heat recovery loops. These loops transfer sensible (and where relevant, latent) heat from donor streams (such as methanation intercoolers, char cooling, or hot reformer-related streams) into upstream consumers such as pyrolysis heating, feed preheating, or steam generation for reforming and electrolysis. Designing such loops with appropriate heat-transfer media (pressurised water for mid-grade uses; thermal oils for higher-grade requirements) reduces dependence on purchased utilities and improves resilience against variability in both feedstock conditions and renewable-energy availability [16], [31], [32]. A key point in the literature is that technology choice reshapes the “cold composite” and thus the integration topology: swapping AEC for SOEC changes the temperature level and magnitude of cold demands, and SOEC benefits disproportionately from matching with mid-to-high grade heat sources due to its elevated inlet-temperature requirements [12].

After internal heat demands are satisfied, any remaining surplus heat can be treated as an export opportunity, most notably through district heating (DH) in a Danish context. In a 20MW hydrogen production case study, district heating integration increased operation hours from 4,150 to 4,950 h/y, boosting hydrogen output and revenue, illustrated in figure 2.16. The rationale in this work is that methanation releases substantial heat at temperature grades compatible with many DH systems. Many modern Danish networks operate with delivery setpoints typically ~70°C (DKK 150/MWh in summer and DKK 200/MWh in winter) [14], [21]. Supply temperatures as low as ~35°C are also cited, which would require a heat pump and can result in much lower prices. The most natural extraction points are the intercoolers between methanation beds, which already exist to control catalyst temperature rise; these exchangers can be designed for dual duty by transferring heat into a hydronic DH circuit while maintaining process-side temperature control [14], [21].

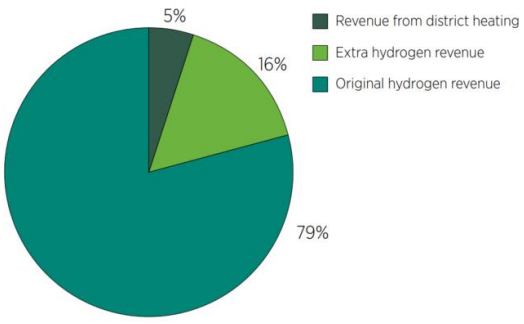

Figure 2.16: District heating adds heat revenue, making more hours profitable. [14]

However, DH export is not “free value” and must be evaluated as a system trade-off. Exporting too aggressively can, in some situations, create deficits in internal cold-duty coverage (visible directly on composite curves when external service streams are included), and therefore may reduce overall fuel-production efficiency if internal duties must then be met with purchased utilities [32]. Consequently, the literature emphasizes that higher-grade surplus should first satisfy internal process needs (e.g., steam generation or high-temperature preheating) before tempering down to DH delivery levels, ensuring the methane-production objective remains primary while surplus is monetised as heat [14], [32].

Practical DH integration also introduces constraints that are often decisive in real projects. First, hydraulic separation between process fluids and network water is essential, typically via plate or shell-and-tube exchangers, because process-side streams may carry moisture and trace contaminants that must not contact public DH water circuits [6]. Second, materials compatibility matters. Straw-derived gases and trace species can promote corrosion (e.g., alkali chlorides), motivating corrosion-resistant alloys/coatings and maintenance regimes that preserve heat-transfer effectiveness over long campaigns [6]. Third, viability is highly sensitive to geographic siting and if plants are located near feedstock collection points rather than population centers, the capital cost and losses associated with insulated pipeline installation can be a major barrier, pushing designs toward co-location with existing network nodes or energy parks —shown in figure 2.17 [9]. Finally, DH demand is seasonal, whereas chemical synthesis is often baseload; bridging this mismatch may require thermal storage (buffer tanks) or alternative heat sinks during low-demand periods, and off-take agreements often need flexibility clauses to manage variability and maintenance downtime [14].

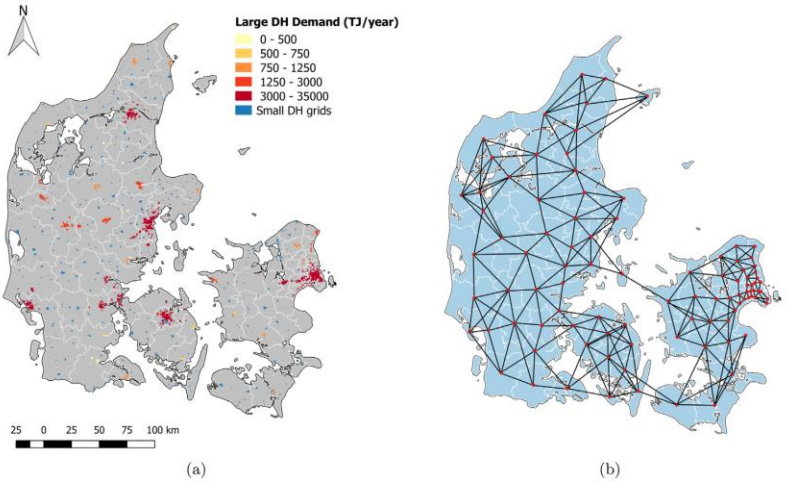

Figure 2.17: Geographical representation in Balmorel-OptiFlow; district heating networks in Denmark (a) and geographical areas for biomass collection with transport links (b). [9]

3. Process Description and System Boundaries

In this thesis a renewable-assisted pathway for producing grid-quality bio-synthetic natural gas (bioSNG) from biomass is evaluated in terms of energy and economics. The studied plant concept is based on slow pyrolysis of wheat straw, followed by gas upgrading via reforming and methanation, where additional renewable hydrogen is supplied through electrolysis to reach the stoichiometry required for high methane yield. The facility is modelled at steady state and at nominal load, with a biomass thermal input of 31.4 MW_{th} (LHV basis, dry biomass).

The plant converts biomass into two main product categories:

1. bioSNG (product gas intended to meet Danish gas grid requirements), and
2. co-products comprising biochar and exportable heat intended for district heating.

The overall process can be divided into four interacting subsystems:

- (S1) *Pyrolysis*: conversion of wheat straw to biochar + pyrolysis volatiles
- (S2) *Reforming*: catalytic conversion of volatiles into permanent gases (reformer syngas)
- (S3) *Electrolysis*: production of renewable H_2 (and O_2 as a by-product)
- (S4) *Methanation*: catalytic conversion of reformer syngas + H_2 into bioSNG

3.1. Feedstock Characterization

The biomass feedstock is wheat straw pellets with 8 wt% moisture content. The total mass flow is 2.00 kg/s, which is represented for modelling convenience as:

- Dry biomass: 1.84 kg/s
- Moisture: 0.16 kg/s (treated as water/steam)

The inherent moisture is necessary to ensure that sufficient steam is available in downstream high-temperature reforming step. The ultimate analyses used in this work, together with other characteristics of biomass and biochar are represented in the table 3-1. Sulfur and chlorine content are neglected.

LHV values for biomass and biochar are calculated from the reference HHVs by subtracting the latent heat associated with the water formed from hydrogen in the fuel:

$$LHV_{dry} = HHV_{dry} - h_{vap} \cdot 9H_{dry}$$

where:

- h_{vap} is the enthalpy of vaporisation of water (2.42 MJ/kg),
- H_{dry} is the mass fraction of hydrogen in the dry fuel (from ultimate analysis),
- the factor 9 represents the mass of water formed per unit mass of hydrogen

Table 3-1: Summary of feedstock characterization used in process modelling.

Parameter	Assumed value
Feedstock	Wheat straw pellets
Total mass flow	2.00 kg/s
Moisture content	8 wt%
Dry biomass mass flow	1.84 kg/s
Moisture (water) mass flow	0.16 kg/s
Biomass Ultimate analysis (dry, wt%)	C 47.3; H 5.64; O 41.24; N 0.67; Ash 5.15
Biochar Ultimate analysis (dry, wt%)	C 71.8; H 2.85; O 7.5585; N 0.1315; Ash 17.66
Biomass HHV (dry)	18.3 MJ/kg_{dry}
Biochar HHV (dry)	28.26 MJ/kg_{dry}
Biomass effective c_p (dry)	1.35 kJ/(kg_{dry}·K)
Biochar effective c_p (dry)	1 kJ/(kg_{dry}·K)
Biomass thermal input (LHV, dry)	~31.4 MW_{th}
Biomass LHV (dry, calculated)	17.06 MJ/kg_{dry}
Biochar LHV (dry, calculated)	27.63 MJ/kg_{dry}
reference: personal communication	

3.2. Process Definition

3.2.1. Subsystem S1: Pyrolysis

Slow pyrolysis is the primary thermochemical conversion step, transforming wheat straw into:

- a solid carbonaceous fraction (biochar) and
- a volatile fraction consisting of pyrolysis vapours and permanent gases.

The reactor, illustrated in figure 3.1, is inspired by the Stiesdal SkyClean technology operating regime, with a characteristic peak temperature around 550°C and outlet gas temperature around 350°C [48]. Pyrolysis process needs heat; in the SkyClean technology, a fraction of the pyrolysis volatiles is compressed, heated to peak temperature, and recirculated to meet the process heat demand. In this work, pyrolysis is treated as a conversion step with defined yields and elemental partitioning, while the thermal demand of heating the feed to peak temperature is accounted for through explicit energy balances and process heating duties.

Performance data for the reference slow pyrolysis concept suggests a mass yield of approximately 29% biochar and 71% volatile products on dry feed basis. The present work adopts a biochar mass yield of 0.291 kg biochar per kg dry biomass, leaving 0.709 kg/kg as volatile products. Because the char is carbon-rich and, unlike the volatile fraction, has a relatively high LHV, the energy content of the biomass is

approximately evenly split between char and volatile products, each representing roughly half of the input thermal power.

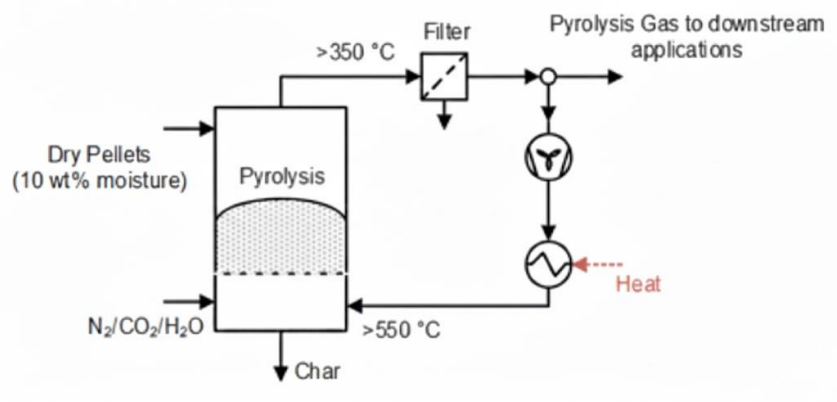

Figure 3.1: Stiesdal SkyClean pyrolysis. [48]

Using the biomass and biochar ultimate analyses and the fixed char yield, the remaining constituents of the biomass are assigned to the volatile fraction, shown in table 3-2. This approach ensures elemental consistency across the full plant model. It is important to note that, based on the referenced ultimate analyses, we assume all ash is retained in the biochar; accordingly, the pyrolysis volatiles are considered completely ash-free.

Table 3-2: Pyrolysis yield and elemental split per kg dry biomass.

Component Yield	**Value**
Biochar yield (kg/kg)	0.291
Volatile fraction (kg/kg)	0.709
• Elements remaining in volatile fraction (kg/kg): C	0.264
• Elements remaining in volatile fraction (kg/kg): H	0.0481
• Elements remaining in volatile fraction (kg/kg): N	0.00632
• Elements remaining in volatile fraction (kg/kg): O	0.390

These values provide the basis for constructing the pyrolysis volatiles stream as an internally consistent mixture of species prior to the subsequent reforming stage. In reality, the volatile stream includes condensables (tars) and light hydrocarbons. In this work however, such species are not included explicitly as final products of pyrolysis; instead, their presence is represented by the overall elemental distribution to the volatile stream and the subsequent conversion of that stream in reforming stage. For simplicity, tar proxies are not modeled.

3.2.2. Subsystem S2: Reforming and syngas conditioning

Illustrated in figure 3.2, using an electrified catalytic reformer (e-reformer) the volatile products of the pyrolysis can be upgraded into a synthesis gas suitable for methanation [20]. In this work, the reformer is assumed to be fully electrified and powered by renewable electricity. Reforming assumes the catalytic cracking and conversion of condensables and hydrocarbons to H_2, CO, CO_2, H_2O, CH_4, N_2. It is treated as a high-temperature equilibrium-limited conversion step, with pressure drop neglected and operating pressure at 1 bar. Additionally, the reforming stage is assumed to proceed without accounting for solid carbon formation. Simplified Chemistry can be represented via the reactions below:

Steam methane reforming (SMR)	$CH_4 + H_2O \leftrightharpoons CO + 3H_2$	$+ 206\ \mathrm{kJ/mol}$
Water gas shift (WGS)	$CO + H_2O \rightleftharpoons CO_2 + H_2$	$- 41\ \mathrm{kJ/mol}$
Overall (SMR + WGS)	$CH_4 + 2H_2O \rightleftharpoons CO_2 + 4H_2$	$+ 165\ \mathrm{kJ/mol}$

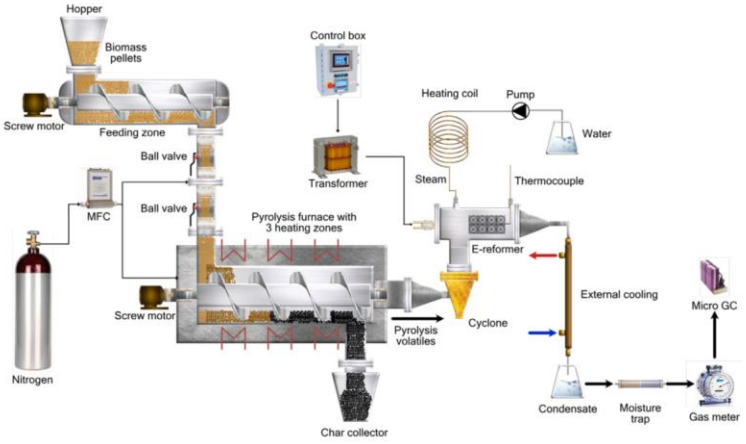

Figure 3.2: Experimental setup from Caballero et al., consisting of a pyrolysis furnace and the e-reformer. [20]

It is important to note that, based on these reactions, the reformer syngas composition is strongly influenced by the amount of steam present in the reformer. In this work, the steam input is assumed to be constant and equal to the inherent moisture of the biomass; no additional steam is supplied to the reformer. The hot reformer outlet (800°C) provides an opportunity for thermal integration and preheating the inlet. Though, a minimum approach temperature of ΔT_{min} = 30°C (gas–gas) is adopted as the heat exchanger design constraint and the inlet is thus preheated to 770°C before entering the reformer. After reforming, the wet reformer syngas is cooled to near ambient temperature to enable condensation and drying. The dry reformer syngas is then compressed to the methanation design pressure of 10 bar. Compressor isentropic and mechanical efficiencies are assumed 90% and 98% respectively.

3.2.3. Subsystem S3: Electrolysis

Hydrogen addition is required to adjust the reformer syngas to the suitable stoichiometric conditions for high methane yield and grid-quality SNG. The plant concept therefore integrates a renewable electricity-driven electrolyser producing H_2 at the same delivery pressure as the methanation feed.

Two electrolysis technologies are evaluated:

- Alkaline electrolysis cells (AEC)
- Solid oxide electrolysis cells (SOEC)

The electrolysis subsystem is treated as an electricity-to-hydrogen converter with an overall efficiency parameter and, where relevant, recoverable thermal streams. Chemistry is simply represented via water splitting:

$$2H_2O \rightleftharpoons 2H_2 + O_2 \qquad +286\,\text{kJ/mol}$$

For AEC, as illustrated in figure 3.3, liquid water at 20°C is pressurized to 10 bar, prior to entering the electrolyser. The electrolyser is set to operate at 10 bar and 80°C, producing hydrogen and oxygen. An overall electrical efficiency is assumed 67.5%. Electrolysis produces heat due to ohmic effect, which should be removed to maintain constant temperature. This is done by cooling and recirculating a fraction of the water. In this work, the difference between the reaction enthalpy and the actual electrical input (calculated using the electrical efficiency) is treated as low-grade heat available for recovery (e.g., district heating).

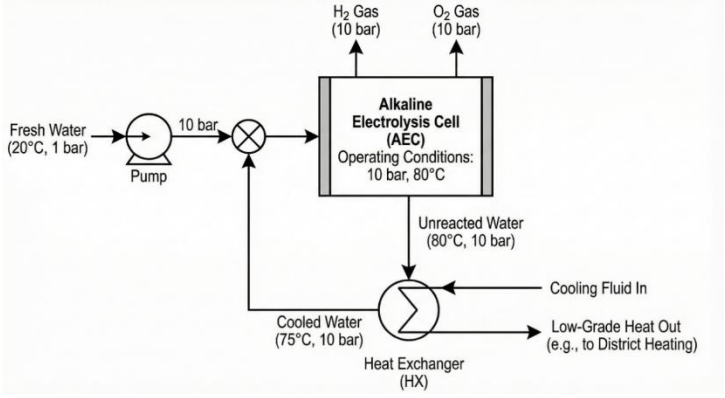

Figure 3.3: AEC subsystem overview.

For the SOEC, steam is supplied at 650 °C and 10 bar, and electrolysis is performed at 700 °C. in the case of SOEC, an overall electrical efficiency of 80% is assumed. In contrast to AEC, except for the recoverable waste heat from outlet hydrogen and oxygen streams, no recoverable waste heat directly from SOEC stacks is assumed. On the other hand, the heat required to generate the steam feed is assumed to be met through

integration with available high-temperature heat sources within the plant, thereby minimising the need for additional external heating.

3.2.4. Subsystem S4: Methanation and product conditioning

Methanation converts the reformer syngas, together with renewable hydrogen, into a methane-rich product gas. Illustrated in figure 3.4, the methodology adopts a multi-step, adiabatic fixed-bed concept inspired by industrial TREMP-type configuration [41][49], with:

- A recycle of the first step product gas (temperature control)
- inter-stage cooling (heat recovery)
- water condensation before the last step (drying)

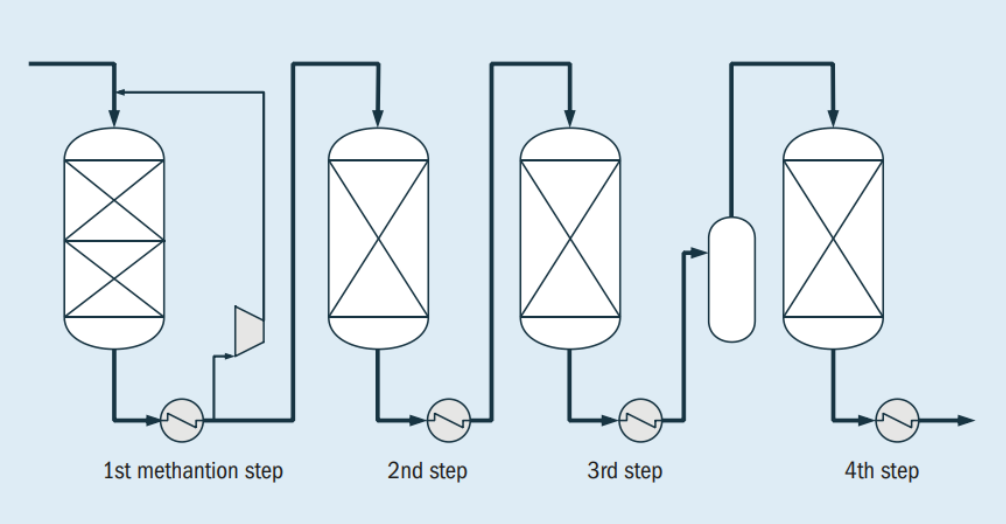

Figure 3.4: The Haldor Topsøe TREMP™ methanation process. [41]

Operating pressure is assumed 10 bar in this work (neglecting any pressure drop), and based on the reference, operating temperatures can span 200–700°C, without damaging the catalysts. Temperature control is critical due to the strongly exothermic nature of methanation reaction. Thus, a recycle of product gas to the first step inlet is included at the process model to control the maximum reactor outlet temperature (to remain below ~690°C). The methanation chemistry is captured through the following reactions:

CO methanation:	$CO + 3H_2 \rightleftharpoons CH_4 + H_2O$	-206 kJ/mol
CO_2 methanation (Sabatier):	$CO_2 + 4H_2 \rightleftharpoons CH_4 + 2H_2O$	-165 kJ/mol

Because these reactions are strongly coupled, the methanation outlet composition depends on inlet stoichiometry. To ensure high methane yield and avoid hydrogen deficiency, the inlet gas composition is targeted using the stoichiometric number/ syngas module commonly used for methanation feeds:

$$\mathrm{SN} = \left(n_{H_2} - n_{CO_2}\right)/\left(n_{CO} + n_{CO_2}\right)$$

A target of SN = 3 is imposed in modelling, consistent with typical requirements for high methane yield when both CO and CO_2 are present. The feed water rate to electrolyser, and consequently hydrogen mass flow rate, is adjusted to achieve this target module at the methanation inlet. The de-watered and dry product stream is expected to exceed 95% methane with minor residual hydrogen, nitrogen, and carbon dioxide. The product is assumed to comply with Danish grid specifications for synthetic natural gas.

The integrated process model is summarized in table 3-3. Pressure drops are neglected throughout the whole process.

Table 3-3: Key operating assumptions by subsystem (process summary).

Subsystem / unit	Key assumptions
Pyrolysis	T ≈ 550°C; 1 bar; biochar yield 0.291 kg/kg; heat loss neglected
Reforming	Equilibrium-limited; 1 bar; 800°C (catalytic); ΔT_{min} 30°C for gas–gas heat recovery; powered by renewable electricity
Reformer Syngas compression	1 → 10 bar; η_{is} = 90%; η_{mech} = 98%
Electrolysis (AEC)	80°C; 10 bar H_2 delivery; overall electrical efficiency 67.5%; low-grade heat potentially recoverable
Electrolysis (SOEC)	~700°C; 10 bar H_2 delivery; superheated steam fed at 650°C; overall electrical efficiency 80%; requires high-temperature heat integration
Methanation	Multi-stage, catalytic, adiabatic fixed beds; 10 bar; ~200–700°C; inter-stage cooling and water removal; module M ≈ 3 at inlet

3.3. Aspen Plus modelling and implementation

3.3.1. Thermodynamic property methods and component list

A single consistent thermodynamic framework is used for conventional components in the gas and liquid phases. The Peng–Robinson equation of state with *Boston–Mathias modification (PR-BM)* is selected as the global property method to represent phase equilibria and enthalpy for the conventional species. The *conventional* component set includes:

- H_2, CO, CO_2, CH_4, H_2O, N_2, O_2, NH_3

Solid biomass, biochar, and ash are treated as *non-conventional solids*. Their properties (enthalpy and density) are set to be calculated using standard Aspen correlations:

- *HCOALGEN* for enthalpy

- *DCOALIGT* for density

Non-conventional component attributes are assigned in section *Pure Components* (HCOMB as higher heating value and CP2C as heat capacity). Ultimate analyses of biomass and biochar are later implemented in *simulation* environment.

3.3.2. Pyrolysis implementation

Because biomass is defined as a non-conventional component, Aspen Plus requires an initial decomposition of the feed into conventional species before any equilibrium calculations can be performed. Pyrolysis is therefore represented using a conceptual two-step reactor hierarchy, shown in figure 3.5 (noting that, physically, pyrolysis occurs within a single reactor):

- Yield-based decomposition reactor (RYield; DECOMP): converts the non-conventional biomass into conventional constituents and a solid biochar fraction according to the prescribed elemental split. The heat released in this block is evaluated from the biomass higher heating value (HHV) specified for the feed.
- Gibbs-equilibrium reactor (RGibbs; RECOMB): receives the decomposed volatile constituents and recombines them to the equilibrium distribution of a set of gas species, energetically balanced according to the heat released in the previous reactor.

To ensure that the calculated heat effect is attributed solely to reaction chemistry (and not to sensible heating), both reactors are specified at the feed conditions (20 °C and 1 bar). This constraint prevents any portion of the reaction heat (derived from the HHV-based heat calculation) from being consumed in raising stream temperature within the reactor blocks. Such a reaction is considered balanced; heat is released from decomposition, and is simultaneously absorbed to recombine the elements.

Moisture is treated explicitly as a separate stream, bypassing both reactor blocks, and avoiding participation in the decomposition and equilibrium reactions. It is subsequently recombined with the equilibrium pyrolysis gas downstream to form the final wet “pyrogas” stream.

The solid biochar is separated from the volatile products using a separator block. To reflect the actual operating condition of the pyrolysis unit, all relevant product streams (biochar, volatiles, and the bypassed moisture stream) are heated to the peak pyrolysis temperature (550 °C) using dedicated heater blocks. The individual heater duties are then aggregated to obtain the total thermal requirement of the overall pyrolysis process, enabling transparent extraction of pyrolysis heat demands for the subsequent plant-wide energy integration and techno-economic analyses.

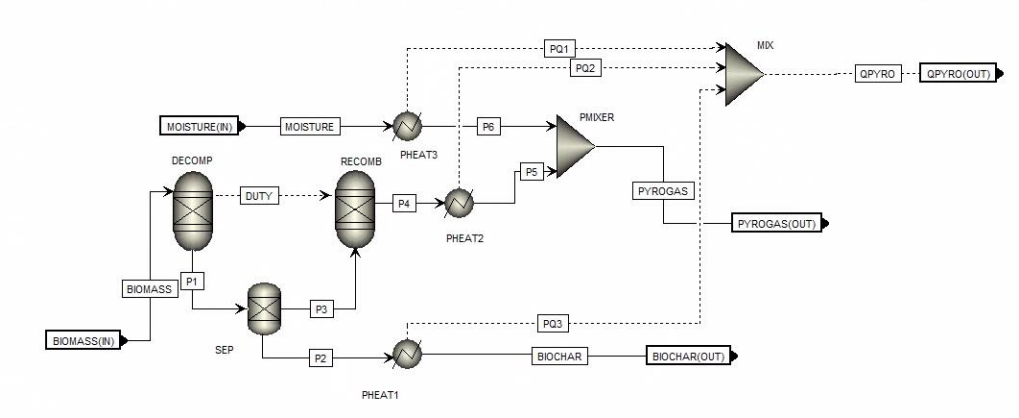

Figure 3.5: Pyrolysis hierarchy in Aspen Plus.

To represent how process heat would be supplied to the pyrolysis unit in a real plant, the total thermal demand calculated previously is mapped to a dummy heat exchanger block outside the hierarchy in the main flowsheet. In practice, this heat would be delivered by heating a recycled fraction of the volatile stream from approximately 350 °C (pyrolysis outlet) back to 550 °C and recirculating it to provide the required heat input.

Accordingly, such dummy exchanger, shown in figure 3.6, is configured to impose the same temperature lift (350 → 550 °C) while delivering the assigned duty (2.91 MW in our case). The identity of the working fluid in this exchanger is intentionally non-physical; only the heat duty and temperature increase are required for plant-level energy accounting. A design specification is therefore used solely to adjust the dummy stream flow rate so that the exchanger achieves the specified outlet temperature at the imposed duty. This approach makes the pyrolysis heat demand explicit in the flowsheet and enables simplified integration with the overall heat and utility balance.

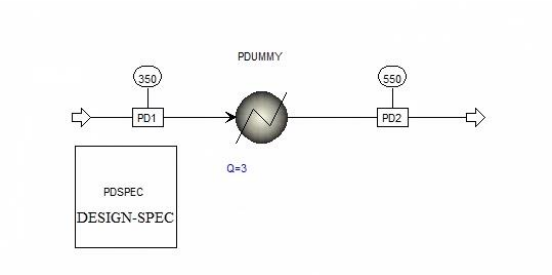

Figure 3.6: Pyrolysis heat integration in Aspen Plus.

3.3.3. Reforming implementation

Reforming is modelled using a RGibbs reactor operating at 800°C and 1 bar, allowing the conventional component set (H_2, CO, CO_2, CH_4, H_2O, N_2) to reach equilibrium. A heater is set to preheat the inlet flow

to the reformer to 770°C, while the outlet flow, wet reformer syngas, is then cooled to near ambient temperature and the water is removed using a flash separator. Compression to 10 bar is implemented using a compressor block with predefined efficiencies.

3.3.4. Electrolysis implementation

The alkaline electrolysis cell is modelled as a dedicated Aspen Plus hierarchy, shown in figure 3.7. Feedwater at 20 °C and 1 bar is first pressurised to 10 bar using a pump, and is then routed to the hierarchy. The hierarchy provides three outputs: a hydrogen product stream (H_2), an oxygen by-product stream (O_2), and a heat stream (QELEC) representing the net heat that must be removed from the electrolysis block.

Within the hierarchy, electrolysis is represented using an RStoic reactor operated at 80 °C and 1 bar, based on the water-splitting reaction. The reactor computes the reaction enthalpy associated with this stoichiometric conversion. A downstream separator splits the gaseous products into hydrogen and oxygen; oxygen is treated as a waste by-product, while hydrogen at 10 bar is exported as the product stream to be mixed with dry reformer syngas.

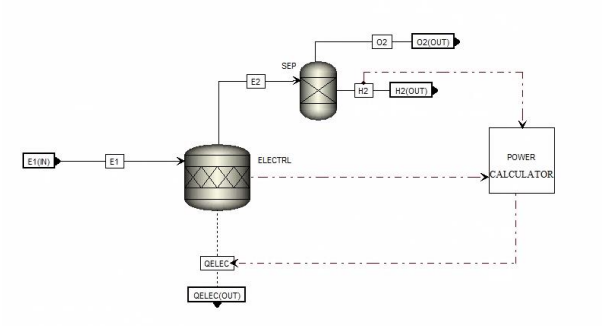

Figure 3.7: Alkaline electrolysis cell hierarchy in Aspen Plus.

Because Aspen's RStoic block does not intrinsically translate reaction enthalpy into electrical power demand, a dedicated calculator block ("POWER") is used to compute the actual electrical power requirement. The calculator imports (i) the hydrogen mass flow rate and (ii) the reaction enthalpy calculated in the RStoic reactor, and then estimates the electrical input using the hydrogen lower heating value and the assumed electrolyser efficiency according to:

$$P_{el} = \frac{\dot{m_{H_2}} \cdot LHV_{H_2}}{\eta_{el}}$$

The difference between this required electrical input and the reaction enthalpy is interpreted as waste heat that must be removed to maintain the specified operating temperature. This removable heat is exported via the heat stream QELEC.

To make this cooling duty explicit in the overall energy balance, the calculated QELEC load is assigned to a dummy heat exchanger, shown in figure 3.8, analogous to the approach used for the pyrolysis heat demand. The exchanger is configured to impose the specified temperature decrease (80 → 75 °C) while removing 5.55 MW of heat in the case of AEC (the calculated difference).

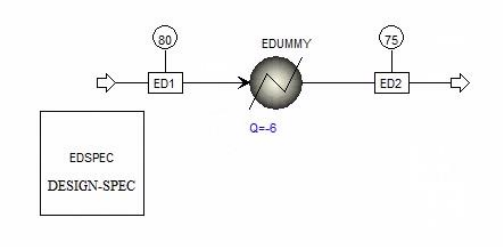

Figure 3.8: Recoverable heat in alkaline electrolysis cell.

For the SOEC case, the electrolysis subsystem is modified to reflect the steam-fed, high-temperature operation. As in the AEC configuration, liquid water enters at 20 °C and 1 bar and is pressurised to 10 bar. However, before entering the SOEC hierarchy, the pressurised water is converted to a suitable high-temperature feed. It is heated to 650 °C in a dedicated heater block (STGEN) to generate superheated steam, which is then supplied to the SOEC hierarchy. This explicitly captures the steam generation duty associated with SOEC operation.

Within the SOEC hierarchy, shown in figure 3.9, the electrolysis reaction is again implemented using an RStoic reactor to enforce the water-splitting stoichiometry and to calculate the reaction enthalpy. Hydrogen and oxygen are separated downstream, with O_2 treated as a waste by-product. A calculator block is again used to calculate the required electrical input based on the assumed efficiency of the cell, but in contrast to AEC, no recoverable waste-heat stream directly from the "ELECTRL" block is defined for SOEC.

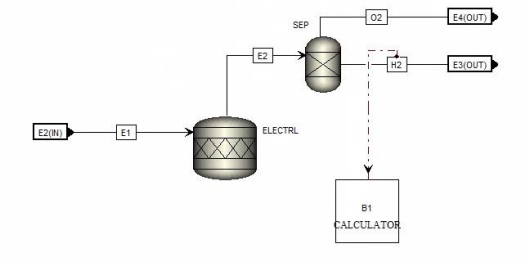

Figure 3.9: Solid oxide electrolysis cell hierarchy in Aspen Plus.

In both AEC and SOEC cases, products streams of oxygen and hydrogen are cooled down to 20°C to account for the recoverable waste heat of their product streams.

3.3.5. Methanation implementation

Methanation is implemented following the conceptual features described previously, i.e., an adiabatic, multi-bed reactor train, each working at 10 bar, with interstage cooling and targeted temperature control to avoid excessive outlet temperatures.

Upstream of the methanation train, and using a mixer block, the compressed dry reformer syngas is mixed with electrolytically produced hydrogen (both at 10 bar) to achieve the required stoichiometry for complete conversion of CO/CO_2 to methane. A design specification at the mixer outlet is configured such that $M = 3$, by varying the water feed to the electrolysis section, thereby controlling the hydrogen production rate and, consequently, the mixed-feed composition. The resulting syngas is then preheated to 200 °C, and is directed to the methanation train.

Methanation reactor beds are modelled as adiabatic RGibbs blocks. To ensure that the first reactor outlet temperature remains below the limit (690 °C), a recycle loop (controlled by a design spec) is implemented such that a substantial fraction of the first reactor effluent (after being cooled to 250 °C) is recirculated to dilute reactants and reduce the effective reaction driving force, thereby limiting the adiabatic temperature rise. After each reactor, the effluent is cooled to 250 °C to re-establish an appropriate inlet temperature for the subsequent step.

Prior to the final stage, the stream is cooled to 20 °C, condensed water is removed in a flash separator, and the dry gas is then preheated to 250 °C before entering the last adiabatic reactor. After the final reactor, the outlet is again cooled to 20 °C and residual water is removed. The final product is a bioSNG stream of approximately 96 wt% CH_4.

The integrated process to produce bioSNG, modelled in Aspen Plus, is illustrated in figures 3.10 and 3.11.

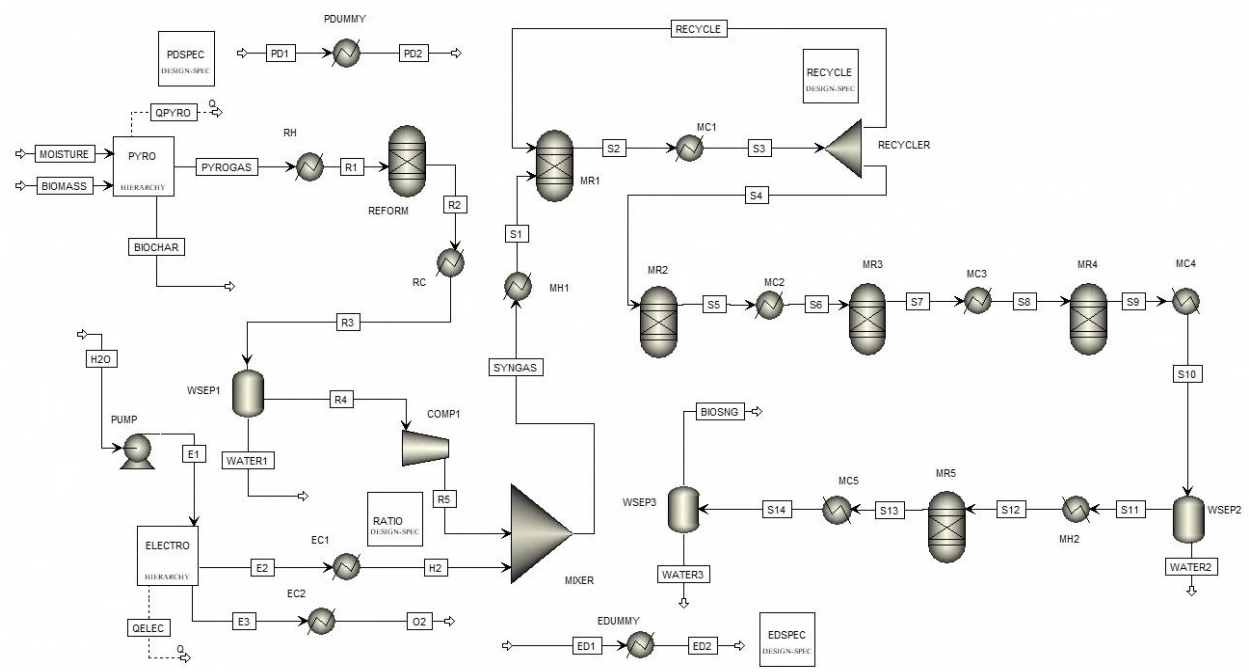

Figure 3.10: Overall system flowsheet (AEC-based layout).

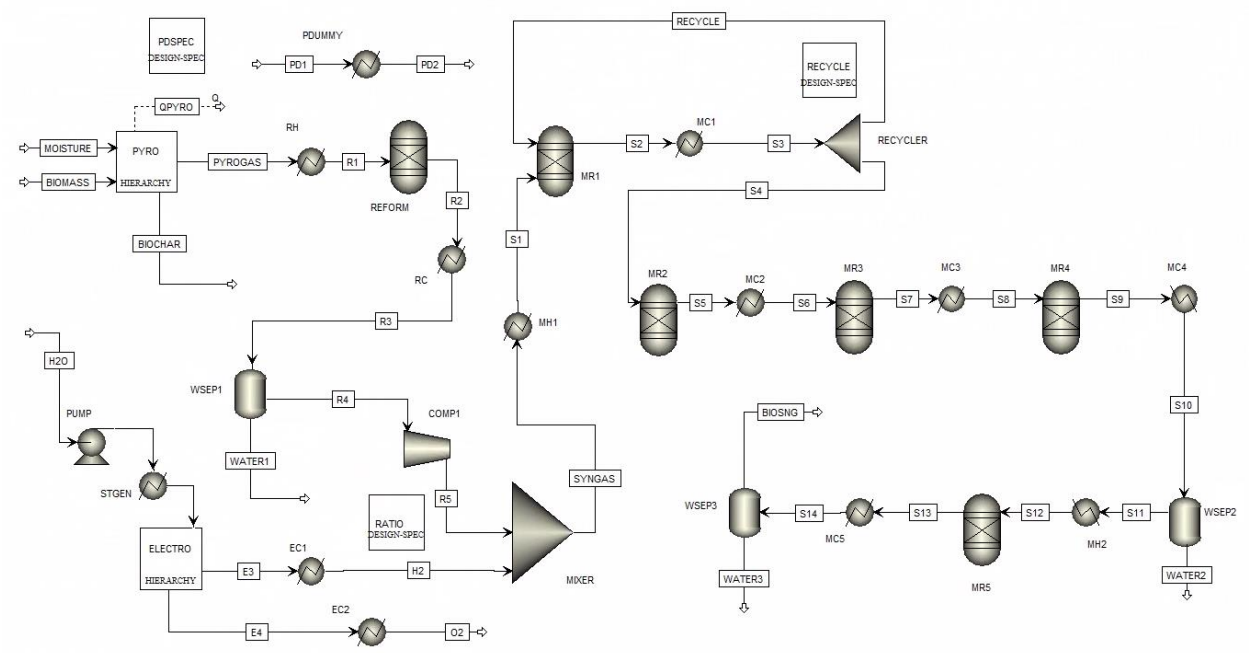

Figure 3.11: Overall system flowsheet (SOEC-based layout).

Having implemented the full process model in Aspen Plus, the simulation can be executed to obtain a consistent steady-state solution. A successful run is indicated by normal convergence of all blocks, without warnings or errors, confirming that the specified mass and energy relationships are satisfied across the flowsheet. The resulting stream and block outputs, which effectively constitute the model's mass and energy balances, are then taken forward as the quantitative basis for subsequent analyses and performance evaluation. In addition, composite curves are generated using the Aspen Energy Analyzer tool to support heat-integration assessment.

3.4. Process performance assessment

3.4.1. Key performance indicators

Across both the AEC and SOEC layouts, all subsystems other than the electrolysis units are modeled identically, and the biomass feed to both configurations is the same. Moreover, the hydrogen production rate is identical in both cases due to the imposed design specification to achieve the target syngas module. As a result, both layouts produce the same amount of bioSNG; the primary differences are their electricity consumption and plant-wide heat integration. With that in mind, a set of key performance indicators is defined to quantify the energetic performance of the proposed biomass-to-SNG pathway, tabulated in table 3-4. All indicators are formulated on a dry, lower heating value basis and are expressed as ratios between the chemical energy flow of product streams (reformer syngas, methanation-ready syngas, bioSNG, biochar) and the chemical/electrical energy flow of the feed (biomass, hydrogen) and utility streams (electricity) within the system boundary. Assuming a fully heat-integrated process, no external heat input is considered; this is subsequently verified and demonstrated using plant-wide composite curves. For any stream i, the chemical energy flow is defined as:

$$\dot{E}_\iota = \dot{m}_\iota \cdot LHV_i$$

where:

- $\dot{m}_\iota$ is the mass flow rate
- and LHV_i is the lower heating value.

Table 3-4: Definition of key performance indicators.

Metric	Equation
Biomass → reformer syngas efficiency	$\eta_{BM\rightarrow refsyn} = \frac{\dot{E}_{refsyn}}{\dot{E}_{BM}}$
Biomass → SNG efficiency	$\eta_{BM\rightarrow SNG} = \frac{\dot{E}_{SNG}}{\dot{E}_{BM}}$
(Biomass + H_2) → syngas efficiency	$\eta_{BM+H_2\rightarrow syn} = \frac{\dot{E}_{syn}}{\dot{E}_{BM} + \dot{E}_{H_2}}$
Syngas → SNG conversion efficiency	$\eta_{syn\rightarrow SNG} = \frac{\dot{E}_{SNG}}{\dot{E}_{syn}}$
(Biomass + H_2) → SNG efficiency	$\eta_{BM+H_2\rightarrow SNG} = \frac{\dot{E}_{SNG}}{\dot{E}_{BM} + \dot{E}_{H_2}}$
(Biomass + H_2) → (SNG + biochar) efficiency	$\eta_{BM+H_2\rightarrow SNG+char} = \frac{\dot{E}_{SNG} + \dot{E}_{char}}{\dot{E}_{BM} + \dot{E}_{H_2}}$
Total electrical power demand Sum of electrical power requirements for electrolysis, e-reformer, compression, and pumping.	$\dot{W}_{tot} = \dot{W}_{elec} + \dot{W}_{e-ref} + \dot{W}_{comp} + \dot{W}_{pump}$
Overall efficiency (biomass + total power → SNG)	$\eta_{BM+\dot{W}_{tot}\rightarrow SNG} = \frac{\dot{E}_{SNG}}{\dot{E}_{BM} + \dot{W}_{tot}}$
Overall efficiency (biomass + total power → SNG + biochar)	$\eta_{BM+\dot{W}_{tot}\rightarrow SNG+char} = \frac{\dot{E}_{SNG} + \dot{E}_{char}}{\dot{E}_{BM} + \dot{W}_{tot}}$

Moreover, a carbon utilization indicator is calculated as the fraction of biomass carbon that appears in the final bioSNG stream, on a mass-flow basis. The mass flow of carbon in the bioSNG stream is obtained directly from the stream properties in Aspen. The mass flow of carbon in the biomass is calculated as the biomass mass flow multiplied by the biomass carbon mass fraction (from the elemental analysis). The remainder is almost entirely retained in the biochar, consistent with the earlier assumption that coke formation is neglected.

$$X_C = \frac{\dot{m}_{C,SNG}}{\dot{m}_{C,BM}} \qquad 1 - X_C \approx \frac{\dot{m}_{C,char}}{\dot{m}_{C,BM}} \qquad \dot{m}_{C,BM} = w_{C,BM} \cdot \dot{m}_{BM}$$

Finally, hydrogen specific consumption indicators quantify the amount of externally supplied hydrogen required per unit of SNG produced. The mass-based indicator, $s_{H_2}^{mass}$, expresses the hydrogen demand on a gravimetric basis and is therefore directly linked to material balances and storage/supply requirements. The

energy-based indicator, $s_{H_2}^{energy}$, expresses the hydrogen demand relative to the chemical energy output of SNG, enabling an energy-normalized comparison across operating points and configurations.

$$s_{H_2}^{mass} = \frac{\dot{m_{H_2}}}{\dot{m_{SNG}}} \qquad s_{H_2}^{energy} = \frac{\dot{E_{H_2}}}{\dot{E_{SNG}}}$$

3.4.2. Heat integration and export potential

For heat integration, both layouts are evaluated using their composite curves and the heating and cooling duty breakdowns. The curves and breakdowns are taken directly from Aspen. From the duty breakdowns, the internally supplied process heat demands are identified as reformer inlet preheating, pyrolysis heat input, methanation train preheating, and superheated steam generation in the SOEC case. The total internally supplied heat demand is defined as the sum of these contributions.

$$\dot{Q_{tot}} = \dot{Q_{pyr}} + \dot{Q_{ref}} + \dot{Q_{meth}} + \dot{Q_{steam}}$$

The final term is included only for the SOEC case.

The total cooling load is obtained in the same way. The main cooling duties are the cooling of electrolysis outlet streams to 20°C, the intercooling duties in the methanation train, the electrolysis heat removal in the AEC case, and the cooling of the reformer outlet stream from 800°C to 20°C. The electrolysis outlet streams cooling is most significant in the SOEC case because the product streams are cooled from 700°C to 20°C, while in the AEC case they are cooled from 80°C to 20°C.

$$\dot{C_{tot}} = \dot{C_{ele,out}} + \dot{C_{meth}} + \dot{C_{ele,waste}} + \dot{C_{ref}}$$

The third term is included only for the AEC case.

Assuming that all heating duties can be supplied internally, which is later checked against the composite curves, the net balance between heating and cooling duties is used to define tentative export potentials. Two options are considered.

- The first is district heating based on heating water from 40°C to 70°C.
- The second is process heat export as superheated steam generation by heating water from 20°C to 200°C.

4. Simulation results

4.1. Key performance indicators

As previously explained, the only differences between the two layouts relate to electricity consumption and heat integration. Accordingly, all the metrics defined in previous chapter are identical for both configurations except for the total electrical power demand and, consequently, the overall efficiencies of each layout. The results are tabulated in table 4-1.

Table 4-1: Key performance indicators for the studied layouts.

Metric	Value	
	AEC	SOEC
$\eta_{BM \rightarrow refsyn}$	0.66	
$\eta_{BM \rightarrow SNG}$	1.03	
$\eta_{BM+H_2 \rightarrow syn}$	0.79	
$\eta_{syn \rightarrow SNG}$	0.80	
$\eta_{BM+H_2 \rightarrow SNG}$	0.63	
$\eta_{BM+H_2 \rightarrow SNG+char}$	0.92	
$\dot{W_{tot}}$	34.50 MW	29.93 MW
$\eta_{BM+\dot{W_{tot}} \rightarrow SNG}$	0.49	0.53
$\eta_{BM+\dot{W_{tot}} \rightarrow SNG+char}$	0.72	0.77
X_C	0.56	
$S_{H_2}^{mass}$	0.25	
$S_{H_2}^{energy}$	0.61	

The results indicate that the energy content of the produced SNG is close to that of the fed biomass. About 56% of the biomass carbon ends up in the main product, SNG. This explains why treating biochar as a main product, or not, can change the metric substantially. Hydrogen is also critical. About 61% of the SNG energy originates from the supplied hydrogen. In both layouts, electricity consumption is dominated by the electrolyser and accounts for more than 80% of the total. Most of the remaining demand is associated with the reformer. The pump demand is negligible in both cases. The higher efficiency of the SOEC based layout leads to a lower electrical power demand and therefore a higher overall efficiency than the AEC based layout. The electrical power breakdowns for both layouts are shown in the figure 4.1.

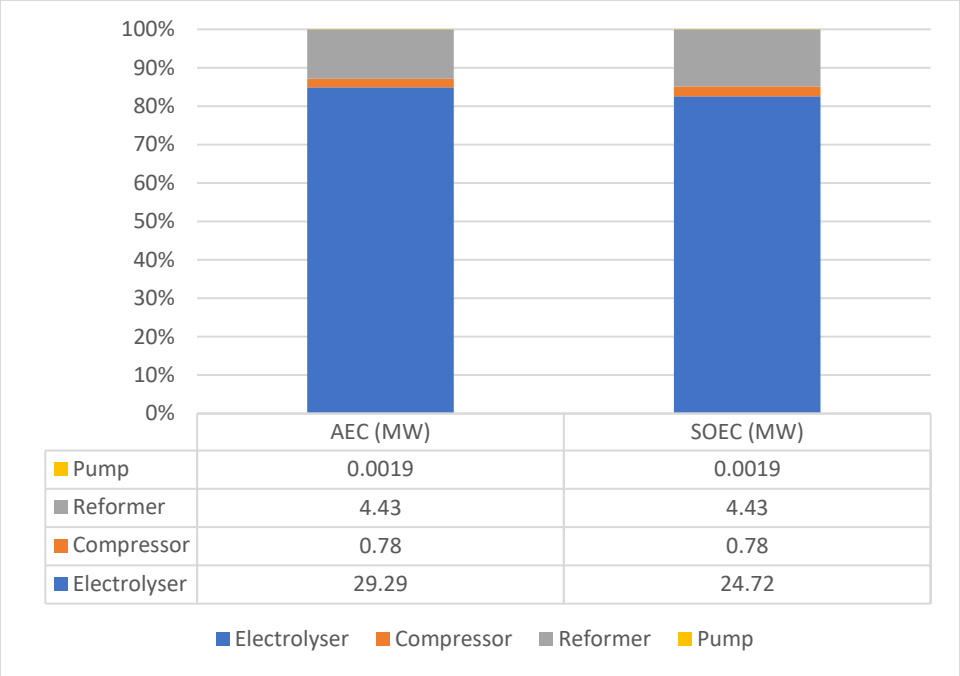

Figure 4.1: Electrical power breakdown of the studied layouts.

4.2. Heat integration and export potential

The composite curves indicate that no external heat input is required in either the AEC or SOEC case. While the curves show an approximately 4.4 MW unmet heating duty from 770°C to 800°C (blue curve), this duty corresponds to the e-reformer, which is assumed to be fully electric and its energy demand is already included in the electrical power breakdown.

In the AEC-based layout, additional heating duties are also visible on the blue curve. These include reformer inlet preheating from 550°C to 770°C, the pyrolysis heat input, and the preheating of the syngas sent to the methanation train. The red curve represents the total cooling duties. Since it lies entirely above the blue curve, it confirms that no external heat input is required. The near-horizontal red segment highlights the heat that must be removed during operation of the alkaline electrolyser. From the composite curves of the AEC-based layout in figures 4.2 and 4.3, and treating enthalpy below 1 MW as non-usable due to too low temperature levels, the district heating potential is tentatively estimated at 14.5 MW. Under the alternative export option of steam at 200°C, the usable process heat is estimated at about 9 MW.

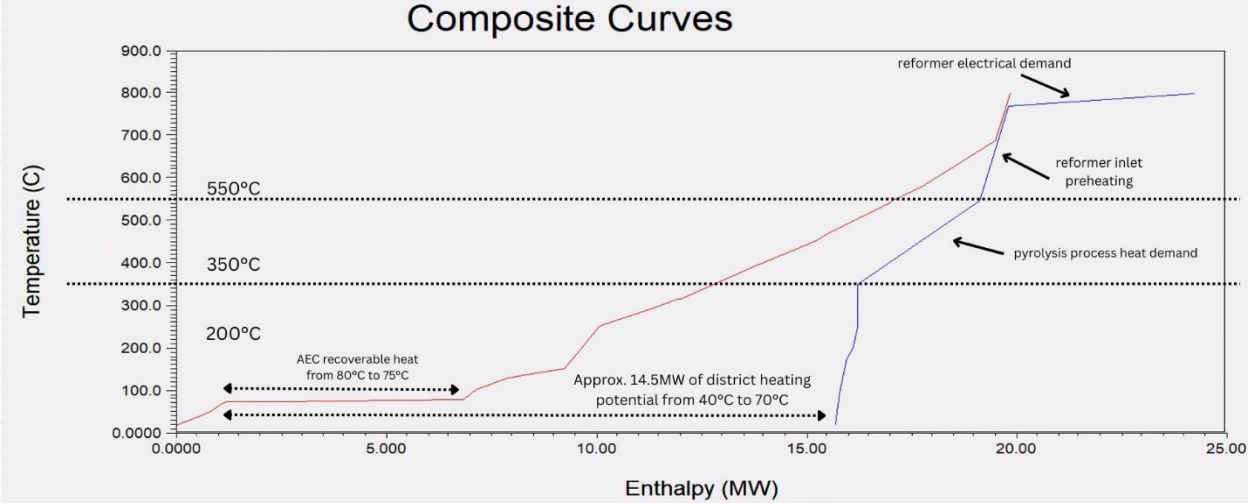

Figure 4.2: Composite curves for AEC-based layout.

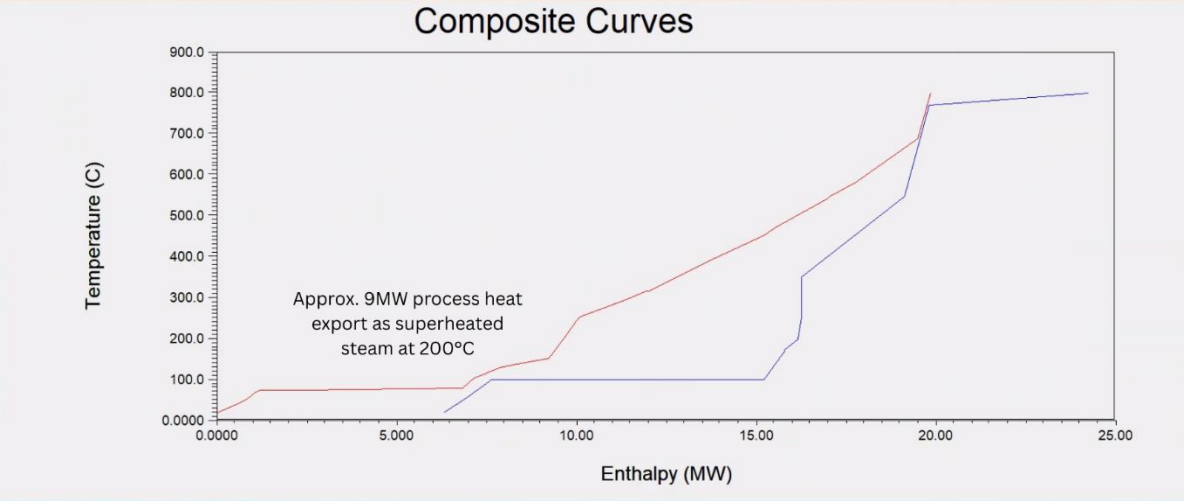

Figure 4.3: Composite curves for AEC-based layout with process heat export.

The same approach is applied to the SOEC-based layout. The composite curves, shown in figures 4.4 and 4.5, differ markedly in this case. A large share of the available heat is used internally to generate superheated steam at 650°C for the electrolyser inlet. As a result, the surplus heat available for the predefined export programs is much lower. The district heating and process heat export potentials are both estimated at about 5 MW. Even so, the blue curve remains fully below the red curve, which confirms that the internal heating demands are met without external heat input in this layout as well.

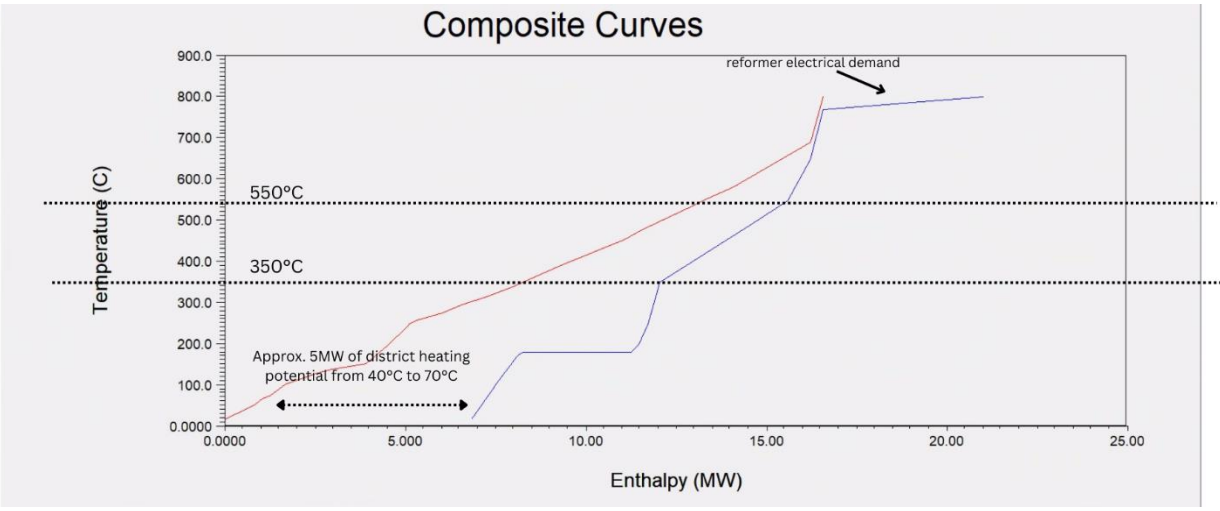

Figure 4.4: Composite curves for SOEC-based layout.

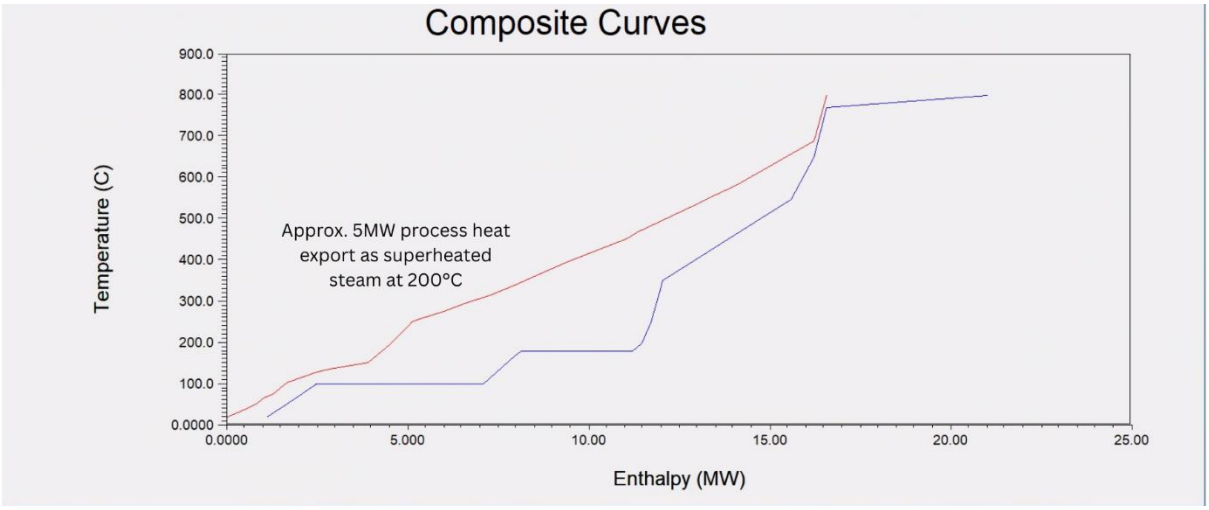

Figure 4.5: Composite curves for SOEC-based layout with process heat export.

Based on Figure 4.6, which compares the heating and cooling duties of both layouts, the dominant heat demand is pyrolysis in the AEC case, while it is the electrolysis steam generator in the SOEC case. In both layouts, the methanation train remains the largest source of available heat.

These differences mainly reflect how the electrolyser is integrated into the process. The AEC-based layout leaves more surplus heat for export. The SOEC-based layout instead uses a larger share of the available heat internally. As a result, even without relying on heat export, it achieves higher overall efficiency and makes more effective use of internally available heat.

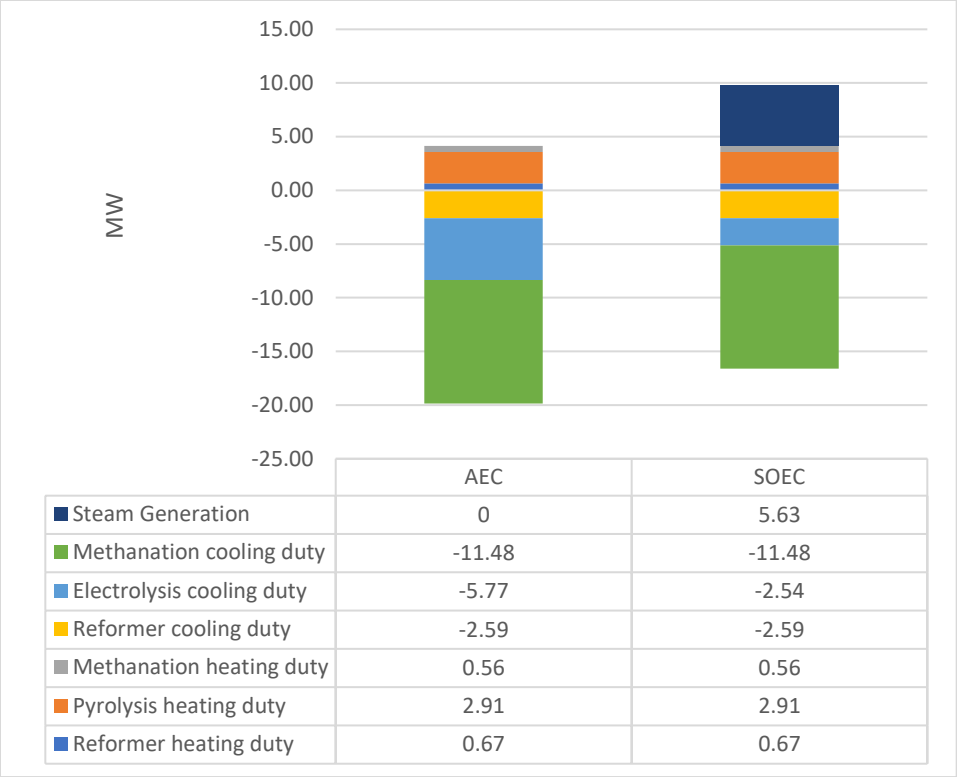

	AEC	SOEC
Steam Generation	0	5.63
Methanation cooling duty	-11.48	-11.48
Electrolysis cooling duty	-5.77	-2.54
Reformer cooling duty	-2.59	-2.59
Methanation heating duty	0.56	0.56
Pyrolysis heating duty	2.91	2.91
Reformer heating duty	0.67	0.67

Figure 4.6: Heating and cooling load breakdown (AEC vs. SOEC).

Note that the electrolysis cooling duty in the AEC case is the sum of direct waste heat released from the stacks, which is significant, and the recoverable heat from the product stream as it cools from 80°C to 20°C. In contrast, for SOEC there is no direct waste heat from the stacks, but a substantial amount of heat is available from the product streams as they cool from 700°C to 20°C.

5. Techno-economic analysis

This section presents the cost-estimation methodology used to quantify the total investment cost (TIC), cost of operations and maintenance (O&M), total annual cost (TAC), and the levelized cost of fuel (LCOF) for the evaluated plant configurations. The economic boundary is consistent with the process boundary defined previously. Biomass enters at the pyrolysis section inlet, and fuel (dry bioSNG) exits at the plant fence. The boundary therefore includes integrated electrolysis, auxiliary power consumption, and the major heat-exchange and cooling functions represented in the simulation model.

Rather than applying a component-by-component costing method, a technology-based approach is used to estimate subsystem costs within the boundary—namely pyrolysis, e-reforming, electrolysis, and methanation. Assumptions, references, and intermediate results are documented throughout the chapter. Assuming a base case scenario for each layout, sensitivity analyses are performed to assess the impact of key cost drivers on the LCOF, and literature data are ultimately used to define lower and upper bounds for the LCOF.

5.1. Preliminary assumptions

Financial data for pyrolysis, AEC, and SOEC are taken from the Danish Energy Agency (Technology Data for Renewable Fuels [8]). Cost data for the e-reformer and methanation, as well as other economic inputs such as commodity prices (renewable electricity, district-heating sales price, biochar sales price, etc.), are sourced from peer-reviewed literature. As noted previously, a base case is defined, and a summary table of the corresponding input data is provided at the end of this section.

5.1.1. Reference year

Techno-economic data obtained from the Danish Energy Agency catalogues are already aligned with the study's reference year (2025). For data from other sources, costs are updated to the reference year either using the CEPCI index or by applying a flat inflation rate, as described by the equations below.

$$C_{2025} = C_y * \left(CEPCI_{2025}/CEPCI_y\right) \qquad C_{2025} = C_y * (1+i)^{(2025-y)}$$

5.1.2. Reference capacity

When a reference cost is provided for a different plant size, capacity scaling is performed using the standard scaling relation given below. However, the Danish Energy Agency catalogue data are either module-based or already match the capacities used in this work; therefore, linear scaling is assumed (scaling exponent $n = 1$). All the preliminary assumptions are tabulated in table 5-1.

$$C = C_0 * (S/S_0)^n$$

Table 5-1: Preliminary financial assumptions for the base case.

Reference year	2025
Plant lifetime	25 years
Annual operation hours	8000
CEPCI 2025	818
Flat inflation rate (*i*)	2.79%
Electrolysis efficiencies: AEC / SOEC	67.5% / 80%
Weighted average cost of capital (*WACC*)	5%
Electricity price (of renewable origin)	80 €/MWh
Euro to Dollar conversion rate (2025 average)	1.13

5.2. Subsystem TIC/O&M estimation

5.2.1. Subsystem S1: Pyrolysis

The DEA technology catalogue provides techno-economic data (2025) for slow pyrolysis of wheat straw based on the Stiesdal SkyClean pyrolysis technology [8]. In the catalogue, the typical plant input is 20 MW_{th} (thermal), with an indicated capacity range of 50–150% of this reference. Using the upper end of this range, the biomass input in this work (31.4 MW) falls almost within the stated applicability window; the catalogue data are therefore adopted with linear scaling.

The catalogue reports a typical useful output (biochar, volatile fraction, and heat) of 16.6 MW, corresponding to an efficiency of 83%. The specific investment cost for 2025 is given as 1.4 M€ per MW of pyrolysis output, of which 75% is attributed to equipment and 25% to installation. In this work, the useful pyrolysis output is taken as the sum of biochar and volatile products and, consistent with the modelling assumption of 100% conversion efficiency, is set equal to 31.4 MW. The pyrolysis total investment cost is therefore estimated by multiplying the specific investment (M€/MW_{out}) by the modelled output capacity.

The catalogue further reports uncertainty bounds for the specific investment cost of 60–140% of the nominal value; these bounds are applied later to quantify the impact of pyrolysis-cost uncertainty on the overall economics.

Operating and maintenance (O&M) costs are also provided in the catalogue and will be used in subsequent TAC/LCOF calculations. Fixed O&M (labour and maintenance, expressed as an annual cost per unit output) is reported as 0.048 M€ per MW_{out} per year, while variable O&M is reported as 6.8 € per MWh_{out}. Total O&M is taken as the sum of the fixed and variable components.

Finally, the catalogue specifies a forced outage of 4% and a planned outage of two weeks per year. Accounting for these outages yields approximately 8,073 operating hours per year, consistent with the assumption of 8,000 annual operating hours. The technical lifetime is given as 25 years, also consistent with the assumed lifetime in this work. The adopted inputs are summarized in the table 5-2.

Table 5-2: Financial input for the pyrolysis system.

Typical input (Biomass)	20 MW_{th} (50-150%)
Specific investment	1.4 M€ per MW_{out} (60-140%)
Fixed O&M	0.048 M€ per MW_{out} per year
Variable O&M	6.8 € per MWh_{out}

5.2.2. Subsystem S2: Reforming

As noted previously, not all techno-economic inputs are sourced from the DEA technology catalogues, and the e-reformer is one such subsystem. The process definition and operating concept for the electrically heated reformer are taken from Caballero et al. [20]; however, Caballero et al. do not originate the investment-cost data and instead cite Mion et al. [50] as the underlying source. In Mion et al., it is stated that the e-SMR cost is evaluated on an energy (electricity consumption) basis and implemented as multiple 3 MW modules installed in parallel, with each module costing approximately 1.7 M€. Mion et al. further state that this results in a total electrically heated reformer cost comparable to the traditional fired configuration. Importantly, Mion et al. use wording that vaguely implies the cost is an installed cost (i.e., already reflects installation), but they do not provide a fully explicit breakdown, which introduces ambiguity. The reported cost basis corresponds to year 2019, associated with a CEPCI value of 607.5.

In contrast, when Caballero et al. conduct their techno-economic assessment, they treat the same reformer cost as a bare erected cost (BEC) and apply additional factors to obtain a total overnight cost (approximately 42% higher). The factor methodology used is as follows:

- Total bare equipment cost (BEC): installation cost of all units
- Engineering procurement and construction costs (EPCC): 10% of BEC
- Project contingency (PC): 15% of (BEC + EPCC)
- Total plant cost (TPC): BEC + EPCC + PC
- Owner costs: 12% of TPC
- Total overnight cost (TOC): TPC + Owner costs

This creates a clear inconsistency between the two sources. Mion et al. report a module cost that is vaguely described as "installed," whereas Caballero et al. explicitly apply a structured set of indirect-cost adders to reach TOC. This inconsistency is interpreted here as uncertainty in the appropriate interpretation of the reformer module cost, particularly given that electrically heated reforming remains a comparatively new technology with limited mature cost data available in the open literature. In addition, much of the available reforming techno-economic literature pertains to autothermal reforming (ATR), where heat is provided via partial oxidation of a fraction of the gas. Nevertheless, ATR costs remain informative for context because Mion et al. explicitly indicate that electrically heated reformer costs are similar to "traditional" configurations.

Accordingly, and to reflect this uncertainty transparently, this work treats the Mion approach as a lower bound and the Caballero factor-based approach as an upper bound for the e-reformer investment cost. For an order-of-magnitude cross-check, the cost of a traditional reformer was also estimated based on Hamelinck (2004) [51], and it was found that an autothermal reformer at the scale relevant to the present model would cost approximately 5 M€, which is broadly consistent with Mion et al.'s statement. For further context, additional scholarly sources reporting techno-economic data for reforming technologies are also suggested for the interested reader: [22][47][52][32][6].

With this framing, the costing is then applied to the present model. The e-reformer electrical demand in this work is approximately 4.4 MW. Since the cost basis is given in discrete 3 MW modules, and to conservatively account for modular implementation and uncertainty, two 3 MW modules installed in parallel are assumed for the cost estimate, which is then interpreted as the lower-bound e-reformer TIC. For the upper-bound estimate, the Caballero TOC methodology described above is applied on top of the base cost level. The resulting lower and upper bounds are subsequently propagated to the overall plant economics as part of the uncertainty treatment.

Regarding O&M assumptions, explicit e-reformer-specific O&M datasets are limited and are often only available as plant-wide assumptions. Based on the referenced studies and to reflect the fact that this is not yet a highly developed technology, fixed O&M is assumed as 5% of TIC per year. For variable O&M, only

catalyst replacement cost is included, as electricity use is accounted for separately in the plant-wide electrical power consumption. Catalyst-related assumptions follow the basis used by Caballero et al., namely:

- GHSV = 2500 h^{-1}
- catalyst bulk density = 3630 kg m^{-3}
- catalyst price = 5 EUR kg^{-1}
- catalyst lifetime = 6 months

The volumetric flow to the reformer inlet is taken directly from Aspen and equals 18,215 m^3/h. Using this volumetric input and the above assumptions, the catalyst inventory and replacement cost for the present model are calculated and reported in the O&M results section. The adopted inputs for this technology are summarized in the table 5-3.

Table 5-3: Financial input for the electrically heated reformer.

Cost basis (2019, *CEPCI* = 607.5)	3 MW modules of 1.7 M€ each Upper bound factor: 1.42
Fixed O&M	5% of TIC per year
Variable O&M	Catalyst replacement cost
Catalyst assumptions	• GHSV = 2500 h^{-1} • catalyst bulk density = 3630 kg m^{-3} • catalyst price = 5 EUR kg^{-1} • catalyst lifetime = 6 months

5.2.3. Subsystem S3: AEC

Returning to the DEA technology catalogues [8], the required techno-economic inputs for alkaline electrolysis (AEC) are extracted. For the reference year 2025, the catalogue specifies a typical AEC module size of 10 MW. Because this reference is module-based, linear scaling is adopted with respect to the catalogue's specific investment cost. The specific investment for an alkaline electrolyzer is reported as 1.4 M€ per MW of total electrical input (2025 basis). In the AEC base case modelled in this work, the electrolyzer electrical demand is 29.29 MW, and the TIC is therefore obtained by multiplying 29.29 MW by 1.4 $M€/MW_{in}$. The catalogue also reports an uncertainty range for the specific investment, suggesting lower/upper bounds of 80–120% of the nominal value; this range is later used to quantify uncertainty in the electrolysis investment cost.

A further important point is that the 1.4 M€/MW total specific investment includes a contribution attributed specifically to the electrolyzer stack. The stack-specific investment component is reported as 0.187 M€ per MW of electrical input in 2025. The catalogue also specifies a stack lifetime of 80,000 hours, which, under the assumed 8,000 operating hours per year, corresponds to approximately 10 years of operation per stack set. In this work, stack replacements are incorporated within the electrolysis TIC for simplicity (rather than being treated separately as periodic replacement costs), meaning that future stack purchases are included directly in the investment accounting.

Because replacement stacks are not purchased in the reference year (2025) but later during plant operation, the stack-specific investment is adjusted to reflect the year of purchase. The catalogue provides stack cost data only for 2025, 2030, 2040, and 2050; therefore, intermediate years are estimated by linear interpolation. Using this approach, a stack replacement schedule is formulated:

- 0.104 M€ per MW_{in} for AEC stacks purchased in 2035 (with 93500 hours of lifetime)
- 0.072 M€ per MW_{in} for AEC stacks purchased in 2047 (with almost 100000 hours of lifetime)

Because the second series of stacks would be purchased near the end of the plant's life, only about one quarter of their useful life would be utilized by 2050. Accordingly, the second-series replacement is treated as a partial-life replacement, and the associated cost is prorated by multiplying by 0.25.

Finally, additional AEC economic inputs used in the TAC/LCOF calculations are taken directly from the catalogue: fixed O&M is assumed as 4% of TIC per year, and variable O&M is assumed to be zero. The adopted inputs for AEC technology are summarized in the table 5-4.

Table 5-4: Financial input for the AEC.

Specific investment	1.4 M€/MW_{in}
AEC stacks purchased in 2035	0.104 M€ per MW_{in}
AEC stacks purchased in 2047	0.072 M€ per MW_{in} (multiplied by 0.25)
Fixed O&M	4% of TIC per year
Variable O&M	0

5.2.4. Subsystem S3: SOEC

This subsection follows the same approach as the AEC cost estimation, using techno-economic inputs taken from the DEA technology catalogues. For the reference year 2025, the catalogue specifies a typical SOEC module size of 10 MW, and since the reference is module-based, linear scaling is adopted. In the SOEC base-case configuration modelled in this work, the electrolyzer electrical demand is 24.72 MW, and the TIC is therefore obtained by multiplying this electrical input by the catalogue's specific investment cost of

2.075 M€ per MW of total input electricity (2025 basis). As for AEC, the catalogue suggests that the specific investment is uncertain and recommends lower/upper bounds of 80–120%, which are later applied in the uncertainty analysis.

The catalogue also provides an explicit decomposition of the SOEC investment, including a stack-related contribution. For SOEC, the stack contribution is reported as 0.882 M€ per MW of total input electricity (2025 basis), with 34500 hours of lifetime. As in the AEC case, a stack replacement schedule is formulated:

- 0.58 M€ per MW_{in} for SOEC stacks purchased in 2029 (with almost 48000 hours of lifetime)
- 0.486 M€ per MW_{in} for SOEC stacks purchased in 2035 (with almost 58000 hours of lifetime)
- 0.42 M€ per MW_{in} for SOEC stacks purchased in 2042 (with almost 70000 hours of lifetime)

Finally, additional SOEC economic inputs used in the TAC/LCOF calculations are also taken from the catalogue: fixed O&M is assumed as 12% of TIC per year, and variable O&M is assumed to be zero. The adopted inputs for SOEC technology are summarized in the table 5-5.

Table 5-5: Financial input of the SOEC.

Specific investment	2.075 M€/MW_{in}
SOEC stacks purchased in 2029	0.58 M€ per MW_{in}
SOEC stacks purchased in 2035	0.486 M€ per MW_{in}
SOEC stacks purchased in 2042	0.42 M€ per MW_{in}
Fixed O&M	12% of TIC per year
Variable O&M	0

5.2.5. Subsystem S4: Methanation

The techno-economic inputs for the methanation section are not taken from the DEA catalogues, but are instead extracted from reports and peer-reviewed literature, similar to the approach used for the reformer. In this work, the primary basis is taken from Subramanian et al. (2020) [53], who in turn reference a NETL (National Energy Technology Laboratory) report for methanation cost estimation [54]. In the Subramanian et al. dataset, the reference methanation process is defined for a syngas feed of 90.9 kg/s and is reported to have a total investment cost of 76.3 million USD. The cited methodology applies a capacity scaling exponent of 0.6, and the reported cost basis corresponds to year 2007, associated with a CEPCI value of 525.4.

In the present model, the syngas feed to the methanation train is 1.52 kg/s. Using the above reference point (90.9 kg/s, 76.3 MUSD) and the stated scaling methodology, the methanation train TIC for the present work is obtained by scaling the reference cost from the stated basis to the modelled syngas feed. It is, however,

critical to recognize that the reference capacity (90.9 kg/s) is substantially larger than the capacity in this work (1.52 kg/s). As a result, applying a conventional 0.6 scaling exponent over such a large extrapolation introduces a high level of uncertainty. To explicitly reflect this uncertainty in the subsequent uncertainty analysis, an alternative exponent of 0.45 is adopted as an upper-bound case for capacity scaling (i.e., to test the sensitivity of cost to a more conservative scaling behaviour at small scale).

With respect to operating and maintenance costs, fixed O&M is estimated using a rule-of-thumb consistent with the maturity of industrial methanation technologies (e.g., TREMP), which are considered highly developed. Accordingly, fixed O&M is taken as 4% of TIC per year. For variable O&M, only catalyst replacement cost is considered, consistent with the treatment used for the reformer (i.e., variable O&M is represented by catalyst consumption rather than plant-wide utilities). Subramanian et al. report a catalyst replacement cost of 1.26 million USD per year, noting that this value is also based on the same 2007 reference basis. In the present work, this catalyst replacement cost is first updated from the 2007 basis to the 2025 reference year using a flat inflation rate. Since the catalyst cost is a consumable (rather than a piece of equipment), and because it is fundamentally tied to throughput, it is then scaled linearly with syngas feed capacity from the 90.9 kg/s reference plant to the 1.52 kg/s plant modelled here. The adopted inputs for methanation technology are summarized in the table 5-6.

Table 5-6: Financial input for the methanation train.

Cost basis (2007, *CEPCI* = 525.4)	90.9 kg/s syngas feed, 76.3 million USD
	Base exponent: 0.6
	Upper exponent: 0.45
Fixed O&M	4% of TIC per year
Variable O&M	Catalyst replacement cost

Finally, additional literature sources providing useful methanation techno-economic data are also surveyed for context and comparison and are listed for the interested reader: [49][55][6][35][56][57].

5.2.6. Results of TIC/O&M estimation

The results for the two layouts (AEC-based and SOEC-based) were obtained, and the corresponding total investment cost (TIC) and annual O&M costs were calculated; the breakdowns are shown in figures 5.1 and 5.2. For the AEC-based layout, the total TIC is 102.15 M. For the SOEC-based layout, the total TIC is 145.59 M€.

Several observations follow directly from these TIC breakdowns. First, in the AEC-based layout, TIC is largely dominated by pyrolysis and the electrolyzer, which contribute 43.96 M€ and 41.01 M€, respectively (together 83.2% of the total), while the stack replacement cost is marginal in comparison (3.57 M€, i.e., 3.5% of total TIC). Second, in the SOEC-based layout, the electrolyzer remains a major cost driver (51.29 M€, i.e., 35.2% of total TIC) and is 10.28 M€ higher than the AEC electrolyzer cost (51.29 M€ vs. 41.01 M€). In addition, stack replacement becomes a major cost driver in the SOEC case, amounting to 36.73 M€ (25.2% of total TIC). This stack replacement cost is only 7.23 M€ lower than the pyrolysis TIC (43.96 M€), which aligns with the qualitative conclusion that SOEC investment is driven not only by a higher electrolyzer cost but also by significantly higher stack-related CAPEX. This is attributable to both the higher cost level of SOEC stacks and their shorter lifetime necessitating more frequent replacement than in the AEC case.

For annual O&M, the AEC-based layout totals 5.74 M€/y. The SOEC-based layout totals 10.25 M€/y. Hence, while pyrolysis dominates O&M in the AEC-based layout (3.22 M€/y, i.e., 56%), the electrolyzer dominates O&M in the SOEC-based layout (6.15 M€/y, i.e., 60%).

Finally, the combined contribution of methanation plus e-reformer remains secondary in both configurations. In TIC terms, methanation plus reforming contribute 13.61 M€ (13.3%) in the AEC-based layout and 13.61 M€ (9.35%) in the SOEC-based layout. In O&M terms, methanation plus reforming contribute 0.88 M€/y (15.3%) in the AEC-based layout and 0.88 M€/y (8.6%) in the SOEC-based layout.

Overall, the AEC configuration is characterized by two comparable TIC cost drivers (pyrolysis and electrolyzer), whereas in the SOEC configuration the electrolyzer-related costs (electrolyzer CAPEX, stack replacement CAPEX, and electrolyzer O&M) clearly dominate both TIC and O&M.

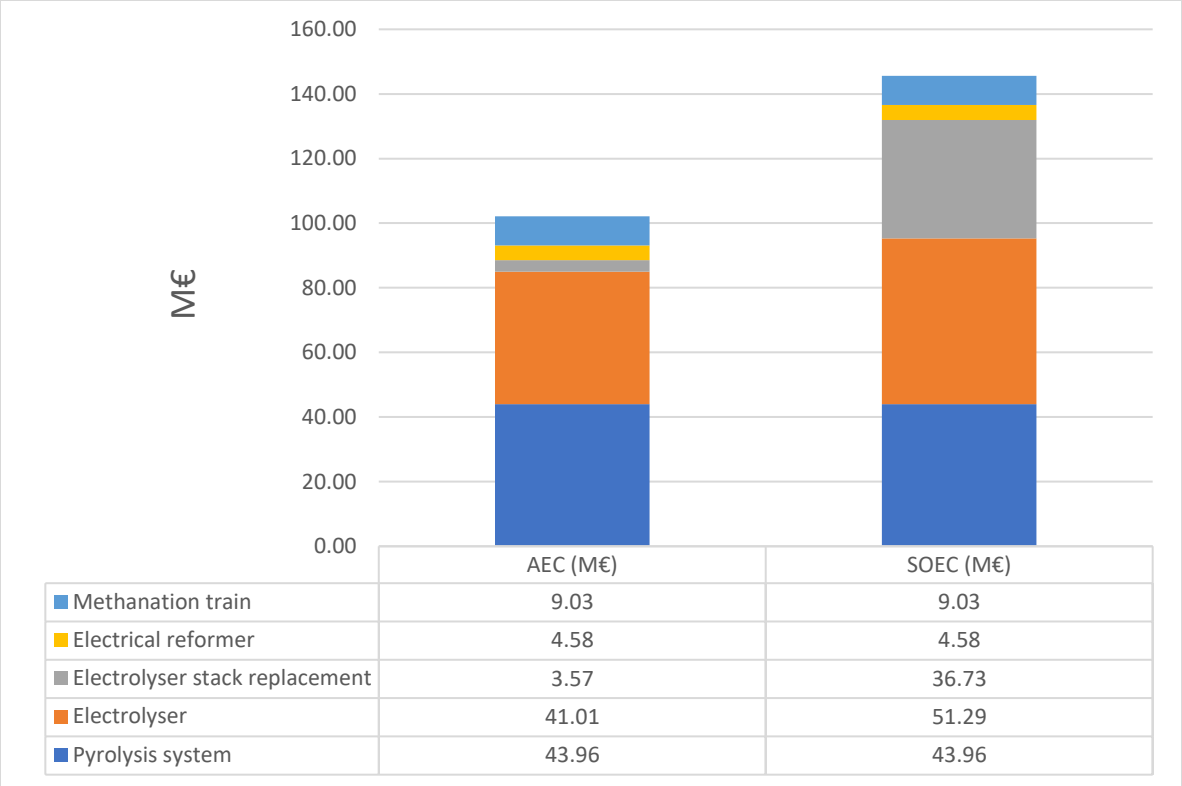

	AEC (M€)	SOEC (M€)
Methanation train	9.03	9.03
Electrical reformer	4.58	4.58
Electrolyser stack replacement	3.57	36.73
Electrolyser	41.01	51.29
Pyrolysis system	43.96	43.96

Figure 5.1: Total investment cost breakdown by subsystems.

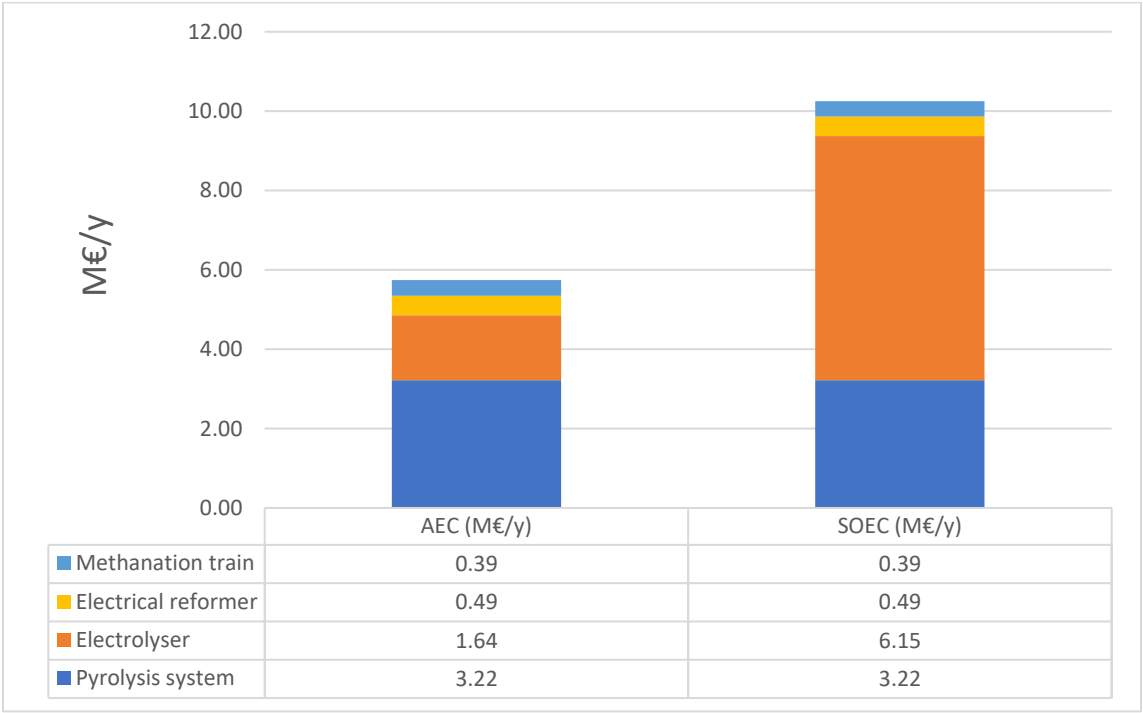

	AEC (M€/y)	SOEC (M€/y)
Methanation train	0.39	0.39
Electrical reformer	0.49	0.49
Electrolyser	1.64	6.15
Pyrolysis system	3.22	3.22

Figure 5.2: O&M annual cost breakdown by subsystems.

5.3. Total annual expenses

In the previous section, the total investment cost (TIC) and the annual operation and maintenance (O&M) costs were quantified for both layouts. These terms constitute key inputs to the total yearly expenses, which are evaluated in the present section. Total yearly expenses represent the net annual cost of plant operation within the defined economic boundary and include both cost items and revenue credits. In this work, they are calculated as the sum of: annuity (annualized capital cost), O&M, plant-wide electricity consumption, wheat straw consumption, and purified water consumption, minus revenues from district heating and biochar sales (both treated as negative terms). The annuity term is treated in detail in the subsequent subsection; briefly, it is computed as the TIC multiplied by the capital recovery factor (CRF). The resulting total yearly expenses are then used as the primary economic input for calculating the levelized cost of bioSNG (LCOF).

5.3.1. Annuity

The annuity represents the annualized capital cost of the plant and is calculated by converting the total investment cost (TIC) into an equivalent series of equal yearly payments over the plant lifetime. This conversion is performed using the capital recovery factor (CRF), which accounts for the time value of money. In this work, the annuity is therefore computed as:

$$Annuity = TIC * CRF$$

The CRF is calculated as:

$$CRF = i(1+i)^n/((1+i)^n - 1)$$

where:

- i is the weighted average cost of capital (WACC), and
- n is the economic lifetime of the project (years), taken as the plant lifetime assumed in this work.

The WACC is inherently context-dependent (e.g., country, financing structure, perceived risk, revenue certainty, and technology maturity). In Danish Energy Agency (DEA) technology-catalogue contexts, WACC assumptions are often relatively low for mature, low-risk infrastructure financing; values around ~3.5% are commonly used for cases with strong risk mitigation (e.g., regulated revenue, state-backed or low-risk frameworks) [58][59]. The DEA also indicates that 5% can serve as a Denmark-anchored benchmark for a private investor case where the technology is not considered overly risky. However, the plant concept assessed here exhibits certain first-of-a-kind (FOAK) characteristics that can justify a higher

risk premium; correspondingly, many hydrogen/electrolyzer techno-economic studies adopt higher WACC values in the mid-to-high single digits, and an example electrolyzer $LCOH_2$ analysis applies 8% [60].

Considering these ranges, this work adopts WACC = 5% as the base-case assumption, which yields a CRF of approximately 7.10% (for the assumed project lifetime). The influence of financing risk is then explicitly addressed through a sensitivity analysis of LCOF versus WACC, illustrating how the economic performance shifts under higher-risk (higher-WACC) conditions.

5.3.2. Plant-wide operating costs

The next components of total yearly expenses are the variable operating costs associated with plant-wide electricity consumption, biomass (wheat straw) feed, and purified water required for electrolysis, tabulated in table 5-7. In this work, the renewable electricity price is assumed to be 80 € per MWh, the wheat straw price is assumed to be 92.8 € per tonne, and the water (high purity water for process use) price is assumed to be 0.06 € per tonne, all based on literature sources [61]. These unit prices are combined with the corresponding annual consumptions obtained from the process simulation to determine the annual cost contributions of each item.

As shown previously in the electrical power breakdown, the overall electricity demand is strongly dominated by the electrolyzer subsystem. Consequently, electricity-related expenses represent a key cost driver, and two sensitivity analyses are performed later to quantify their impact on the levelized cost of fuel (LCOF): (i) the effect of electricity price on LCOF, and (ii) the effect of electrolyzer efficiency, which directly determines the plant-wide electricity consumption and therefore propagates strongly to LCOF.

Table 5-7: Financial input for the commodities of the systems.

Electricity price	80 €/MWh
Wheat straw	92.8 €/tonne
Purified water	0.06 €/tonne

5.3.3. Revenues

Revenues within the economic boundary considered in this work arise from biochar sales and district heating export, tabulated in 5-8, and the same literature source used for electricity, biomass, and water price assumptions is also used here [61]. The assumed revenue values are 118.5 € per tonne of biochar and 20 € per MWh of district heat. The source explicitly motivates these values as follows. For biochar, it states that:

"The revenue for biochar was calculated as income for CO_2-certificates per mass of carbon in the biochar. The average CO_2-certificate price of 2022 (86.5 €/tCO_2) was used." For district heating, it states that: "Maximum willingness to pay for waste heat from power-to-X plants in a scenario of biomass and heat pumps, and biogas for peak loads as an alternative was used." In the present economic model, both revenues are implemented as negative terms in the total yearly expense balance.

The available district-heating export potential is taken from the heat-integration analysis presented previously (i.e., derived from the composite curves). While the plant is assumed to operate 8,000 hours per year, district heating revenue is not credited over the full operating year; instead, it is assumed that heat can be exported only during the cold season. Accordingly, 4,000 hours per year are assumed for district-heating delivery when calculating the annual district-heating revenue.

Table 5-8: Financial input for the revenue byproducts.

Biochar selling price	118.5 €/tonne
District heating price	20 €/MWh (4000 hours of annual operation)

5.3.4. Results for total yearly expenses

Finally, the total yearly expense breakdowns were compiled for both layouts and are presented in the figure 5.3. These results illustrate the main trade-offs between the layouts and how they propagate to the levelized cost of bioSNG. The SOEC case has a substantially higher annuity, which is consistent with its higher electrolysis-related investment costs (electrolyzer and stack replacement). However, this is partially offset by a lower annual electricity cost in the SOEC layout, reflecting the higher electrical efficiency of SOEC and the resulting reduction in plant-wide electricity consumption. At the same time, the SOEC layout benefits significantly less from district heating, consistent with the lower district-heating export potential identified previously, and it also exhibits considerably higher O&M costs. Overall, the AEC-based layout yields lower total yearly expenses, amounting to 40.19 M€/y compared to 45.25 M€/y for the SOEC-based layout, i.e., approximately 5.06 M€/y lower on an annual basis.

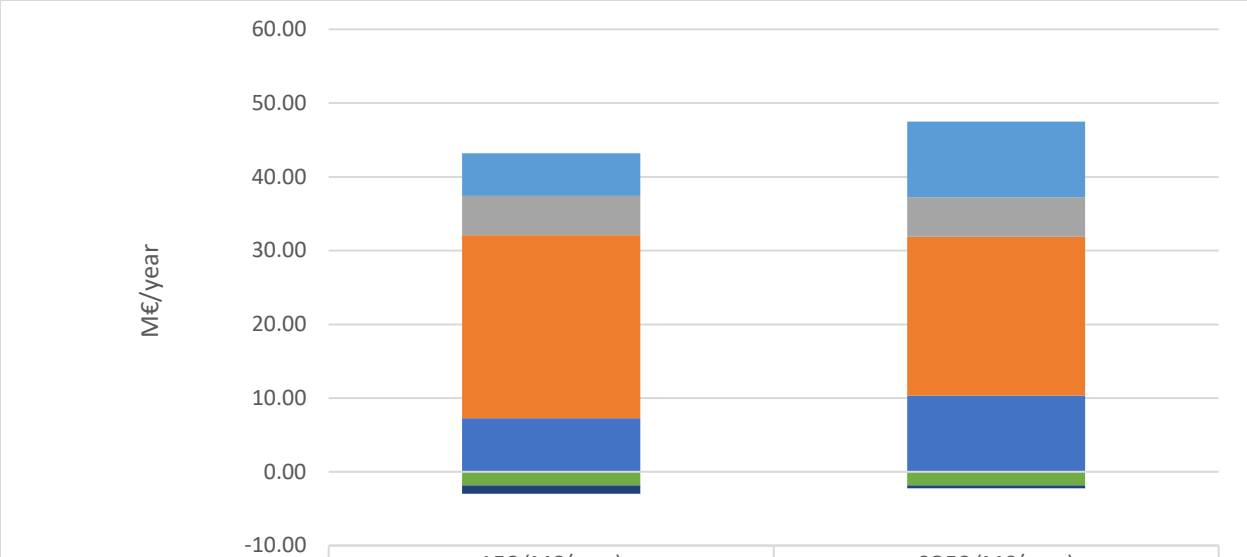

	AEC (M€/year)	SOEC (M€/year)
District heating (revenue)	-1.16	-0.40
Biochar (revenue)	-1.83	-1.83
O&M	5.74	10.25
Electrolysis water	0.0025	0.0025
Wheat straw	5.35	5.35
Electricity	24.84	21.55
Annuity (WACC=5%)	7.25	10.33

Figure 5.3: Total annual expenses breakdown (drivers of LCOF).

5.4. Levelized cost of BioSNG

At this stage, the base-case levelized cost of bioSNG (LCOF) is calculated for both layouts, shown in table 5-9. The mass flow rate and lower heating value (LHV) of the dry bioSNG product stream are taken directly from Aspen and are identical for the AEC- and SOEC-based configurations. Multiplying the bioSNG mass flow rate by its LHV yields a net plant output of 32.43 MW_{th} (dry bioSNG). Assuming 8,000 operating hours per year, the corresponding annual bioSNG production is 259,440 MWh/y. The LCOF is then obtained by dividing the total annual expenses by the annual bioSNG production. Using the previously calculated total annual expenses, the resulting base-case LCOF values are obtained. It is observable that a difference of approximately 5.06 M€/y in total yearly expenses translates into an LCOF increase of roughly 20 €/MWh, illustrating the strong sensitivity of the fuel cost to plant-wide annual costs.

Table 5-9: Base-case LCOF values for the studied layouts.

Layout	Levelized cost of BioSNG €/MWh
AEC-based	154.88
SOEC-based	174.38

6. Sensitivity analysis

6.1. Effect of electrolyser efficiency

The next chapter presents the sensitivity analyses. As previously indicated, the first sensitivity considers the effect of electrolyzer efficiency on the levelized cost of bioSNG (LCOF) for both layouts. The results clearly show that lower electrolyzer efficiency leads to higher LCOF. Importantly, this effect is not limited to electricity consumption alone. A lower efficiency does increase plant-wide electricity demand; however, because the plant must still deliver the same hydrogen requirement (imposed by the syngas-module design specification), a lower efficiency also implies that more electrolyzer capacity must be installed to achieve the same hydrogen production rate. In practical terms, this means purchasing additional modules, which increases TIC and, consequently, fixed O&M (given the O&M costs are defined as a fraction of TIC). In other words, when electrolyzer efficiency is reduced, the economic penalty is amplified by simultaneous increases in electricity cost, investment cost, and O&M cost.

In the AEC-based layout, illustrated in figure 6.1, the examined efficiency range is 50% to 67.5%, where 67.5% corresponds to the base case and also represents the most optimistic value considered in this work. This range was selected because commercial AEC systems are frequently reported at substantially lower efficiencies (commonly around 55%), making it important to test performance below the base-case assumption. Over this range, the calculated LCOF increases from 154.89 €/MWh at 67.5% efficiency (base case) to 186.66 €/MWh at 50%. The total change across the examined range is therefore 31.77 €/MWh.

In the SOEC-based layout, illustrated in figure 6.2, the examined efficiency range is 70% to 90%, with the base case at 80%. This range reflects SOEC efficiencies can reach much higher numbers under favourable operating conditions. The calculated LCOF rises from 161.45 €/MWh at 90% to 191.00 €/MWh at 70%. The total change across the examined range is therefore 29.55 €/MWh.

A further implication of reduced efficiency is the change in heat-recovery conditions. With lower efficiency (and therefore higher electrical input and larger installed electrolyzer capacity), more low-grade heat may become available, which can marginally increase district-heating revenue. This effect is only relevant to the AEC-based layout; however, it remains a weak benefit because the district-heating selling price is relatively low and the revenue credit is typically small compared with the additional costs introduced by higher electricity consumption and higher electrolysis-related TIC and O&M.

A key observation from these results is that the LCOF variation is slightly larger for the AEC layout than for the SOEC layout over the respective tested ranges (31.77 €/MWh vs. 29.55 €/MWh). This may be explained by the fact that electricity is the dominant annual expense term in both layouts. Consequently,

changes in electrolyzer efficiency propagate strongly through electricity consumption in the AEC layout, and this electricity consumption-driven effect can outweigh the intuitive expectation that SOEC would be "more sensitive" due to its higher electrolysis-related TIC/O&M.

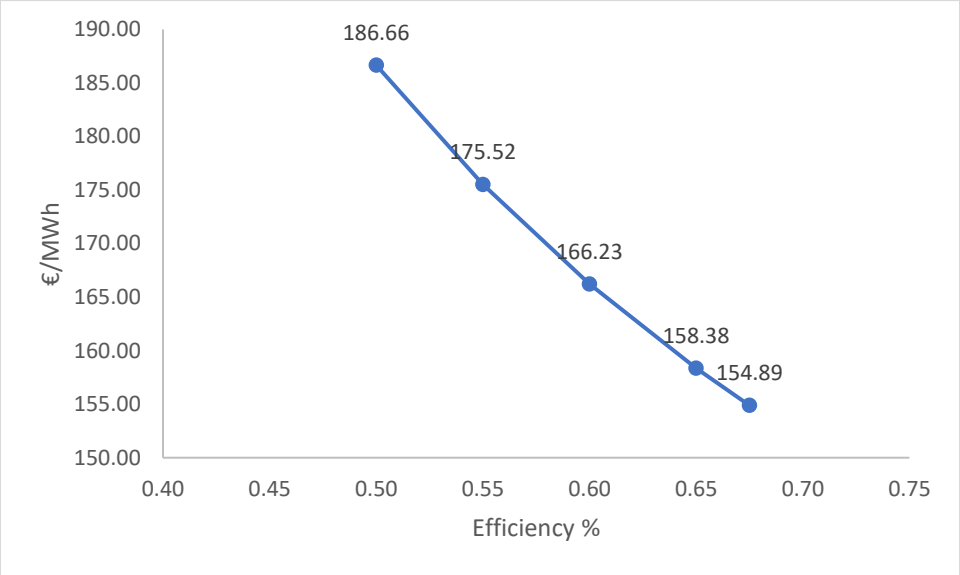

Figure 6.1: Effect of AEC efficiency on LCOF.

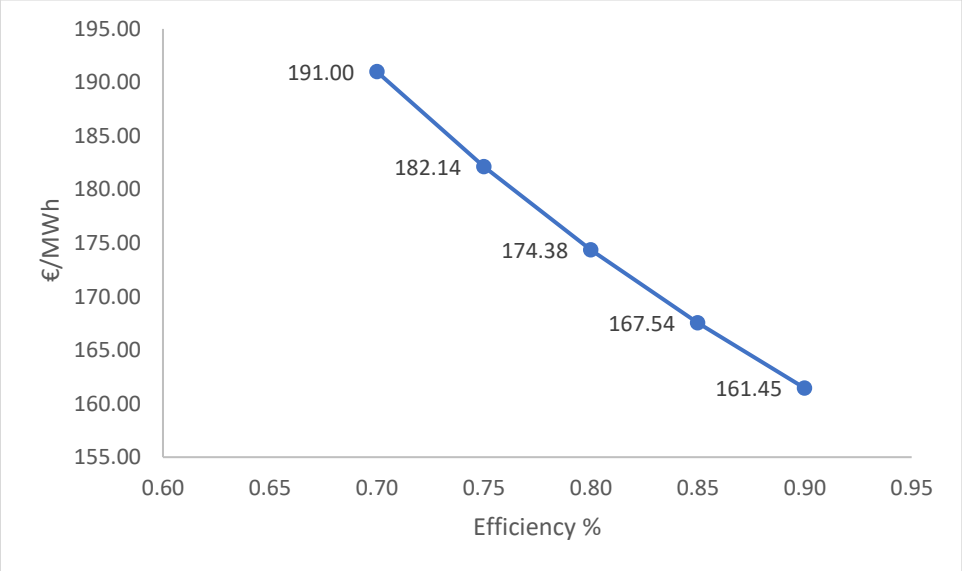

Figure 6.2: Effect of SOEC efficiency on the LCOF.

6.2. Effect of electricity price

The next sensitivity examines the effect of renewable electricity price on the levelized cost of bioSNG (LCOF), and the results show a pronounced impact in both layouts. Electricity price was varied from 0.07 to 0.11 €/kWh (i.e., 70–110 €/MWh), and in both cases the LCOF response is close to linear, reflecting the fact that electricity is a dominant contributor to total yearly expenses. For the AEC-based layout, shown in figure 6.3, the LCOF increases from 133.60 €/MWh at 0.07 €/kWh, to 176.16 €/MWh at 0.11 €/kWh, corresponding to a total swing of 42.56 €/MWh across the tested range (approximately +10.64 €/MWh per +0.01 €/kWh). For the SOEC-based layout, shown in figure 6.4, the corresponding values swing from 155.92 €/MWh at 0.07 €/kWh to 192.83 €/MWh at 0.11 €/kWh, giving a total change of 36.91 €/MWh (approximately +9.23 €/MWh per +0.01 €/kWh). The slightly steeper slope in the AEC case is consistent with the earlier observation that the AEC layout has higher plant-wide electricity costs (i.e., greater exposure to electricity-price variation), whereas the SOEC layout partially mitigates electricity-price sensitivity through lower electricity consumption driven by higher electrolysis efficiency.

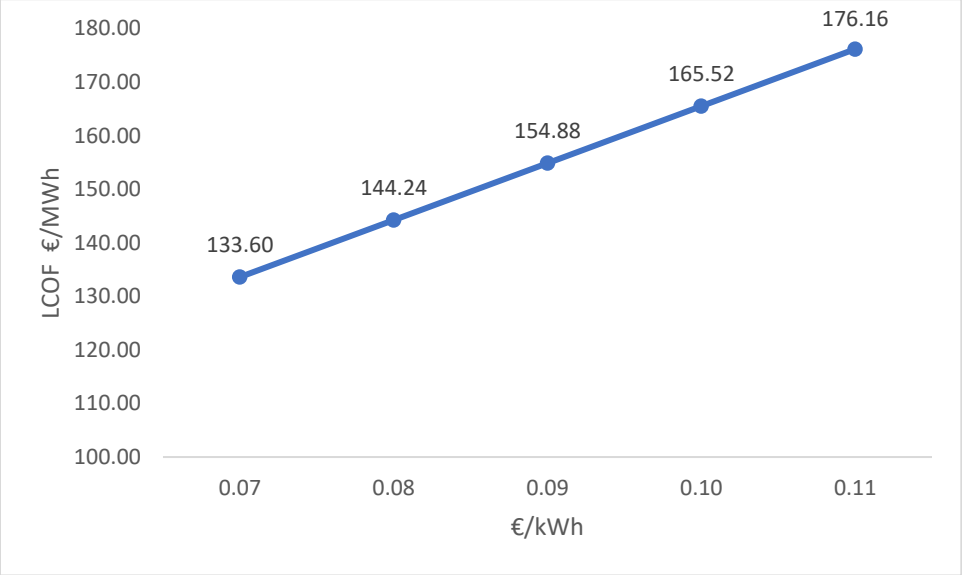

Figure 6.3: Effect of electricity price on LCOF (AEC layout).

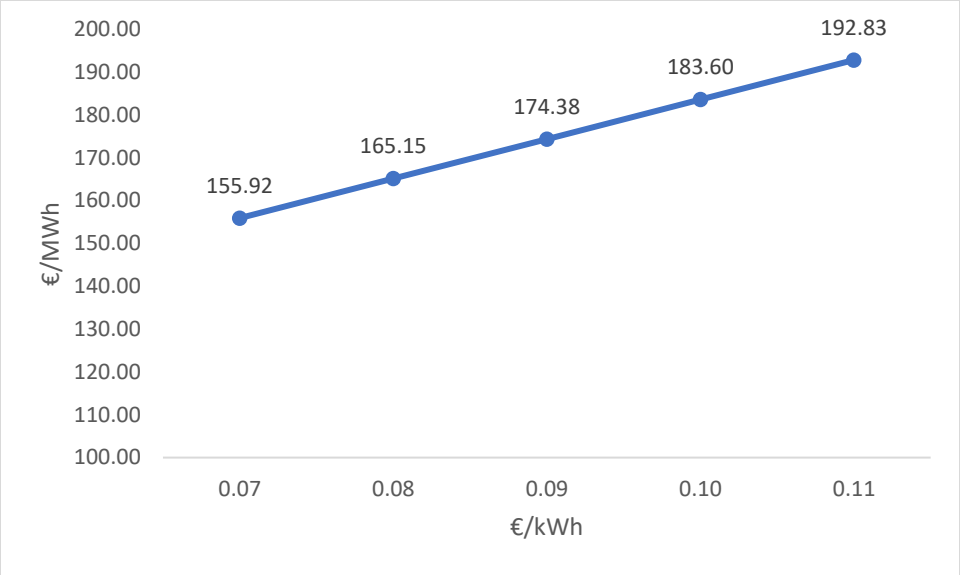

Figure 6.4: Effect of electricity price on LCOF (SOEC layout).

6.3. Effect of WACC

The next sensitivity examines the effect of the weighted average cost of capital (WACC) on LCOF through its direct influence on the capital recovery factor (CRF) and, consequently, the annuity term. Increasing WACC represents a higher financing cost and is commonly interpreted as a proxy for increased perceived financial and technology risk. Because CRF is a monotonic function of WACC, a higher WACC increases CRF, which increases the annualized capital charge (annuity = TIC × CRF). This higher annuity propagates directly to higher total yearly expenses and therefore a higher LCOF.

As shown in the figure 6.5, for the AEC-based layout, increasing WACC from 5% (base case) to 9% increases the LCOF from 154.88 €/MWh to 167.03 €/MWh, respectively. Over this range, the total increase is 12.15 €/MWh.

For the SOEC-based layout, shown in figure 6.6, the same WACC variation yields a larger absolute impact because the SOEC configuration has a higher TIC and therefore a larger annuity contribution. Specifically, the LCOF increases from 174.38 €/MWh at 5% WACC (base case) to 191.69 €/MWh at 9%. The total increase across the range is therefore 17.31 €/MWh, confirming that LCOF in the SOEC-based layout is more exposed to financing assumptions due to its higher capital intensity.

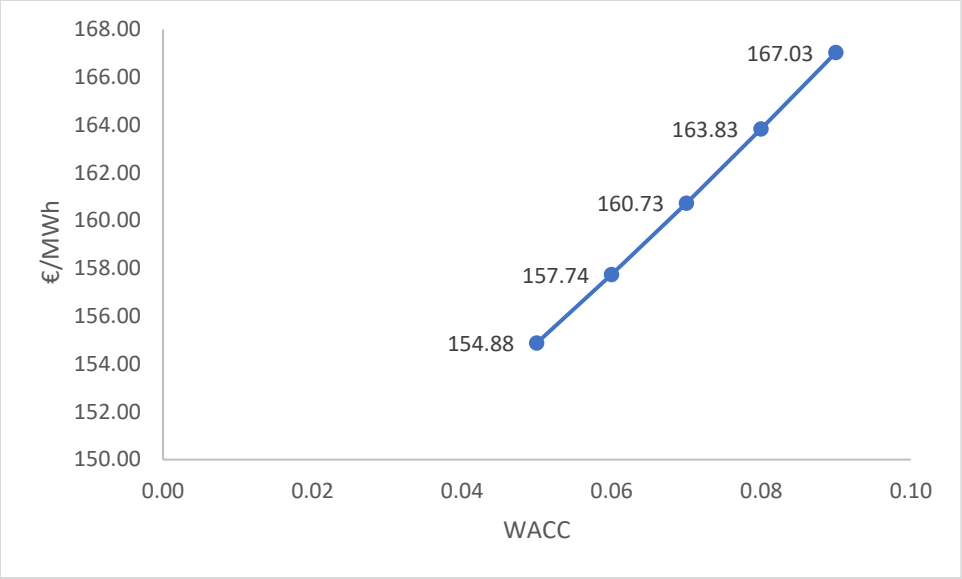

Figure 6.5: Effect of WACC (annuity) on LCOF (AEC layout).

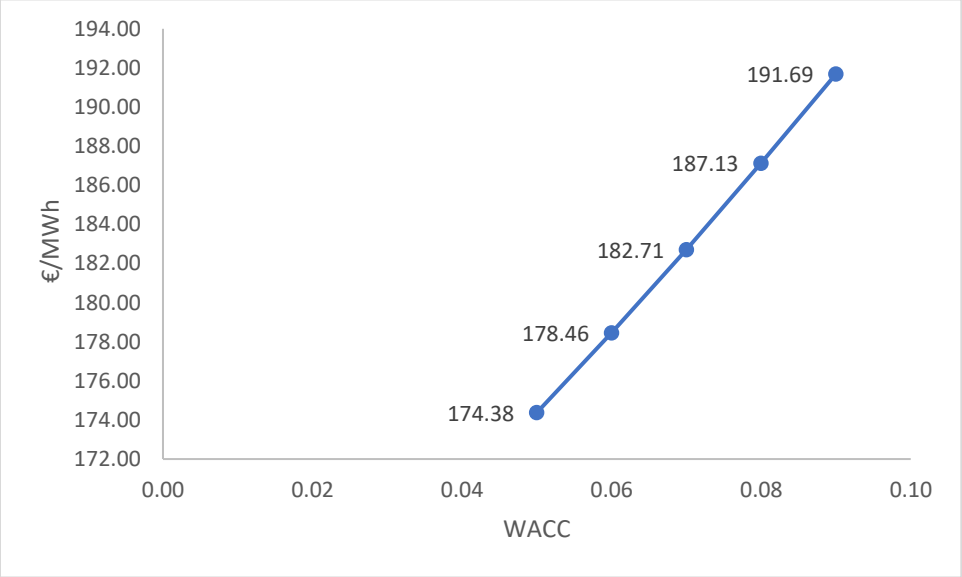

Figure 6.6: Effect of WACC (annuity) on LCOF (SOEC layout).

6.4. Uncertainty band for LCOF

Lastly, an uncertainty band is constructed for both layouts to quantify the impact of investment-cost and cost-model assumptions on the resulting LCOF. As defined earlier in the TIC and O&M estimation sections, lower and upper bounds were assigned to the major subsystems based on the availability and nature of the underlying data. For pyrolysis and electrolysis (AEC/SOEC), the uncertainty ranges are taken directly from the DEA technology catalogues (i.e., catalogue-provided lower/upper bounds on specific investment). For the e-reformer, a source-consistency issue was identified: the original cost statement from Mion et al. is interpreted as the lower bound and also adopted as the base-case approach, whereas the factor-based total overnight cost methodology applied by Caballero et al. is taken as the upper bound. For the methanation train, the reference dataset adopts a capacity scaling exponent of $n=0.6$; this exponent is used for both the lower bound and base case, while an alternative exponent of $n=0.45$ is used as the upper bound to reflect the high uncertainty associated with scaling from a very large reference plant to the much smaller scale considered here.

These upper-bound assumptions propagate through the economics primarily by increasing TIC and therefore increasing the annuity term (annuity = TIC × CRF). In addition, because fixed O&M is modelled as a percentage of TIC for the relevant subsystems, higher TIC also implies higher annual fixed O&M. By consistently applying the lower-bound assumptions to all subsystems, an optimistic cost case is obtained, whereas applying the upper-bound assumptions to all subsystems yields a pessimistic cost case. Total yearly expenses are recalculated for both cases, and the corresponding LCOF values define the uncertainty band for each layout.

For the AEC-based layout, shown in figure 6.7, the resulting uncertainty band spans from an optimistic case with TIC = 75.65 M€ and LCOF = 146.37 €/MWh, to a pessimistic case with TIC = 138.21 M€ and LCOF = 167.55 €/MWh, with the base case at TIC = 102.15 M€ and LCOF = 154.88 €/MWh. For the SOEC-based layout, shown in figure 6.8, the band spans from an optimistic case with TIC = 110.39 M€ and LCOF = 160.01 €/MWh, to a pessimistic case with TIC = 190.33 M€ and LCOF = 192.90 €/MWh, with the base case at TIC = 145.58 M€ and LCOF = 174.38 €/MWh. These results illustrate that cost uncertainty translates into a substantial spread in LCOF, with the spread being more pronounced for the SOEC-based layout due to its higher capital intensity and stronger coupling between TIC, annuity, and fixed O&M.

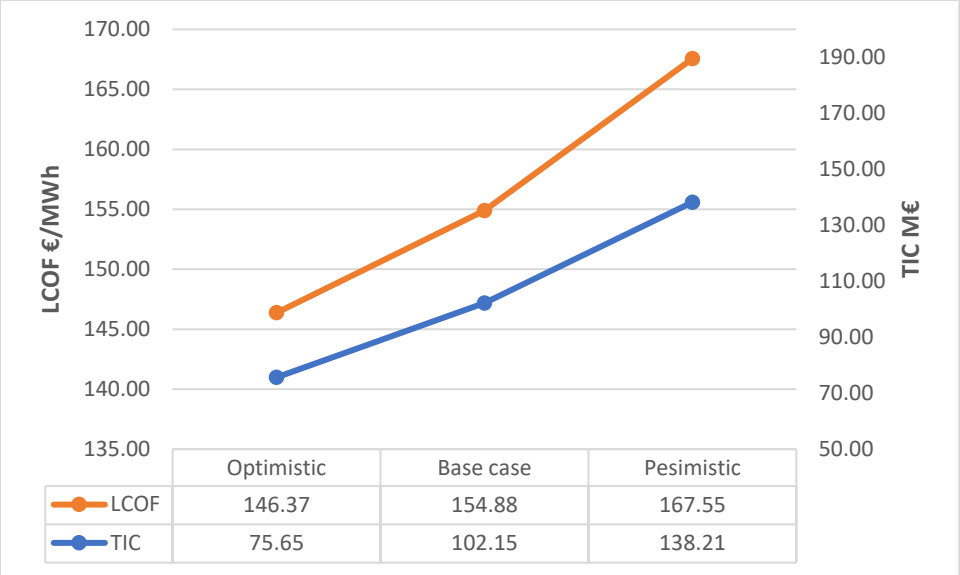

Figure 6.7: Uncertainty band for the AEC layout.

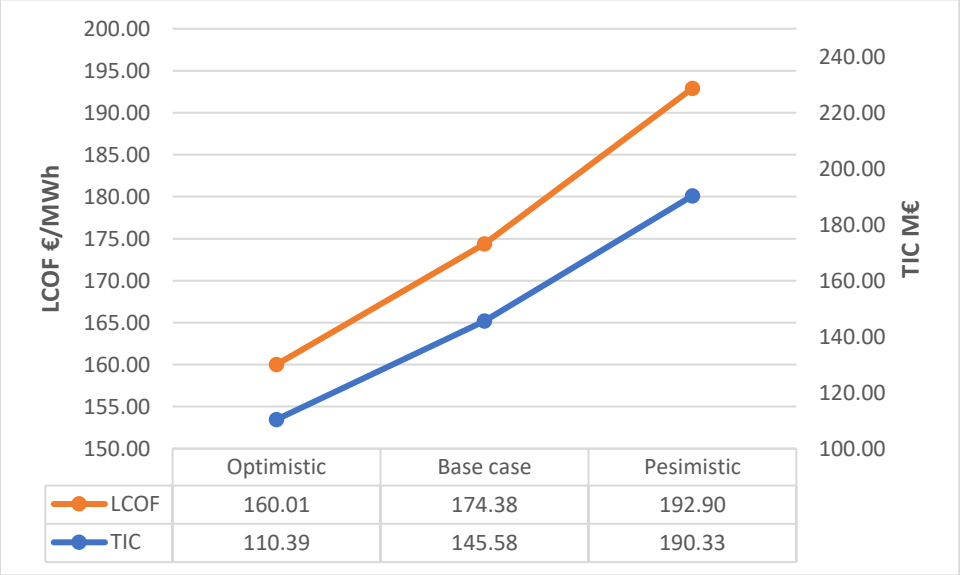

Figure 6.8: Uncertainty band for the SOEC layout.

7. Discussion

7.1. Techno-economic benchmarks for SNG production pathways

To contextualize the levelized cost of bioSNG obtained in the present work, it is useful to summarize techno-economic benchmarks reported for other SNG production pathways. The literature spans, conventional biomass gasification followed by syngas conditioning and methanation, pyrolysis–reforming–methanation pathways (including electrified reforming concepts), and biogas-based routes producing biomethane or e-methane via CO_2 methanation with renewable hydrogen.

7.1.1. Conventional BioSNG (biomass gasification and methanation)

A recent Aspen-based techno-economic assessment compares three biomass-to-SNG configurations centered on gasification and methanation, explicitly including cases with electrolysis-derived hydrogen in addition to a non-electrolysis case [5]. The authors define:

- a DFB gasification route with methanation and CCS
- a DFB gasification route integrated with electrolysis and methanation
- a CFB gasification route integrated with electrolysis and methanation

Across these cases, the reported annual biomass use is held constant at 4242 MWh, while the annual SNG production varies from 2684 to 6980 MWh depending on configuration and carbon utilization. Under base assumptions including biomass priced at 9.43 €/MWh (approximately 50 €/t) and renewable electricity at 50 €/MWh, the reported levelized SNG costs are 100 $€/MWh_{SNG}$ for the first case, 112 $€/MWh_{SNG}$ for the second case, and 105 $€/MWh_{SNG}$ for the third case. The study emphasizes that the levelized SNG cost is highly sensitive to assumed biomass and electricity prices, and that the dominant cost components shift with configuration. Where SNG output is comparatively low, capital recovery tends to dominate, while in higher-throughput and more electricity-intensive configurations, operating costs become more influential. In the 2022 scenario explored by the same authors, the electrolysis-integrated DFB case (second case) is reported to span approximately 58–98 $€/MWh_{SNG}$ across the electricity (0–100 €/MWh) and biomass (50–100 €/t) price range, illustrating how strongly electrolysis-linked SNG economics depend on power-price assumptions. The same reference situates these results within a broader literature range for larger-scale plants, cited as approximately 42–133 $€/MWh_{SNG}$.

Complementing this, an earlier process-integration analysis evaluates hydrogen addition to gasification-based SNG via electrolysis and frames feasibility explicitly through an electricity “break-even” threshold

[62]. Under the assumptions applied in that study, continuous electrolysis-derived hydrogen addition increases production costs at prevailing electricity prices, and the authors report a break-even electricity price on the order of 38.8–40.2 €/MWh_{el} (depending on gasification configuration) at which the electrolysis-integrated concept becomes cost-competitive with the non-electrolysis baseline.

7.1.2. Pyrolysis/reforming-based BioSNG production

A close comparator in "process shape" to pyrolysis-based BioSNG concepts is an electrified chain combining biomass pellet conversion, reforming, CO_2 removal, and methanation, evaluated at industrially relevant scale with explicit financial assumptions [20]. In that study, biomass pellets are converted via an electrified pyrolyser and then upgraded through a reformer concept (either electrified catalytic steam reforming, eCSR, or an alternative oxygen/partial oxidation route referred to as ACPOX), followed by CO_2 removal and multi-stage methanation (implemented using a TREMP-type approach in the model). The assessment is framed around an 80 MW_{HHV} SNG plant operating 8000 h/y, with a 20-year lifetime, a 10% IRR, and 100% equity financing without subsidy. The reported SNG production cost is presented for eCSR as 18.0–23.9 SEK/kg, increasing as the steam-to-biomass ratio rises from 1 to 4. The sensitivity discussion identifies biomass pellet price as the strongest cost lever, with electricity price representing the next most influential factor. The same reference reports a base equipment cost signal of approximately 627 MSEK for the eCSR pathway and 1154 MSEK for the ACPOX case, highlighting that reforming configuration can significantly reshape the capital profile even when final SNG output scale is comparable.

7.1.3. Biogas-based pathways

In the Danish context, several studies provide explicit benchmark cost bands for biomethane and electro-methane (CO_2 methanation using renewable hydrogen), and they are especially informative because they highlight how electrolysis and co-product monetization can dominate outcomes. A Denmark-oriented assessment reports biomethane costs in the approximate range of 460–550 DKK/MWh under 2020 assumptions, while electro-methane is reported in a substantially higher range of roughly 1200–1600 DKK/MWh under the same period assumptions [55]. The same reference projects that electro-methane costs can decline to approximately 450–600 DKK/MWh by 2030 under improved conditions, and it further shows that monetization of co-products such as waste heat and oxygen can reduce the apparent electro-methane cost significantly down toward roughly 300 DKK/MWh under favourable crediting assumptions.

Additional Danish screening work provides representative scale and sizing context for biogas methanation concepts [57]. In one illustrative case, a plant processing roughly 12,000 tonnes/year of substrate is associated with around 500 Nm^3/h raw biogas production, and the screening indicates an illustrative methanation-integrated configuration delivering on the order of 437 Nm^3/h output under the stated assumptions. The same table implies an electrolyser size around 1.6 MW and a methanation unit around 0.5 MW for that design point, underscoring that electrolysis sizing can be material relative to the biogas scale depending on targeted CO_2 conversion.

A dedicated report evaluating biogas–SOEC–methanation integration provides an additional benchmark that is valuable specifically for high-temperature electrolysis coupling [49]. In that concept, the report references a biogas plant producing approximately 500,000 Nm^3 biogas/year and a resulting SNG production of roughly 450,000 Nm^3 SNG/year, with an indicated cost level around 0.70 €/Nm^3 SNG. For interpretability, this unit basis can be approximately converted to an energy basis for methane-rich gas. Using a typical conversion of roughly 1 Nm^3 CH_4 ≈ 9.97 kWh (LHV), 0.70 €/Nm^3 corresponds to approximately 70 €/MWh (LHV) on an indicative basis. The same report highlights operational integration implications, such as differences in optimal hydrogen storage inclusion between near-term and future-year scenarios (e.g., no hydrogen storage in a 2020 optimization case versus roughly seven hours of hydrogen storage in a 2035 optimization case) and corresponding differences in SOEC utilization (reported as 100% in 2020 versus about 88% in 2035 under the stated optimization framing).

7.1.4. Non-biomass SNG

Although not renewable pathways, coal- and waste-derived SNG assessments can provide contextual cost ranges for methane synthesis under different feedstock and emissions assumptions. A coal-to-SNG benchmark reports levelized SNG costs of 18.87 $/MMBtu (30-year basis, 2007$) and 31.67 $/MMBtu (3-year basis, 2008$) [54]. On an energy-only conversion basis (1 MMBtu ≈ 0.293 MWh), these correspond to approximately 64 $/MWh and 108 $/MWh, respectively (currency-year and exchange-rate differences not adjusted). Separately, a waste-tyre-to-liquefied SNG pathway reports a production cost around 10.75 €/GJ [53], corresponding to approximately 38.7 €/MWh on an energy-only basis (again subject to boundary and basis details in the original reference).

7.1.5. Summary of insights

Across these pathway benchmarks, summarized in table 7-1, three useful patterns emerge. First, pathways that incorporate electricity use are structurally sensitive to electricity price assumptions and utilization. Multiple studies frame feasibility around power-price thresholds or show wide cost bands across electricity-price scenarios. Second is the importance of scale and operating hours. Industrially scaled assessments often assume high annual operating hours and long plant lifetimes, and cost outcomes may shift significantly when storage or flexible operation is introduced as part of an optimized strategy rather than assuming steady baseload operation. Third, co-product monetization can reshape the apparent fuel cost in methane pathways. Heat and oxygen credits are shown to significantly reduce the net cost of electro-methane under Danish assumptions, and comparable integration logic applies in methanation-heavy systems where recoverable heat is large and can offset other duties or generate revenue if district heating export is feasible.

Table 7-1: Summary table of the benchmarking studies.

Pathway family	**Ref.**	**Key boundary conditions**	**Reported cost metric (as stated)**	**Notes on main drivers**
Biomass gasification and methanation (BioSNG)	[5]	DFB/CFB; includes electrolysis cases; biomass 4242 MWh/y	100–112 €/MWh_{SNG}	Strong dependence on biomass and electricity prices
Gasification BioSNG + electrolysis threshold	[62]	Electrolysis H_2 addition economics	Break-even electricity ~38.8–40.2 €/ MWh_{el}	Electricity price threshold framing for H_2-assisted carbon utilization
Pyrolysis + reforming and methanation	[20]	80 MW_{HHV} SNG; 8000 h/y; 20 y; 10% IRR	18.0–23.9 SEK/kg SNG (eCSR) (109-146 €/MWh HHV basis)	Pellet cost strongest; electricity second; CAPEX differs strongly by reforming configuration
Biomethane and e-methane (Danish context)	[55]	Danish assumptions, 2020 and 2030	Biomethane 460–550 DKK/MWh (62-74 €/MWh); e-methane 1200–1600 DKK/MWh (2020) (162-216 €/MWh); 450–600 DKK/MWh (2030) (60-81 €/MWh)	Electrolysis cost exposure; heat/oxygen credits can materially lower net cost
Biogas + SOEC + methanation	[49]	System integration framing; storage/operation varies by year	~0.70 €/Nm³ SNG (63 €/MWh HHV basis)	Operational strategy (storage, utilization) influences outcomes; metric may reflect system context
Coal-to-SNG	[54]	Cost-year dependent	18.87–31.67 $/MMBtu (55-93 €/MWh)	Context benchmark only
Waste tyre to L-SNG	[53]	Waste-derived	~10.75 €/GJ (38.7 €/MWh)	Context benchmark only
Hydrogen-assisted wheat straw to bioSNG	*This work*	*32.4 MW_{LHV}, 8000h annually, Electrolysis H_2 addition*	*154.88 €/MWh for the AEC-based layout and 174.38 €/MWh for the SOEC-based layout*	*Strong dependence on electrolyser efficiency and electricity prices, significant stack replacement costs in the SOEC-based layout*

7.2. Interpretation of the base case techno-economic results

The techno-economic results show that the studied pathway can produce grid quality methane while relying on a substantial hydrogen input. This creates a cost structure where electricity related expenditures and electrolyser related capital recovery dominate the final fuel cost. Under the base assumptions used in this thesis, the levelized cost of BioSNG is 154.88 €/MWh for the AEC-based layout and 174.38 €/MWh for the SOEC-based layout. The difference is large enough to matter, but small enough that it can plausibly change under different cost and performance assumptions.

The AEC-based layout is cheaper in the base case even though it consumes more electricity than the SOEC-based layout. The main reason is that the SOEC-based layout carries higher annualized capital cost and higher fixed operating costs in the economic inputs applied here. This offsets the electricity savings that SOEC delivers through higher electrolysis efficiency. This trade-off is consistent with the way high temperature electrolysis is often framed in the literature. It can reduce electrical input if high-grade heat is available, but it tends to rely on more demanding hardware and tighter operating constraints. These features usually appear as higher investment and cost uncertainty when compared with mature alkaline systems. This is reflected in technology catalogue style inputs and in comparative SOEC costing discussions [3], [14], [40].

Section 7.1 shows that reported SNG costs vary widely across pathways and assumptions. In that context, the base case values from this thesis sit above many gasification based BioSNG estimates that assume lower electricity prices and larger plants [5]. They are closer to the cost levels reported for electricity intensive methane pathways, particularly when electrolysis is a major energy input and when co-product credits are modest [55]. This does not imply that the present concept is uncompetitive by definition. It indicates that its economic performance is especially sensitive to electricity related assumptions and to electrolysis cost and efficiency inputs, which is also a consistent message in benchmark studies that add electrolysis-derived hydrogen to methane synthesis chains [62].

7.3. What drives cost in the hydrogen-assisted BioSNG pathway

A central finding is that electricity is the dominant cost line under the base assumptions. Electricity is the largest component of annual expenses in both layouts. It is larger in the AEC-based case because more electrical energy is required to produce the same hydrogen flow at lower electrolysis efficiency. This is consistent with the process results where the total electrical power demand is 34.50 MW for the AEC-based layout and 29.93 MW for the SOEC-based layout for the same BioSNG output basis. The hydrogen specific

consumption indicators reported in the results chapter reinforce why this happens. The energy-based indicator of 0.61 shows that hydrogen provides a large share of the chemical energy that ends up in the product fuel. This makes the cost of electricity and the efficiency of electrolysis structurally important.

Capital recovery is the next major driver. The annuity term is materially higher in the SOEC-based layout than in the AEC-based layout under the same financing assumptions. This is important because it limits how much the SOEC electricity advantage can reduce the final fuel cost in the base case. This is also where the scope of the thesis matters. The cost inputs applied here are largely based on literature and catalogue sources and on scaling from reference plants that are not identical to the modeled plant. This means that the capital side of the results should be interpreted as indicative rather than definitive, especially for SOEC where cost maturity is still evolving [14], [40].

Operating and maintenance assumptions also matter. In the present inputs, fixed operating costs are notably higher for SOEC than for AEC. This acts in the same direction as the capital cost effect. It reinforces the base case result that SOEC improves energy efficiency but does not necessarily minimize cost under current style assumptions.

7.4. Role of heat integration, district heating export, and biochar revenue

The thesis results indicate that heat integration and heat export can reduce net annual expenses, but the effect is secondary relative to electricity and capital. In the base case economics, biochar sales and district heating export reduce the levelized cost by a moderate amount. The biochar credit is similar in both layouts because the biochar output is defined by the same pyrolysis front-end. The district heating credit is larger in the AEC-based layout because more low temperature waste heat is available from electrolysis and auxiliaries, which aligns with common discussions of alkaline electrolysis waste heat levels [14]. Additionally, a large portion of available heat in the SOEC-based layout is utilized to provide superheated steam for the electrolysis cell.

The magnitude of heat export benefits depends strongly on assumed heat price and annual delivery hours. The thesis uses a conservative style assumption of limited annual district heating export hours and a modest heat price. Under such conditions, heat export improves results but does not change the overall ranking of major cost drivers.

The process results also show that a substantial fraction of biogenic carbon is retained in biochar while the remainder is converted to BioSNG. This strengthens the sustainability narrative of the concept, but it also means the pathway does not maximize fuel yield per unit of biomass. In economic terms, this tends to

increase the share of fixed costs per unit of fuel, unless biochar revenue or carbon crediting is high. The literature suggests that value stacking can materially change methane pathway economics when co-products are strongly monetized [55]. In this thesis, the assumed biochar price provides a meaningful but not dominant offset, which makes the BioSNG cost remain primarily electricity and capital driven.

7.5. Interpretation of the sensitivity analyses

The sensitivity analyses confirm that the conclusions above are robust in direction. They also clarify when the ranking between layouts can change.

Electrolyser efficiency is a strong driver. In the AEC-based layout, the tested efficiency range leads to a levelized cost range from 154.89 to 186.66 €/MWh. In the SOEC-based layout, the tested range leads to a levelized cost range from 161.45 to 191.00 €/MWh. These ranges are large relative to the difference between the base-case layouts. They imply that realistic achieved efficiency and degradation behavior can be as important as the technology choice itself. This aligns with how comparative electrolysis studies frame the importance of real operating efficiency and long-term durability [14], [40].

Electricity price sensitivity is expected to be strong because electricity is the largest annual expense. A simple way to interpret the results is to translate electricity price changes into fuel cost changes using the modeled electricity consumption per unit of BioSNG output. In this work, a ten €/MWh change in electricity price corresponds to roughly a ten to twelve €/MWh change in the fuel cost, with the AEC-based layout being more exposed because it consumes more electricity per unit output. This is consistent with the threshold logic found in electrolysis assisted SNG literature where economic feasibility is often described in terms of the electricity price level [62].

Financing assumptions also matter and they matter more for the SOEC-based layout. Over the tested WACC range, the AEC-based layout increases from 154.88 to 167.03 €/MWh, while the SOEC-based layout increases from 174.38 to 191.69 €/MWh. This confirms that capital intensive configurations become more sensitive to financing conditions and that the comparative advantage of SOEC depends partly on whether its higher capital cost can be reduced or financed cheaply.

The uncertainty band constructed in the thesis is best read as a reminder of model and data limitations rather than as a precise probabilistic interval. It captures how sensitive the final cost is to investment and operating cost assumptions that are scaled from reference plants and literature ranges. This matters most for the subsystems where cost maturity is still changing and where scale effects are significant, especially electrolysis and high temperature components.

7.6. Limitations of the study

Several limitations follow directly from the scope and simplifying assumptions of the present thesis.

- First, the cost estimates rely on literature and catalogue-based inputs and on scaling from reference systems that differ from the modeled plant in size and integration detail. This is unavoidable at this stage but it limits how strongly individual cost items should be interpreted.
- Second, the analysis assumes a fixed annual operating profile and a single electricity price level in the base case. This is suitable for comparing layouts under consistent conditions, but it does not capture the full value of flexible operation or the potential to target low price hours for electrolysis.
- Third, process modelling choices such as equilibrium-based reactions and simplified representations of catalyst behavior affect the calculated heat duties and gas compositions. This can influence both energy performance and the sizing of key equipment.
- Fourth, revenue assumptions for biochar and district heating are uncertain and site dependent. This affects the size of the co-product offset and the extent to which value stacking can change the cost outlook.

7.7. Recommendations for future work

Future work can strengthen the discussion and reduce uncertainty without requiring a full redesign of the approach.

- A first priority is to improve the representation of electrolysis in long-term operation. This includes degradation, stack replacement logic, and realistic part-load efficiency for AEC and SOEC under process relevant integration constraints.
- A second priority is to refine electricity price treatment. Using time varying electricity prices and testing simple operating strategies would clarify how much the fuel cost can be reduced by flexible electrolysis and whether the relative ranking of AEC and SOEC changes under realistic price distributions.
- A third priority is to strengthen heat integration assessment. A more explicit heat exchanger network design and clearer temperature level accounting would improve the credibility of district heating export estimates and of internal heat recovery potential.
- Finally, if the concept is to be assessed in a Danish deployment context, it would be useful to add a location sensitive layer for straw logistics, district heating access, and biochar offtake conditions. This would help separate the intrinsic process trade-offs from site dependent feasibility.

8. Conclusions and outlook

This thesis developed and evaluated a hydrogen-assisted BioSNG pathway integrating slow pyrolysis of wheat straw, volatile reforming, electrolysis, and catalytic methanation. An Aspen Plus model was used to quantify mass and energy balances, and the results were translated into a transparent techno-economic framework to estimate the levelized cost of BioSNG for two integration layouts. Both configurations were found capable of producing grid-quality methane, while the economics were shown to depend strongly on hydrogen provision and electrolysis integration.

Under base-case assumptions, the levelized cost of BioSNG was estimated at 154.88 €/MWh for the AEC-based layout and 174.38 €/MWh for the SOEC-based layout. Although the SOEC case reduced total electricity demand, this advantage was outweighed by higher annualized capital and fixed costs in the present framework. The results therefore show that higher efficiency does not necessarily lead to lower fuel cost. Instead, overall performance depends on the combined effects of electricity price, electrolyser efficiency, capital recovery, and heat recovery.

Sensitivity analysis confirmed that electricity and electrolysis-related parameters are the dominant cost drivers, while also showing that the ranking between AEC and SOEC could shift under different assumptions. Comparison with literature further supports this conclusion, as electrolysis-based renewable methane pathways are consistently found to be highly sensitive to electricity price, utilization, and the treatment of co-product credits.

The main contribution of this thesis is a coherent and transparent assessment of a specific hydrogen-assisted BioSNG concept and its key trade-offs, rather than a definitive identification of the lowest-cost renewable methane route. While the analysis is constrained by literature-based cost inputs, simplified operational assumptions, and uncertain credits for heat and biochar, it provides a structured basis for future refinement. Overall, the study indicates that such pathways are technically feasible, but under conservative assumptions remain cost intensive unless supported by low-cost electricity, strong utilization, and credible valorization of heat and co-products.

9. References

[1] IEA, “Denmark 2023 - Energy Policy Review,” 2023. [Online]. Available: www.iea.org

[2] E. and U. Danish Ministry of Climate, “The Government’s Strategy for Power-to-X,” 2021.

[3] A. Singlitico, “Overview of the Power-to-X potential integration within the Danish energy system,” 2022.

[4] M. Puig Arnavat, M. Thoisen Fog, A. K. Sejbjerg, P. Stoholm, and W.-R. Kiebach, “Danish roadmap for a sustainable gas grid transition-status and potential role of thermal gasification,” 2020.

[5] D. Katla-Milewska, S. M. Nazir, and A. Skorek-Osikowska, “Synthetic natural gas (SNG) production with higher carbon recovery from biomass: Techno-economic assessment,” *Energy Convers. Manag.*, vol. 300, Jan. 2024, doi: 10.1016/j.enconman.2023.117895.

[6] JOSÉ JUAN BOLÍVAR CABALLERO, “Catalyst Development and Distributed Electrified Heating in Reforming Processes for Efficient Renewable Syngas and Fuel Production,” KTH Royal Institute of Technology, Stockholm, 2025.

[7] J. ; Ahrenfeldt, B. ; Jørgensen, and T. Thomsen, “Bio-SNG potential assessment: Denmark 2020,” 2010.

[8] Danish Energy Agency, “Technology Data for Renewable Fuels.” Accessed: Jan. 19, 2026. [Online]. Available: https://ens.dk/en/analyses-and-statistics/technology-data-renewable-fuels

[9] G. Venturini, A. Pizarro-Alonso, and M. Münster, “How to maximise the value of residual biomass resources: The case of straw in Denmark,” *Appl. Energy*, vol. 250, pp. 369–388, Sep. 2019, doi: 10.1016/j.apenergy.2019.04.166.

[10] D. Hidalgo, A. Urueña, J. M. Martín-Marroquín, and D. Díez, “Integrated Approach for Biomass Conversion Using Thermochemical Routes with Anaerobic Digestion and Syngas Fermentation,” Apr. 01, 2025, *Multidisciplinary Digital Publishing Institute (MDPI)*. doi: 10.3390/su17083615.

[11] N. S. Bentsen, D. Nilsson, and S. Larsen, “Agricultural residues for energy - A case study on the influence of resource availability, economy and policy on the use of straw for energy in Denmark and Sweden,” *Biomass Bioenergy*, vol. 108, pp. 278–288, Jan. 2018, doi: 10.1016/j.biombioe.2017.11.015.

[12] R. Nogueira Nakashima *et al.*, "Techno-economic evaluation of pyrolysis and electrolysis integration for methanol and char production," *Renew. Energy*, vol. 242, Apr. 2025, doi: 10.1016/j.renene.2025.122388.

[13] B. Nath, G. Chen, L. Bowtell, and T. Nguyen-Huy, "Pyrolysis of wheat straw pellets in a pilot-scale reactor: Effect of temperature and residence time," *Energy Sci. Eng.*, vol. 12, no. 8, pp. 3524–3539, Aug. 2024, doi: 10.1002/ese3.1833.

[14] Dansk Fjernvarme (Danish District Heating Association), Grøn Energi, COWI, and TVIS, "Power-to-X and District Heating," 2021.

[15] R. M. Swanson, J. A. Satrio, R. C. Brown, A. Platon, and D. D. Hsu, "Techno-Economic Analysis of Biofuels Production Based on Gasification," 2010. [Online]. Available: http://www.osti.gov/bridge

[16] H. Zhang, L. Wang, J. Van herle, F. Maréchal, and U. Desideri, "Techno-economic evaluation of biomass-to-fuels with solid-oxide electrolyzer," *Appl. Energy*, vol. 270, Jul. 2020, doi: 10.1016/j.apenergy.2020.115113.

[17] R. Kofler and L. R. Clausen, "Increasing carbon efficiency for DME production from wheat straw and renewable electricity – Analysis of 14 system layouts," *Energy Convers. Manag.*, vol. 281, Apr. 2023, doi: 10.1016/j.enconman.2023.116815.

[18] M. F. U. Hasnain *et al.*, "Optimization and Techno-Economic analysis of catalytic gasification of wheat straw biomass using ASPEN PLUS model," *Arabian Journal of Chemistry*, vol. 17, no. 7, Jul. 2024, doi: 10.1016/j.arabjc.2024.105821.

[19] F. S. João Roberto, J. B. Ribeiro, and L. Durães, "e-Fuel production process technologies and trends: A bibliometric-based review," *Energy Reports*, vol. 13, pp. 3351–3368, Jun. 2025, doi: 10.1016/j.egyr.2025.02.030.

[20] J. J. Bolívar Caballero *et al.*, "Electrified catalytic steam reforming for renewable syngas production: Experimental demonstration, process development and techno-economic analysis," *Appl. Energy*, vol. 377, p. 124556, Jan. 2025, doi: 10.1016/j.apenergy.2024.124556.

[21] T. P. Thomsen, "Climate Footprint Analysis of Straw Pyrolysis & Straw Biogas: Assessment of the Danish climate crisis mitigation potential of two new straw management options.," 2021.

[22] T. Van Nguyen and L. R. Clausen, “Techno-economic analysis of polygeneration systems based on catalytic hydropyrolysis for the production of bio-oil and fuels,” *Energy Convers. Manag.*, vol. 184, pp. 539–558, Mar. 2019, doi: 10.1016/j.enconman.2019.01.070.

[23] H. Honkanen and J. Kataja, “Technological aspects of nonfood agricultural lignocellulose transformations,” in *Bioenergy Systems for the Future: Prospects for Biofuels and Biohydrogen*, Elsevier Inc., 2017, pp. 43–59. doi: 10.1016/B978-0-08-101031-0.00002-8.

[24] M. Hassan and V. Strezov, “Wheat straw pyrolysis fundamentals during production of biochar,” *J. Therm. Anal. Calorim.*, Oct. 2025, doi: 10.1007/s10973-025-14766-9.

[25] M. Gylling, T. Nord-Larsen, A. Bruhn, M. Thomsen, M. Ambye-Jensen, and U. Jørgensen, “Potential Danish biomass production and utilization in 2030,” 2023.

[26] K. Akubo, M. A. Nahil, and P. T. Williams, “Pyrolysis-catalytic steam reforming of agricultural biomass wastes and biomass components for production of hydrogen/syngas,” *Journal of the Energy Institute*, vol. 92, no. 6, pp. 1987–1996, Dec. 2019, doi: 10.1016/j.joei.2018.10.013.

[27] M. Abou Rjeily, M. Chaghouri, C. Gennequin, E. Abi Aad, H. Pron, and J. H. Randrianalisoa, “Biomass Pyrolysis Followed by Catalytic Hybrid Reforming for Syngas Production,” *Waste Biomass Valorization*, vol. 14, no. 8, pp. 2715–2743, Aug. 2023, doi: 10.1007/s12649-022-02012-4.

[28] L. Santamaria *et al.*, “Progress on Catalyst Development for the Steam Reforming of Biomass and Waste Plastics Pyrolysis Volatiles: A Review,” *Energy & Fuels*, vol. 35, no. 21, pp. 17051–17084, Nov. 2021, doi: 10.1021/acs.energyfuels.1c01666.

[29] L. Elsgaard *et al.*, “KNOWLEDGE SYNTHESIS ON BIOCHAR IN DANISH AGRICULTURE,” 2022.

[30] M. Laghari, D. S. Müller-Stöver, M. Puig-Arnavat, T. P. Thomsen, and U. B. Henriksen, “Evaluation of Biochar Post-Process Treatments to Produce Soil Enhancers and Phosphorus Fertilizers at a Single Plant,” *Waste Biomass Valorization*, vol. 12, no. 10, pp. 5517–5532, Oct. 2021, doi: 10.1007/s12649-021-01358-5.

[31] S. Heyne and S. Harvey, “Assessment of the energy and economic performance of second generation biofuel production processes using energy market scenarios,” *Appl. Energy*, vol. 101, pp. 203–212, 2013, doi: 10.1016/j.apenergy.2012.03.034.

[32] C.-C. Cormos, A.-M. Cormos, L. Petrescu, and S. Dragan, "Techno-economic assessment of decarbonized biogas catalytic reforming for flexible hydrogen and power production," *Appl. Therm. Eng.*, vol. 207, p. 118218, May 2022, doi: 10.1016/j.applthermaleng.2022.118218.

[33] T. Thomsen, "Introduction to Production and Use of Biochar 2022 working towards a more circular and bio-based Danish economy," 2022.

[34] T. Van Nguyen and L. R. Clausen, "Thermodynamic analysis of polygeneration systems based on catalytic hydropyrolysis for the production of bio-oil and fuels," *Energy Convers. Manag.*, vol. 171, pp. 1617–1638, Sep. 2018, doi: 10.1016/j.enconman.2018.06.024.

[35] (S&T)2 Consultants Inc., "Review of Technology Data for Advanced Bioenergy Fuels," 2014.

[36] J. Zhang, N. Fatah, S. Capela, Y. Kara, O. Guerrini, and A. Y. Khodakov, "Kinetic investigation of carbon monoxide hydrogenation under realistic conditions of methanation of biomass derived syngas," *Fuel*, vol. 111, pp. 845–854, 2013, doi: 10.1016/j.fuel.2013.04.057.

[37] S. Simon Araya, X. Cui, N. Li, V. Liso, and S. L. Sahlin, "Aalborg Universitet Power-to-X Technology overview, possibilities and challenges," 2022.

[38] R. N. Nakashima *et al.*, "Integration of electrolysis with pyrolysis: effects of carbon conversion in methanol production," APA, 2022, pp. 20–23.

[39] G. Butera, S. H. Jensen, and L. R. Clausen, "A novel system for large-scale storage of electricity as synthetic natural gas using reversible pressurized solid oxide cells," *Energy*, vol. 166, pp. 738–754, Jan. 2019, doi: 10.1016/j.energy.2018.10.079.

[40] N. Campion, R. Gutiérrez-Alvarez, J. T. F. Bruce, and M. Münster, "The potential role of concentrated solar power for off-grid green hydrogen and ammonia production," *Renew. Energy*, vol. 236, p. 121410, Dec. 2024, doi: 10.1016/j.renene.2024.121410.

[41] J. H. Jensen, J. M. Poulsen, and N. U. Andersen, "Substitute Natural Gas: From coal to clean energy," *Nitrogen+Syngas*, 2011.

[42] Haldor Topsøe, "From solid fuels to substitute natural gas (SNG) using TREMP™ Topsøe Recycle Energy-efficient Methanation Process," 2009.

[43] F. Celoria *et al.*, "Kinetic study and deactivation phenomena for the methanation of CO2 and CO mixed syngas on a Ni/Al2O3 catalyst," *Chemical Engineering Journal*, vol. 512, May 2025, doi: 10.1016/j.cej.2025.162113.

[44] S. Rönsch *et al.*, “Review on methanation - From fundamentals to current projects,” Feb. 15, 2016, *Elsevier Ltd*. doi: 10.1016/j.fuel.2015.10.111.

[45] D. Schmider, L. Maier, and O. Deutschmann, “Reaction Kinetics of CO and CO2Methanation over Nickel,” *Ind. Eng. Chem. Res.*, vol. 60, no. 16, pp. 5792–5805, Apr. 2021, doi: 10.1021/acs.iecr.1c00389.

[46] H. Er-rbib and C. Bouallou, “Modeling and simulation of CO methanation process for renewable electricity storage,” *Energy*, vol. 75, pp. 81–88, Oct. 2014, doi: 10.1016/j.energy.2014.05.115.

[47] T. N. Do, H. Kwon, M. Park, C. Kim, Y. T. Kim, and J. Kim, “Carbon-neutral hydrogen production from natural gas via electrified steam reforming: Techno-economic-environmental perspective,” *Energy Convers. Manag.*, vol. 279, p. 116758, Mar. 2023, doi: 10.1016/j.enconman.2023.116758.

[48] European Sustainable Phosphorus Platform, “Stiesdal SkyClean pyrolysis.” Accessed: Jan. 17, 2026. [Online]. Available: https://www.phosphorusplatform.eu/activities/p-recovery-technology-inventory?view=article&id=2400

[49] Haldor Topsøe A/S, “Biogas-SOEC: Electrochemical upgrading of biogas to pipeline quality by means of SOEC electrolysis,” 2012. Accessed: Jan. 17, 2026. [Online]. Available: https://www.ea-energianalyse.dk/en/publications/1110-biogas-soec-electrochemical-upgrading-og-biogas-to-pipeline-quality-by-means-of-seoc-electrolysis/

[50] A. Mion, F. Galli, P. Mocellin, S. Guffanti, and G. Pauletto, “Electrified methane reforming decarbonises methanol synthesis,” *Journal of CO2 Utilization*, vol. 58, p. 101911, Apr. 2022, doi: 10.1016/j.jcou.2022.101911.

[51] C. HAMELINCK, A. FAAIJ, H. DENUIL, and H. BOERRIGTER, “Production of FT transportation fuels from biomass; technical options, process analysis and optimisation, and development potential,” *Energy*, vol. 29, no. 11, pp. 1743–1771, Sep. 2004, doi: 10.1016/j.energy.2004.01.002.

[52] E. Rezaei and S. Dzuryk, “Techno-economic comparison of reverse water gas shift reaction to steam and dry methane reforming reactions for syngas production,” *Chemical Engineering Research and Design*, vol. 144, pp. 354–369, Apr. 2019, doi: 10.1016/j.cherd.2019.02.005.

[53] A. S. R. Subramanian, T. Gundersen, and T. A. Adams, “Technoeconomic analysis of a waste tire to liquefied synthetic natural gas (SNG) energy system,” *Energy*, vol. 205, p. 117830, Aug. 2020, doi: 10.1016/j.energy.2020.117830.

[54] NETL - US Department of Energy, “Cost and Performance Baseline for Fossil Energy Plants Volume 2: Coal to Synthetic Natural Gas and Ammonia.” Accessed: Jan. 19, 2026. [Online]. Available: https://www.netl.doe.gov/sites/default/files/netl-file/SNGAmmonia_FR_20110706.pdf

[55] Henrik Iskov, Torben Kvist, and Johan Bruun, “Biogas, Biomethane and Electro-methane cost comparison,” 2019. Accessed: Jan. 19, 2026. [Online]. Available: https://dgc.dk/media/g1bn0xut/electrolyser-and-methanisation-economics_final-1.pdf

[56] M. Kraussler, F. Pontzen, M. Müller-Hagedorn, L. Nenning, M. Luisser, and H. Hofbauer, “Techno-economic assessment of biomass-based natural gas substitutes against the background of the EU 2018 renewable energy directive,” *Biomass Convers. Biorefin.*, vol. 8, no. 4, pp. 935–944, Dec. 2018, doi: 10.1007/s13399-018-0333-7.

[57] I. R. Skov, S. Nielsen, M. S. Nørholm, and J. P. Vestergaard, “Screening of biogas methanation in Denmark: Resources, technologies and renewable energy integration,” Aalborg , 2019.

[58] Danish Energy Agency, “Technology Brief: Update of offshore wind in the Technology Catalogue,” Feb. 2025. Accessed: Jan. 20, 2026. [Online]. Available: https://ens.dk/media/6572/download

[59] Danish Energy Agency, “Determining the Cost of New Entry (CONE) for Denmark,” Dec. 2024. Accessed: Jan. 20, 2026. [Online]. Available: https://ens.dk/media/6428/download

[60] Willem Hazenberg, “Green Hydrogen Cost and reduction potential,” 2024. Accessed: Jan. 20, 2026. [Online]. Available: https://greenskillsforhydrogen.eu/wp-content/uploads/2024/07/2024-Juni-4-V03-Masterclass-WHB_-Greenskill4h2_Green-Hydrogen-Cost-and-reduction.pdf

[61] R. Kofler, N. Campion, M. Hillestad, W. Meesenburg, and L. R. Clausen, “Techno-Economic Analysis of Dimethyl Ether Production from Different Biomass Resources and Off-Grid Renewable Electricity,” *Energy and Fuels*, vol. 38, no. 10, pp. 8777–8803, May 2024, doi: 10.1021/acs.energyfuels.4c00311.

[62] M. Gassner and F. Maréchal, “Thermo-economic optimisation of the integration of electrolysis in synthetic natural gas production from wood,” *Energy*, vol. 33, no. 2, pp. 189–198, Feb. 2008, doi: 10.1016/j.energy.2007.09.010.